HOMOGENOUS PLANAR WAVEGUIDE LENSES IN INTEGRATED OPTICS

A Thesis Submitted to the Faculty of Engineering of the University of Glasgow for the degree of Doctor of Philosophy

by **Pisu Jiang**, B.Eng., M.Sc.

April 1992

DECLARATION

The author declares that the work of this thesis has not been previously submitted for any other degree or award.

ProQuest LLC.
789 East Eisenhower Parkway
P.O. Box 1346
Ann Arbor, MI 48106 – 1346

To My Wife Yishan

ACKNOWLEDGEMENTS

I wish to thank Professor John. Lamb, late head of the Department, for the use of the research laboratories in the Department of Electronics and Electrical Engineering.

I am greatly indebted to Professor Peter J. R. Laybourn for closely supervising the work. Special thanks are also due to Professor Richard M. De La Rue, Dr. Armando Loni (now with BT & D Technologies), Dr. Feng Zhou, Dr. Raj Shenoy (now with the Indian Institute of Technology, Delhi), Mr. Dejie Li (now with Tsinghua University, P. R. China), Mr. Yan Zhou, Mr. Zhuangqi Cao and Dr. Robert Keys (now with BNR), for many interesting suggestions and discussions. Many thanks to Mr. Weiping Zhang (now with Shandong University, P. R. China) for providing the experimental results on glass waveguide, to Mr. Weiping Zhang and Dr. Andrzej Jezierski (now with Nottingham University) for preparation of masks of waveguide prism and lenses used in this work, and to Dr Feng Zhou for co– operation in the work on buried waveguide polariser and Er:Ti co– doping.

The technical assistance of Mr. David Clifton, Mrs. Lois Hobbs, Mr. George W. T. Boyle, Mr. Jimmy H. Young, Mr. Kaz Piechowiak, Mr. Hugh Moy and Mr. Ray Darkin was much appreciated.

Grateful acknowledgement is made to the University of Glasgow for the D. J. Gray Postgraduate Scholarship, Overseas Research Student Committee of the Committee of Vice Chancellor and Principal of UK for an ORS award, and Mrs. Margaret Hows and Mr. Fred Hows in Montreal, Canada for their concern and support.

ABSTRACT

Waveguide lenses are a key element in integrated optical devices. Even though several types of waveguide lenses have been developed, they do not fully satisfy the requirements of their applications. Existing waveguide lenses were reviewed and it was pointed out that the homogenous refracting lens has advantages over other types of waveguide lenses. Resolution, field of curvature, signal–to–noise ratio, field of view and relative aperture are the main characteristics of lens performance. A comprehensive understanding of the homogenous lens performance was obtained by raytracing and Huygens–Fresnel analysis. Anisotropic aberration was studied and the lens performance in an anisotropic waveguide was analysed.

Even though the multi–element lens design provided excellent optical performance, even on anisotropic waveguide, the boundary losses limited its application. The existing one–element lenses had curvature of the focal field and anisotropic aberration was not taken into consideration in the design. A new one–element lens design lens was proposed, which, taking anisotropic aberration into consideration, was free of field curvature and had an acceptable resolution.

Mode matching between two disparate waveguides was studied and it was shown that by careful design and choice of processing parameters mode mismatch would not significantly affect the coupling between two fundamental modes in high and low index waveguides. However, boundary scattering reduced the transmission of light power across the boundary and therefore the number of lens elements should be minimised.

The fabrication of waveguide lenses was studied. Ti indiffused waveguide had

advantages over dilute– proton– exchanged waveguide as a low index waveguide, but was subject to the risk of producing a spurious out– diffused waveguide. SiO_2 gave the best behaviour in blocking proton exchange and was easy to process.

Waveguide optical components, prisms and one– element lenses, were successfully fabricated, while the experimental four– element lens suffered low light power transmission due to boundary losses.

In addition to the study of waveguide lenses, some other integrated optical devices were developed. Ti indiffused waveguide was buried by a subsequent proton exchange and annealing. The buried waveguide had low scattering loss, nearly symmetric optical intensity profile and single polarisation. The co– doping of Er and Ti enhanced the indiffusion rate of Er and much less annealing time was used than required in Er– only– doping.

CONTENTS

CHAPTER ONE: INTRODUCTION

I.1. Background of the Project

I.1.1. The Lens Application in Integrated Optical Devices

The emergence of integrated optics (IO) has activated a new research field, to which numerous scientists have contributed. New results are reported almost daily and a new technology era is expected. Unlike integrated circuit (IC) technology, in most cases IO is not, as the term suggests, simply the integration or reduction of the existing optical systems. Many new physical phenomena, optically and electronically, take place in the size scale of IO devices, several micrometers. The phenomena inspire many completely new ideas and provide new products or possibilities, and at the same time new challenges.

One aspect of IO is in the fields of computing and signal processing. Utilizing the properties of particular materials and new ideas and technologies in IO, computing and signal processing could be much easier, more compact, more functional or cheaper. Many designs have been reported [Verber 1984, Taylor 1987, Tsai 1988]. A key element in many devices is a waveguide lens which acts to collimate a light wave source such as a laser diode and to Fourier transform the angle of a surface-acoustic-wave (SAW) diffracted light beam into a new focal spot position. A typical application is the so-called integrated optics spectrum analyser (IOSA) as depicted in figure 1-1, where the lens on the left hand is a collimating lens and the lens on the right hand is a Fourier transform lens. The SAW diffracts the parallel beam into a parlicular angle, depending on the frequency of the SAW. The lens focuses the beam onto the detection plane. The position of the focused spot in the

plane depends on the angle of the diffracted beams and therefore on the frequency of the SAW.

The IOSA has been developed on $LiNbO_3$ [Zang 1986, Suhara 1986] and on GaAs [Vu 1989a, 1989b]. The best result was an IOSA on $LiNbO_3$ which had a frequency resolution of 2MHz in the bandwidth of 1GHz corresponding to 500 resolvable spots of 2μm within the angle range of $\pm 7^0$ [Suhara 1986]. Much higher frequency resolution could be achieved if the lens were to have better resolution; more research is necessary to improve the lens performance and therefore the IOSA performance.

I.1.2. Existing Lenses in Integrated Optical Devices

At the very inception of IO, a waveguide was fabricated by depositing a high index layer on a substrate. Another top layer induced effective refractive index increase. Different thickness resulted in different effective refractive index and then formed two waveguide. Refraction, reflection and lens focusing were realized by this means [Shubert 1968, Ulrich 1971]. Fresnel lenses were also made by the same method [Valette 1982]. Besides the high attenuation of such a thin film waveguide, the substantial difference between the depths of two waveguides, required for a large difference in effective refractive indices, led to severe mismatch of mode profiles, and then the transmission of the guided wave energy was inefficient.

A waveguide region with changing effective refractive index profile in waveguide can act as a lens, the so-called Luneburg lens [Zernike 1974, Anderson 1977]. The effective refractive index profile can be obtained by an index variation in the waveguide or by a thickness variation of the top layer. But, technically, the accurate control of the index profile or the thickness profile is not easy to handle. It is also possible to employ a curved waveguide surface topology which alters the propagation length, instead of the effective refractive index. The guided wave will propagate

along geodesics of the waveguide surface according to Fermat's principle, and so such lenses are named the Geodesic Lens [Righini 1973, Anderson 1977]. A computer controlled grinding machine can grind the surface with the section profile as designed but the machine itself is expensive and the fabrication is still complex. Another intrinsic weakness of Luneburg lenses and Geodesic lenses is their curvature of field even though they can be free of all other aberrations. This is simply because of their circular lens contours and therefore circular focal surface.

Planar processing has been well developed for IC technology and is always preferred in IO fabrication when possible. Conventional photolithography produces the lens pattern and subsequent diffusion processing forms another waveguide in the patterned lens region. In this two-dimensional processing, the lens contour can be of any shape, while in the bulk optical lens even a single non-spherical surface is difficult to make. Since two step waveguide fabrication became possible, i.e. potassium ion exchange and silver ion exchange in glass [Chartier 1986] and titanium indiffusion and proton exchange (TIPE) in lithium niobate [De Micheli 1982], various planar lens configuration have been explored: chirp grating diffraction lens or Fresnel diffraction lens [Suhara 1982, Warren 1983, Suhara 1986, Pitt 1988, Reid 1989] and homogenous refraction lens [Zang 1983, 1985, 1986, Tatsumi, 1988].

It is interesting to note that the Fresnel lens seems more favoured without a fundamental convincing reason. Up to now, the most successful example of waveguide lens application in IOSA is a Fresnel lens on $LiNbO_3$ which could resolve 500 spots in the angle range of $\pm 7^0$, corresponding to a frequency resolution of 2MHz in a bandwidth of 1GHz [Suhara 1986], and recently a Fresnel lens has been fabricated on GaAs [Vu 1989a, 1989b]. The intrinsic drawback of the Fresnel lens is its basically elliptic-shaped (with higher effective index in the lens region) or hyperbolic-shaped (with lower effective index in the lens region) contour, with quantised phase shift, which leads to bad off-axis performance. So it is just addressed with on-axis light [Pitt 1988]. Another disadvantage is its low

transmission efficiency of light energy because of the reduced effective aperture imposed by the phase shifting mechanism and reduced coupling efficiency between the modes in the guide region and the lens region where the effective index is modified [Pitt 1988]. Fabrication difficulties occur in the photolithography of a perfect lens pattern which consists of many small features with dimensions of down to 1 μm.

Another type of planar lens is the homogenous refracting lens, which takes the form of a conventional bulk optical lens but in 2– dimensions. Abundant experience in conventional bulk optical lens design is at hand. Many commercial software packages are available. The acircular lens surface, which is required to overcome aberrations, is no longer a problem and off– plane aberrations do not exist in this two dimensional case, while a contrasting point is the small difference in the indices of the lens and the surrounding medium. A multi element circular lens can give uniform optical quality in an incident angle range of $\pm 9^0$ [Laybourn 1986, Righini 1986] but with too many elements or boundaries, it is difficult to realize in with sufficiently low loss. Using an acircular design, the number of lenses used to eliminate off– axis aberration can be greatly reduced as examplified by the designs of 4– element [Laybourn 1988] and 5– element [Righini 1987] homogenous refracting lenses both of which offer excellent optical performance over a large range of incident angle. A single– element double– convex homogenous refracting lens has been used in an IOSA, but with bad off– axis performance [Zang 1986]. An one– element bi– aspherical lens has been reported to have a uniform optical performance of 1.5 μm spot size at –3dB over the incident angle range of $\pm 6^0$ [Tatsumi 1988].

I.2. Review

The single– element ellipse lens or elliptical– hyperbolic lens has good focusing performance for an on– axis image but the off– axis performance is bad [Laybourn

The single－element double－convex lens [Zang 1986] was an aplanatic lens based on the satisfaction of the sine condition, under which the lens should be aberration free over a very small off－axis angle range. Its off－axis performance was shown experimentally to be poor and the lens focus suffered from field curvature [Zang 1986]. There are at least two reasons for this degradation: 1) the sine condition was not rigorously satisfied; 2) the anisotropic optical aberration was not taken into consideration in the lens design.

The one－element bi－aspherical lens [Tatsumi 1988] consisted of two aspherical surfaces, the contours of which was expressed as polynomial function:

$$y(z) = Cz^2\{1+[1-(1+K)C^2z^2]^{\frac{1}{2}}\}^{-1} + A_1z^4 + A_2z^6 + A_3z^8 + A_4z^{10} \qquad (1-1)$$

where C is the paraxial curvature, K the conic coefficient and the A_i coefficients are the ith－order deformation terms. y and z are refered in figure 2－1 in next chapter. The parameters in the formula and some other parameters were taken as in Table 1－1, but the thickness of the lens and the ratio of the index of the lens and the surrounding material were not given. By analogy, the thickness of the lens was found to be 4.5mm and the index ratio to be 1.49. The lens is depicted in figure 1－2(a).

The lens was optimised by raytracing. The calculated spot width as a function of incident angle is shown in figure 1－2(b). The measured half－power width of the focal spot is also shown in the figure. The spot width was within 1.5μm in the incident angle range of $\pm 5^0$, which is actually a very good result. This was reported in a letter but no further detail about the lens analysis and measurement and its application to IOSA was reported.

The lens design was based on isotropic waveguide. When working on an anisotropic waveguide, the spot size will broaden and the background noise rise as will be seen in the next chapter, even though the calculated result (on isotropic waveguide) was in good agreement with the experiment result on an anisotropic x-cut $LiNbO_3$ waveguide, as shown in figure 1-2(b).

The same parameters are used for raytracing and Huygens-Fresnel analysis in the next chapter. The spot width calculated from raytracing and that from Huygens-Fresnel analysis differ substantially. The spot width from raytracing is bigger than that in figure 1-2(b) and changes with off-axis angle dramatically. The spot width from Huygens-Fresnel analysis is only slightly larger than that in figure 1-2(b) but not as uniform as shown here. However, the best focal surface is a curve. On any fixed plane, the spot width changes with off-axis angle. The analysis shows that when the lens is working on an anisotropic waveguide the spot width is even bigger. One may conclude that even with as small relative aperture as 0.25, the one-element lens still has field curvature, although the spot size could be very small, near diffraction limit.

Using a multi-element lens is an effective means of reducing aberration. There have been some contributions in the study of multi-element acircular lenses [Righini 1987, Laybourn 1988]. It was found that the number of refracting boundaries needed to obtain a well-aberration-corrected lens-set has the following empirical formula [Righini 1987, Laybourn 1988],

$$h = \frac{(1 + m_0^2)}{4 m_0 (n - 1) (1 - a \theta) (f_{\#})_{\theta}} \qquad (1\text{-}2)$$

where $m_0 = 5$ and $a = 0.03$ are empirical coefficients, θ is the working semi-field angle range in degrees, $f_{\#} = f/D$, the f/number, D is the aperture of the entrance

pupil diameter, n is the index ratio of lens and surrounding material, h is the minimum number of the refracting boundaries required for the desired performance. The larger the relative aperture and angle range and the lower the ratio of high index of the lens to the low index of the surrounding waveguide, the more the boundaries. For the $LiNbO_3$ waveguide system and glass waveguide system the index ratio available can be up to a little more than 1.055. For the lens with f/number= 3.0 (relative aperture 0.33) and angle range $\pm 8^0$, at least five acircular lenses must be used [Righini 1987], while for the lens with f/number= 3.3 (relative aperture 0.3) and angle range $\pm 6^0$, a four-element acircular lens is feasible [Laybourn 1988]. For the lens with f/number= 4.0 (relative aperture 0.25), angle range $\theta = \pm 5^0$ and n= 1.049, as used in [Tatsumi 1988], 4 lenses (h= 7.8) are needed, and if n= 1.055 3 lenses (h= 6.9) are needed. For a one-element lens with $\theta = \pm 5^0$ and n= 1.055, the relative aperture has to be less than 0.14 (f/number> 7.1), otherwise the wide beam aberrations will distort the lens performance and then there might be some sacrifice, such as field curvature. For small relative aperture, the diffraction spot will be large and the dynamic range of the device will be small. If two lenses are used the relative aperture can be up to 0.22 (f/number> 4.6). On the other hand, if a one-element lens is to be used with f/number= 4 (relative aperture = 0.25), $\theta = \pm 5^0$, the index ratio n must be bigger than 1.1, which is not available for $LiNbO_3$ waveguide technology at present.

A four-element acircular lens design has been reported [Laybourn 1988]. The lens surfaces have the form of (1-1) and the parameters are as in table 1-2. The lens is depicted in the next chapter. In the next chapter, it will be shown that this four-element lens has an excellent optical performance even on anisotropic waveguide.

The fabrication of multi-element thin-film lenses has not been reported so far. It is apparent that the more the boundaries, the more difficult the fabrication because of the multi-fold coupling losses on the boundaries, which is an intrinsic problem in

integrated optics. The possibility of fabrication of multi-element lenses is the main concern in this work.

x-cut and y-cut $LiNbO_3$ are the most important substrate materials for acousto-optic application. But waveguides on these materials are optically anisotropic. The refractive index varies with the direction of the light beam and so the light is traveling in a different way from that in the normal isotropic optical material. The study of the anisotropic optical performance of the lens is of great important to achieve good lens performance and this is another main object of this work.

I.3. Structure of the Thesis

Chapter Two addresses performance analysis of waveguide lens. At the beginning, it talks about the differences between normal bulk lens and waveguide lens. Then it considers how to assess waveguide lens performance. Anisotropic optical analysis will be the main issue in this chapter. Raytracing and Huygens-Fresnel analysis are used, considering anisotropic behaviour of the light beam. Optical performance of the four-element lens and the one-element bi-aspherical lens, which are optimally designed on isotropic waveguide, are analysed on anisotropic waveguide. The waveguide lens can be designed on anisotropic waveguide, and there will be an example of one-element lens design at the end of the chapter.

Chapter Three presents theoretical modeling of the overlap integral of electromagnetic field, for both TE and TM modes, on the boundary of two waveguides with several index profiles. The waveguide structures for optimum overlap integral are predicted. Optical field profiles were measured experimentally and overlap integrals were calculated for $LiNbO_3$ waveguide and glass waveguide and compared with the theory. Coupling efficiency was mearsured as light intensity distribution in m-line, which

gives the actual optical energy transmission over the lens boundary.

In Chapter Four, $LiNbO_3$ waveguide technologies of TI, PE, DPE and TIPE are described and Li_2O outdiffusion is addressed because it is still a controversial problem. In addition to the main object of producing waveguide lenses, some work on other integrated optical devices was undertaken. Buried TI waveguide and a buried waveguide polariser were developed. A new method of Er:Ti co-doping for a waveguide laser was explored.

In Chapter Five, the process of lens fabrication is discussed where mask layer for blocking PE is addressed. Some fabricated waveguide optical components are shown and the fabrication tolerances on the waveguide lens performances are discussed.

Finally, there is a review of the work and suggestion for future work in Chapter Six.

Table 1-1 Parameters for the single-element bi-aspherical lens [Tatsumi 1988]. D=3mm. f=12mm. D/f=0.25

Parameter	Entrance boundary	Exit boundary
C	8.3265×10^{-1}	-1.0352
K	-5.6803×10^{-1}	-1.0079
A_1	-2.7461×10^{-2}	3.0770×10^{-2}
A_2	-8.4077×10^{-3}	-1.7806×10^{-3}
A_3	1.6716×10^{-3}	-3.2019×10^{-3}
A_4	-1.2687×10^{-3}	7.4345×10^{-4}

Table 1-2. Geometrical and optical characteristics of the four-element acircular homogenous refracting lens [Laybourn 1988]. Dimensions are given in mm. Space is the axial distance to the next surface. Effective focal length f=19.7999, back focal length = 14.8711, system thickness = 9.2585, linear aperture = 6mm, f/number = 3.3 and semi-field angle = $\pm 6^0$.

Boundary	C	K	A_1
1	0.19495521	-1.578775	-1.26524×10^{-4}
2	0.02709186	1.651044	3.08406×10^{-4}
3	0.20621041	-0.048186	-7.98695×10^{-5}
4	-0.12694014	-1.909431	1.47574×10^{-4}
5	0.08921851	-1.750264	-2.74141×10^{-4}
6	-0.18819859	-0.947816	1.28491×10^{-4}
7	0.00755857	142.455762	-3.94214×10^{-4}
8	-0.23764258	-0.888112	6.52229×10^{-4}

	A_2	A_3	A_4	Space
1	-6.11484×10^{-5}	-3.06717×10^{-6}	3.54368×10^{-9}	1.0988
2	-1.10415×10^{-5}	-1.07605×10^{-6}	-3.59955×10^{-9}	0.1140
3	1.23801×10^{-5}	7.76387×10^{-7}	-9.87955×10^{-8}	2.2975
4	-4.77245×10^{-6}	-2.17914×10^{-6}	5.45042×10^{-8}	0.6401
5	1.99732×10^{-5}	5.48246×10^{-7}	-3.79726×10^{-8}	2.6516
6	-1.97849×10^{-5}	-1.06986×10^{-7}	-1.50240×10^{-7}	0.4196
7	-1.28449×10^{-5}	-6.25077×10^{-7}	-1.66811×10^{-7}	2.0369
8	2.63365×10^{-5}	1.49900×10^{-6}	-9.40160×10^{-9}	—

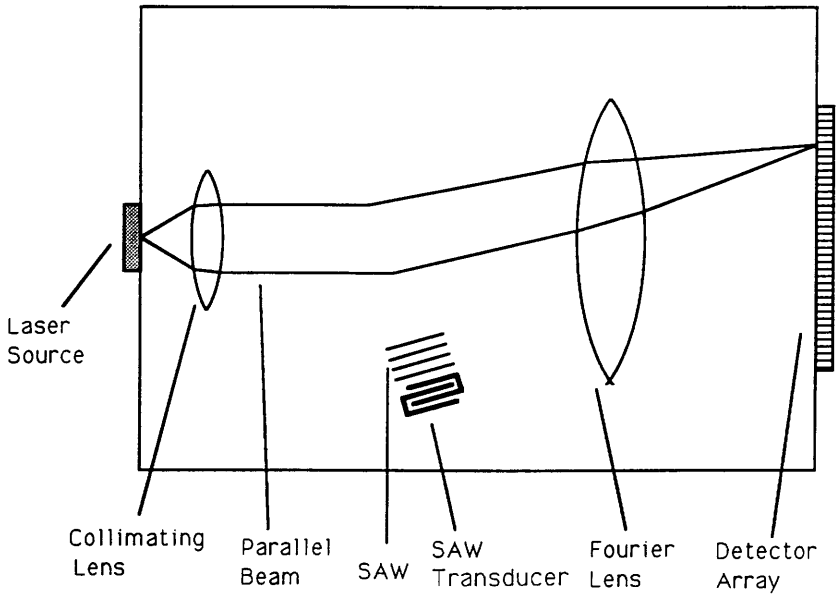

Figure 1－1 The integrated optical spectrum analyser (IOSA)

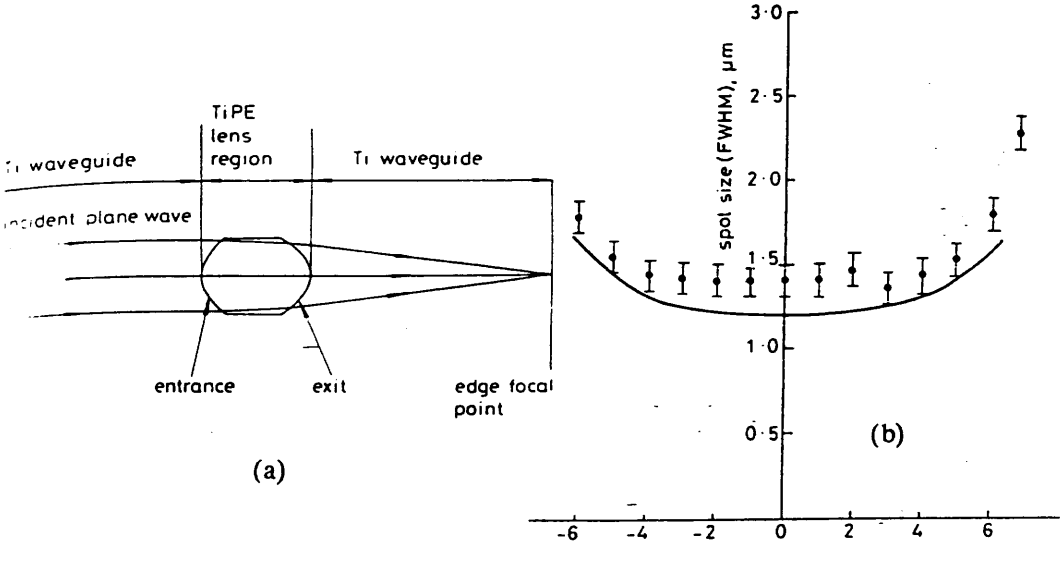

Figure 1－2 (a) the one－element bi－aspherical lens; (b) the dependence of spot width on incident beam angle, —— calculated, · · · · experimental [Tatsumi 1988].

CHAPTER TWO: HOMOGENOUS LENS PERFORMANCE

II.1. Introduction

This chapter deals with some considerations in waveguide lens design. Optical lens design has a long history and there have been abundant papers, books and commercial lens design software. But waveguide lenses have some different characteristics from normal conventional bulk optical lenses. In the second section, there will be some explanation of the differences. In the third section, there will be discussion about how to assess the performance of waveguide lens, where there are again some differences from bulk lens assessment.

Even though anisotropic optical propagation has been well understood in bulk materials and some anisotropic optical components have been developed, it seems that no body would dare to use anisotropic optical lenses because of the tricky behaviour of the light beam. But we may have to wake up the sleeping dog because of the strong interest in $LiNbO_3$ devices which is unfortunately optically anisotropic. In the fourth section, there will be discussion about anisotropic optical analysis in integrated optical devices, which is more complicated than the bulk optical case, and in the fifth and sixth sections there are theoretical results of anisotropic performance of four-element and one-element homogenous lenses. As will be seen in the next chapter, the coupling efficiency on the boundary of the lenses limits the overall power transmission; multi-element lenses have poor overall power transmission efficiency. So, in section seven a new design of single-element lens is provided, considering anisotropic aberration, making some compromises with the optical performances.

II.2. Differences between Waveguide Lens and Bulk Lens

II.2.1. Material Refractive Index and Effective Refractive Index

The basic physical difference between the conventional bulk optical lens and the waveguide lens is in the form of the propagation of an electromagnetic wave. In the bulk lens, the electromagnetic wave is travelling in a 3– dimensional region, uniform in refractive index or with just slow variation, except on the interface of two different media. The propagation of the wave is characterised by its speed $v = c/n$ where c is the speed of electromagnetic wave in vacuum and n is the refractive index of the medium where the light is propagating. Refraction on the interface obeys Snell's law using refractive indices of the two media. In the waveguide lens, the electromagnetic wave is confined in a guiding layer of high refractive index in 2– dimensions, a so– called guided wave. The propagating speed of the guided wave is now characterised by its propagation constant $\beta = kn_e = kc/v_e$, where $k = 2\pi/\lambda$ is the wave vector, n_e is the effective refractive index and $v_e = c/n_e$ could be called the effective propagating speed. β equals the phase change in a unit length and the speed $v_e = c/n_e = kc/\beta$. When the guided wave crosses the boundary of two disparate waveguides, refraction takes place because the guided wave has different propagating speed, and hence effective refractive indices, in the two waveguides and the guided wave must change its direction to preserve the wavefronts on the boundary. Considering that it is the effective index n_e rather than the material refractive index n that decides the wave propagating speed, Snell's law still holds good provided n_e is used instead of n. For any given waveguide structure, the effective refractive index can be calculated by solving wave equation as done in the next chapter, and then it can be used in optical design. Once the effective refractive indices all over the propagating area are known, the optical design can be carried out using the normal procedure.

II.2.2. Ratio of the Indices of the Lens and that of Surrounding Material

In the normal bulk glass optical lenses, the index of the lens material is about $n_h = 1.5$ and that of surrounding material is $n_l = 1.0$. The difference of the indices $\triangle n = 0.5$ and the ratio of them $n_h/n_l = 1.5$. The difference between the refractive indices (and the effective refractive indices) of the lens the surrounding material is very small. For $LiNbO_3$, the effective refractive index of low index waveguide, as surrounding material, is about $n_{eff.l} = 2.208$ and that of high index waveguide, as lens, is about $n_{eff.h} = 2.330$. $\triangle n = 0.122$ and $n_{eff.h}/n_{eff.l} = 1.0553$. For glass waveguide, the effective refractive index of the low index waveguide is about $n_{eff.l} = 1.516$ and that of the high index waveguide is about $n_{eff.h} = 1.600$. $\triangle n = 0.08$ and $n_{eff.h}/n_{eff.l} = 1.0554$. The low ratio of the high index to low index results in poor refraction power at the boundary and one can see that the focusing point would be far away from the lens, which means a small relative aperture. To strengthen the refraction power, the curvature of the lens must be bigger or more lens elements must be used.

II.2.3. Aberrations

In normal bulk optical lens, there are seven defined aberrations: Chromatic Aberration, Spherical Aberration, Coma, Astigmatism, Curvature of Field, Distortion and Lateral Chromatic Aberration. The situation is quite different in the case of the waveguide lens. In integrated optical devices, the light source is laser which is monochromatic. So the Chromatic Aberration and Lateral Chromatic Aberration, which occur only when the light has mixed wavelengths, can be ignored. Astigmatism results from a spatial (out of the optical plane) light beam. Because the waveguide lens lies in a 2-dimensional plane, there is no skew ray into or out of the waveguide plane. Therefore, there is no Astigmatism Aberration. Other aberrations still exist. Distortion is the departure of the actual position of focal spot from the ideal position. It will be no bother, because from the practical point of

view the exact relationship between the angle of the incident beam and the position of the focal spot will be calibrated. If the rays at different positions in the aperture have different optical paths they will not all intersect at a common focus. When the incident beam is along the lens axis the distortion is called Spherical Aberration, and when the beam is at off-axis angle it is called Coma which is also caused by the lack of symmetry and is one of the most objectionable aberrations. In a bulk optical lens Coma appears as a 2-dimensional comet shape on the focal plane, but in a waveguide lens it is turned into a line with varying intensity. The Curvature of Field is the failure of the lens to transform a plane object into a plane image. Among those aberrations, Spherical Aberration, Coma and Curvature of Field are the major factors affecting the lens performance and will be of main concern to the homogenous lens designer.

In an anisotropic material, the light beam has varying refractive index related to the direction, which will obviously change the focusing behaviour and introduce Anisotropic Aberration. Because the most interesting materials for integrated optics acousto-optics applications are x-cut and y-cut $LiNbO_3$ on which the waveguides are anisotropic, Anisotropic Aberration must be taken into consideration.

II.2.4. Flexibility of Design

The surface of normal bulk optical lens is spherical, because of the easy manufacture. Aspherical surfaces can made by computer controlled polishing machine, but are costly. The waveguide lens is actually a 2-dimension shape, and its contour is just a line. Using planar techniques, any shape of contour can be made. So, the equivalent of aspherical surfaces can be used in waveguide lenses, giving great flexibility to the lens design, reducing aberration and the number of lenses.

II.3. Assessment of Lens Performance

With commercial lens design software, the aberrations can be automatically corrected and the lens optimized for the parameters required. The only thing needed to be aware is what parameters are wanted for the lens. The detailed procedure of lens design using commercial software is not part of this project and will not be discussed here. Some excellent designs have been made and have been used in this project. In section seven a single–element lens design is described but it has not been produced by the standard software. Here it is shown how to assess lens performance.

The major parameters of the performance of homogenous lens are as follows:

1. Relative Aperture D/f: where D is the aperture of the entrance pupil diameter. For a fixed focal length, the bigger the D/f is, the more light the lens can collect, and the larger the dynamic range of the device. Correction of aberrations is difficult for large relative aperture. The focal spot size will be limited by diffraction. This diffraction limitation is approximately expressed as $\lambda_0 f/n_e D$, where λ_0 is the wavelength in vacuum, n_e is the refractive index (effective refractive index in the case of a guided wave) in the surrounding area. The larger the D/f, the smaller the diffraction limited spot size. The 4–element lens design [Laybourn 1988] has relative aperture of 0.3 but the lens with relative aperture 0.33 must have 5 elements [Righini 1987];

2. Resolution N: It is the capacity of the lens to discriminate between two closely focused spots. For the Fourier transform lens, high resolution in the focal plane means high resolution of incident beam angle and hence high resolution of the measured parameter, i.e. the frequency in the case of an IOSA. There are two factors affecting the resolution: aberration and diffraction. Aberration increases the spot size and diffraction prevents the focussed spot from further decreasing. Ideally, the aperture of the lens should be as big as possible so that the diffraction limited

spot size is the minimum, and the aberration is reduced to the extent that the spot size is no longer bigger than the diffraction limited spot size, then it is thought aberration free. But increasing the aperture of the lens will increase the difficulty of aberration correction. The 4— element lens has a theoretical resolvable spot size of 2μm and can resolve 2800 spots in the incident angle range of $\pm 8^0$ on isotropic material, as will be shown in the next chapter;

3. Focal length f: It determines the device size, so f should be limited, otherwise the device will be too large and attenuation of the guided wave will increase. In a Fourier lens, the angle resolution $\triangle\alpha$ could be expressed as $\triangle\alpha = \triangle\sigma/f$, where $\triangle\sigma$ is the resolvable spot size on the detection plane. Increasing f could increase anglular resolution. For a bigger lens with the same relative aperture D/f, the diffraction limitation does not increase but the angle resolution increases because of larger f, provided that the spot size is still near diffraction limitation;

4. Field of View 2α: Over the entire field of view, the lens should focus to below the required resolvable spot size. This decides the measurement range. The 4— element lens has field of view of $\pm 8^0$;

5. Curvature of Field: It is where the optimal focused spots with different incident angles are located. Normally, it should be a plane or straight line in the 2— dimensional case so that all these focused spots can be detected by the steady optoelectronic detector. Nevertheless, with the development of hybrid thin film detector on glass or $LiNbO_3$ [Yi— Yan 1989], an optoelectronic detector array with any shape of detection surface maybe possible in the near future. In that case, the curvature of field will not be a trouble and then it is not necessary to restrict the focus to a plane or straight line.

6. Signal Noise Ratio (SNR) by Huygens— Fresnel Analysis: SNR is defined as the ratio of the intensity of the signal to that of the background noise. Obviously a

signal level smaller than the noise level will unlikely to be detectable. The background noise level decides the ability of the component or the system to detect the small signal level. The smaller the background noise level, the larger the range (so called dynamic range) of the detectable signal. There are many sources of noise, but the lens itself introduces noise and this is a concern in the lens design and analysis. All parameters mentioned previously are calculated by geometrical optics analysis. In geometrical analysis, all light rays are thought to be independent. But from the point of view of physical optics they will interfere with each other, when diffraction will happen in the pupil. Taking diffraction into consideration, the physical optics method of Huygens– Fresnel analysis can give optical intensity distribution on the focal plane, and then allow the analysis of the SNR.

II.4. Anisotropic Optical Analysis for Integrated Optics Planar Lenses

All the lens designs mentioned previously were based on isotropic material, i.e. glass, GaAs or z– cut $LiNbO_3$ waveguide on which the propagation is isotropic. However the most interesting materials for acousto– optical applications are planar waveguides grown on y– cut or x– cut $LiNbO_3$, which are anisotropic. Those lenses must have modified parameters when used on anisotropic waveguide. Zhou and Ristic have contributed to the study of anisotropic aberration of a single element homogenous lens using geometrical optical analysis [Zhou 1989]. Such analysis is necessary for lens design, but more comprehensive understanding of the lens behaviour is needed in practice. This section will analyse the anisotropic performances of waveguide lens using ray tracing and Huygens– Fresnel analysis.

The 4– element homogenous planar lens is depicted in figure 2– 1 to help to understand the anisotropic structure of the materials. The substrate material is x– cut $LiNbO_3$, while the analysis is identical for y– cut $LiNbO_3$ because the two are optically similar. The optical axis of $LiNbO_3$ is along the Z direction, so the TE

mode will see the extraordinary refractive index when propagating along the Y direction and see the ordinary refractive index when propagating along the Z direction, while the TM mode has polarisation direction perpendicular to optic axis and sees a constant ordinary refractive index. Because proton exchange (PE) produces an increased extraordinary refractive index and a decreased ordinary index, only the TE mode is guided. In IV.4. it will be seen that TM mode propagation is also possible for the TIPE system.

For refraction to take place, the lens region should be a high refractive index waveguide with effective refractive index $n_{h.eff}(\beta)$ and the surrounding guide region a low refractive index waveguide with effective refractive index $n_{l.eff}(\beta)$. These effective refractive indices vary with the angle β of the ray with respect to the Z axis in the Y− Z plane because the refractive indices of the waveguide material, i.e. $n_s(\beta)$ for the substrate, $n_h(\beta)$ for the high index waveguide and $n_l(\beta)$ for the low index waveguide, vary with β.

Because of the anisotropic performance of x− cut and y− cut $LiNbO_3$, raytracing in the planar waveguide is not straightforward. The light ray E (direction of propagation, see figure 2− 2) and the wave normal K are not in the same direction, and on the boundary of two different waveguides the refraction of the wave normal K, not the ray E, obeys Snell's law, using effective index instead of material index. Ray E is the direction of energy flow and is to be used for raytracing. So it must be kept in mind that the direction and effective index of the ray E are used for raytracing and calculating the optical path, while the direction and effective index of the wave normal K are used for calculating angles of refraction.

II.4.1. Material Refractive Indices

A point light source polarised as a TE wave spreads out in the Y− Z plane with a elliptical energy velocity profile as shown in figure 2− 2(b). The velocity of ray E in

the direction β is expressed as

$$v_E(\beta) = \frac{v_o v_e}{\sqrt{(v_o^2 \sin^2(\beta) + v_e^2 \cos^2(\beta))}} \qquad (2\text{-}1)$$

where v_o and v_e are velocities of ray E along the Z and Y directions respectively.

The wave normal K is in the direction θ. The velocity of K can be obtained as v_K in the figure, the cross point of the tangent through v_E and the wave normal K which is perpendicular to the tangent. The angles θ and β are related by

$$\tan(\beta) = \frac{v_e^2}{v_o^2} \times \tan(\theta) = \frac{n_o^2}{n_e^2} \times \tan(\theta) \qquad (2\text{-}2)$$

where n_o is the ordinary refractive index and n_e is the extraordinary refractive index of the wave normal K. v_K can be obtained from v_E:

$$v_K(\theta) = v_E(\beta) \times \cos(\beta) \times \frac{1 + \tan^2(\beta) \times n_e^2 / n_o^2}{\sqrt{(1 + \tan^2(\beta) \times n_e^4 / n_o^4)}}$$

$$= v_E(\beta) \times \cos(\theta) \times \frac{1 + \tan^2(\theta) \times n_o^2 / n_e^2}{\sqrt{(1 + \tan^2(\theta) \times n_o^4 / n_e^4)}} \qquad (2\text{-}3)$$

The index of the wave normal forms another elliptic section as shown in Fig.2−2(a) and is expressed as

$$n_K(\theta) = \frac{n_o n_e}{\sqrt{(n_o^2 \sin^2(\theta) + n_e^2 \cos^2(\theta))}} \qquad (2\text{-}4)$$

When n_o and n_e take the values in Table 2−1, which are quoted as the parameters of Ti indiffused (TI) waveguide and TI plus proton exchange (TIPE) waveguide, $n_K(\theta)$, expressed in (2−4), becomes the corresponding material indices of the substrate ($n_{Ks}(\theta)$), low index waveguide ($n_{Kl}(\theta)$), and high index waveguide ($n_{Kh}(\theta)$) for the wave normal K, which are plotted as function of θ in figure 2−3.

n_E, the index of the ray E is at the cross point of the tangent at n_K and the ray E which is perpendicular to the tangent. n_E is related to n_K as

$$n_E(\beta) = n_K(\theta) \times \cos(\beta) \times \frac{1 + \tan^2(\beta) \times n_e^2 / n_o^2}{\sqrt{(1 + \tan^2(\beta) \times n_e^4 / n_o^4)}}$$

$$= n_K(\theta) \times \cos(\theta) \times \frac{1 + \tan^2(\theta) \times n_o^2 / n_e^2}{\sqrt{(1 + \tan^2(\theta) \times n_o^4 / n_e^4)}} \qquad (2\text{-}5)$$

Substitute (2−2) and (2−4) into (2−5), giving

$$n_E(\beta) = \sqrt{(n_o^2 \times \cos^2(\beta) + n_e^2 \times \sin^2(\beta))} \qquad (2\text{-}6)$$

The following relationship always holds

$$v_o \times n_o = v_e \times n_e = v_K(\theta) \times n_K(\theta) = v_E(\beta) \times n_E(\beta) = c \qquad (2\text{-}7)$$

where c is the speed of light in vacuum.

II.4.2. Waveguide Effective Index Calculation

The guided wave will see the effective refractive index of the waveguide. As with the material refractive index, an effective refractive index profile can be found for

the wave normal K as a function of θ, $n_{K.eff}(\theta)$, and for the ray E as a function of β, $n_{E.eff}(\beta)$, and then the relationship between $n_{K.eff}(\theta)$ and $n_{E.eff}(\beta)$ may be obtained. Firstly we define the waveguide structure. Perpendicular to the plane Y−Z of propagation, in the X direction, the variation of material refractive index is steplike:

$$n(x,\theta) = \begin{cases} 1 & x > 0 & \text{air} \\ n_w(\theta) & 0 \geqslant x > -d & \text{waveguide} \\ n_s(\theta) & -d \geqslant x & \text{substrate} \end{cases} \qquad (2\text{-}8)$$

The waveguide depth is d, and the values calculated for maximum coupling efficiency on isotropic z−cut $LiNbO_3$ waveguide (see Chapter III) have been used: d is 2.20μm and 2.66μm in the low index and high index guide sections, respectively. $n_s(\theta)$ and $n_w(\theta)$ are calculated from (2−4), using the values of ordinary and extraordinary index in each material layer given in Table 2−1.

The effective refractive indices, $n_{Kl.eff}(\theta)$ and $n_{Kh.eff}(\theta)$ for the wave normal K and $n_{El.eff}(\beta)$ and $n_{Eh.eff}(\beta)$ for the ray E in low and high index waveguide may be obtained by solving the wave equation [Yariv 1973] at any given angle. However, an analytical solution is required in order to establish a relation between θ and β, and an approximation by analogy with the bulk material refractive indices is required. The equations (2−4), (2−6) and (2−2), used to determine $n_K(\theta)$, $n_E(\beta)$ and the relation between θ and β in anisotropic bulk medium, have been applied to the anisotropic waveguides to determine the equivalent effective indices and angles. In order to apply these equations we need the effective indices $n_{o.eff}$ and $n_{e.eff}$, which are the effective refractive indices of the TE mode along the Z and Y directions respectively, in each waveguide. For the low index waveguide they may be calculated, and applied to equations (2−4) and (2−6) to give $n_{Kl.eff}(\theta)$ and $n_{El.eff}(\beta)$. The values of $n_{Kl.eff}(\theta)$ and $n_{El.eff}(\beta)$ calculated from (2−4) and (2−6), using $n_{ol.eff}$ and $n_{el.eff}$ in Table 2−1, agree with values calculated from the

wave equation to $\triangle n_{Kl.eff}(\theta)$ and $\triangle n_{El.eff}(\beta) < 3 \times 10^{-5}$, justifying the extension of the bulk index equation to the waveguide case. The function of $n_{Kl.eff}(\theta)$ is shown in figure 2−3. In the high index waveguide case, because of the anomalous variation of the bulk $n_K(\theta)$ and $n_E(\beta)$ in TIPE waveguide (after proton exchange, the n_o decreases rather than increases), the guide is cut off for $\theta < 31^0$, and there is no physical meaning for $n_{Kh.eff}(0)$ or $n_{Eh.eff}(0) = n_{oh.eff}$. However, a value for $n_{oh.eff}$ can be obtained by calculating $n_{Kh.eff}(\theta)$ from the wave equation at an arbitrary value of θ, near to cut off, and substituting into equation (2−4). The approximated $n_{Kh.eff}(\theta)$ is shown in figure 2−3 and is found to be good for θ large, well away from waveguide cut−off. The values of $n_{Kh.eff}(\theta)$ and $n_{Eh.eff}(\beta)$ calculated from (2−4) and (2−6), using $n_{oh.eff}$ and $n_{eh.eff}$ in Table 2−1, agree with the values calculated from the wave equation to an accuracy of better than 3×10^{-5} in the angle range of $\theta > 75^0$, where in our calculation the light ray lies.

Because the effective refractive index profiles of the wave normal K and the ray E have identical form as material index profiles, the relation between their direction θ and β must be the same as in bulk material, expressed in (2−2). With any direction of ray E or wave normal K, the effective index can be obtained from (2−4) or (2−6), and the direction of the corresponding E or K calculated from (2−2). In the calculations that were made, the ratio of effective extraordinary indices of high and low index waveguide sections, shown in Table 2−1, was 2.3293/2.2080= 1.0549365≅1.055. The ratio 1.0550 was used in optimising the performance of the 4−element lens design on isotropic z−cut $LiNbO_3$ waveguide [Laybourn 1988].

II.4.3. Ray Tracing Procedures

The raytracing is carried out as follows, and illustrated in figure 2−4 where WG1 and WG2 represent two different waveguide divided by refractive planes. A known incident ray $E_1(\beta_1)$ in WG1 is considered, propagating in direction β_1, with respect

to the Z axis. The direction θ_1 of the corresponding wave normal $K_1(\theta_1)$ is obtained through (2−2) with n_o and n_e taking effective values of the related waveguide in Table 2−1. The effective indices $n_{K1.eff}(\theta_1)$ and $n_{E1.eff}(\beta_1)$ are worked out from (2−4) and (2−6). Then the ray $E_1(\beta_1)$ is traced to the first boundary and the optical path calculated. At the boundary the refraction of the wave normal is calculated by a successive approximation routine, necessary since the effective refractive index, $n_{K2.eff}(\theta_2)$ to be used in Snell's law is itself dependent on θ_2, the direction of the wave normal $K_2(\theta_2)$ in the next waveguide section. β_2 is then calculated from θ_2 using equation (2−2) and $E_2(\beta_2)$ is traced to the next boundary. The process is repeated for each ray at every boundary, giving the position, direction and relative phase of each ray at any surface (including the focal plane).

II.5. Anisotropic Performance of Four−Element Waveguide Lens

II.5.1. Raytracing

A program was written for light beam raytracing on anisotropic waveguides. Repeating the computation for 101 rays, forming a parallel incident beam, on all boundaries, the beam waist size can be obtained by ray analysis at the detection plane.

Figure 2−5 shows the performance of the four−element lens on anisotropic material, the parameters of the lens is given in the Chapter One. The waist varies with off−axis angle with back focal length as a parameter. The incident beam is 2mm wide. The back focal length is taken as the distance from the back surface of the lens to the detection plane. As a comparison, the dashed lines in the figure show the waist size of the lens on isotropic material.

Ray analysis breaks down if the focused spot size is within or near to the diffraction limit. The Huygens– Fresnel method allows the calculation of the amplitude and phase of the wave in the focal plane. The data on the positions and phases of all 101 rays on the last surface of the lens, as the result of raytracing, were then fed into another program. Each position was considered as a new wavelet source with a calculated initial phase. All 101 wavelets interfere and, by summing in phase and out of phase components of all wavelets on the detection plane, the optical intensity profile can be obtained. The electric field amplitude from each wavelet is

$$E(r)= \frac{1}{r^{1/2}} \exp(-ik(rn_e(\beta)+\varphi)) \cos(\gamma) \qquad (2\text{-}9)$$

where $k=2\pi/\lambda_0$, r is the distance from the wavelet to detection point, φ is the initial phase at the lens surface, $n_e(\beta)$ is the effective refractive index of the ray E, γ is the angle between the ray and the normal of the lens surface. Note that the energy from the point source is spreading out in an elliptic wavefront with an approximate perimeter of $2\pi r$, but in the normal bulk lenses, the wavefront is spherical with area of $4\pi r^2$. So the intensity on the wavefront is proportional to $1/r$ instead of $1/r^2$, and the amplitude E(r) is proportional to $1/r^{1/2}$ instead of $1/r$. $\cos(\gamma)$ is the declination factor showing the reduction of intensity because of the non– normal radiation from the surface. The back focal length is large compared with lens aperture, so, as confirmed by calculation, $\cos(\gamma)/r^{1/2}$ contributes no significant difference and can be ignored.

An incident Gaussian beam can be constructured by giving an initial amplitude distribution to the incident beam. Figure 2– 6 shows optical intensity profiles on a focal plane for a Gaussian intensity profile incident beam with Gaussian width

A= 6mm, beam width D= 6mm and wavelength $\lambda = 0.633\mu m$ at the incident angle of 0^0, 2^0, 5^0 and 8^0. The spot size σ is listed in table 2−2. From the figures and the table it can be seen that at the focal plane 15.91mm away from the last lens surface the focal spot size can be held to $2.8\mu m$ at −8.1dB of peak intensity in the incident angle range of $\pm 8^0$. The optimum focal surface is still considered to be a plane, or straight line in this 2−D planar lens case. The number of resolvable spots N then is estimated as in table 2−2, assuming an average diffraction spot size of $\sigma = 2.8\mu m$ in the range of Yc on the focal plane, while Yc is the distance between the spot and lens axis in the focal plane (shown in figure 2−1), and $N = 2 \times Yc / \sigma$.

Using a 2mm wide incident beam the focused spot widened, because of stronger diffraction, and the sidelobes were reduced somewhat. Vice versa, with a wider beam, the spot size decreases, but at the same time the background noise increases, as the sidelobes rise up. This fact means that, here, diffraction is limiting the spot size. Reducing the light beam aperture only reduces background noise but not spot size, even though aberration may be reduced somewhat.

As a comparison with the isotropic case (z−cut $LiNbO_3$ waveguide), figure 2−7 shows optical intensity profiles for an incident beam of D= A= 6mm wide and $\lambda = 0.633\mu m$ at the incident angles of 5^0 and 8^0. At the focal plane 14.87mm away from the last lens surface the focal spot size can be maintained at about $2\mu m$ at −17dB in the incident angle range of $\pm 8^0$. The spot sizes and estimated resolvable spot numbers are listed in Table 2−3.

II.6. Performances of One−Element Lens

The same analysis procedures as in the last section for the four−element lens are used for one−element lens analysis. Figure 2−8 shows intensity profiles for an

Elliptical– Hyperbolic lens [Laybourn 1988] used on anisotropic material. The on– axis performance is acceptable but the off– axis performance is greatly degraded.

Raytracing calculations for the one– element bi– aspherical lens [Tatsumi 1988] show that the spot width is bigger than reported (shown in figure 1– 2(b), Chapter One) and it increases dramatically with off– axis angle on isotropic waveguide. The detail calculation was not given in the Letter so there is no way to compare the calculations. The parameters used include some deduced ones which did not appear in the letter, as mentioned in section I.2. The situation on anisotropic waveguide is even worse. Tables 2– 4 and 2– 5 show the spot sizes, back focal lengths and the estimated resolvable number of spots from Huygens– Fresnel analysis. Even though there are enough resolvable spots, the optimum focuses are on the different focal planes. There is field curvature. In addition, as compared with the four– element lens, the background noise is much higher.

II.7. One– Element Lens on Anisotropic Waveguide, a New Design

It seems that some kind of compromise must be made. To get high overall power transmission, the number of lens elements must be reduced to the minimum, and a single– element lens is the ultimate configuration. The index ratio must be no bigger than 1.055, the largest value obtainable from the present $LiNbO_3$ and glass waveguide technologies. The number of resolvable spots should be more than 1000 in the field of view of a few degrees, here $\pm 5^0$ was used. Anisotropic aberration must be taken into consideration. There should be no field curvature. The background noise should be as low as possible. In this section, a new design is provided, of one– element lens on anisotropic waveguide.

There was no lens design software available (specially for anisotropic lenses), so the aberration optimisation can not be done automatically. Because of the huge

computation work, the high power terms in the polynomial form of the lens contour (1−1) are omitted and the the lens contour is expressed as:

$$z(y) = Cy^2\{1+[1-(1+K)C^2y^2]^{\frac{1}{2}}\}^{-1} \qquad (2-10)$$

1). Raytracing.

Using the same programme as in section II.5.1. for anisotropic analysis, the waist sizes are calculated to find the best C and K so that a compromise performances over the whole range of field was obtained. The best C and K for on−axis and off−axis points are not obtained simultaneously and there are some compromises to be made. Several sets of raytracing results were chosen for the Huygens−Fresnel analysis.

2). Huygens−Fresnel analysis.

The same programme as used in the section II.5.2 was used. The optical intensity profiles were calculated for the selected results from raytracing. Finally, one set of C and K giving the best performance in the incident angle range of $\pm 5^0$ was taken as the optimised design. The analysis showed that if the lens is working at a little lower index ratio the off−axis performance would be improved, while this was found in geometrical optic analysis [Laybourn 1988]. So finally the index ratio of 1.0548 was used, which can be obtained by a high effective index of 2.3290 and a low effective index of 2.2080.

The lens is depicted in the figure 2−9 and the parameters of C and K are given in table 2−6. The intensity profiles for the incident angle of $\alpha = 0^0$, 3^0 and 5^0 are shown in figure 2−10. The spot sizes, back focal lengths and the resolvable spot numbers are given in table 2−7, calculated as in section II.5.2. The back focal lengths are slightly different for different incident angles but on some optmised plane

surface a reasonable focusing spot size can be obtained as shown in table 2—7. Even though there is no field curvature, the background noise is high especially for large off—axis angle. A marked improvement would be possible if more calculation time were spent and the higher polynomial terms were re—introduced.

II.8. Discussion and Summary

From the point view of optics, the major differences between the waveguide lens and the normal bulk optical lens are the small refractive index ratio of the lens and the surrounding material, and the relaxation of aberrations. The small index ratio complicates the lens design even though its 2—dimensional form has eased the fabrication of acircular boundaries and provided more freedom for lens design. The light beam is propagating in a form of guided wave which results in a mode mismatch loss on the boundary as will be discussed in next chapter. This limits the use of multi—element lens which otherwise could be used to tackle the problem of small index difference.

The assessment of the performance of a waveguide lens is concentrated on focal length, relative aperture, resolution, field of view, field curvature and signal—to—noise ratio. The successful lens design depends on the reduction of aberrations. Besides the conventionally defined aberrations, anisotropic aberration is addressed, considering the potential application of the lens on x—cut and y—cut $LiNbO_3$.

The method of lens analysis in anisotropic waveguide is developed and comprehensive understanding of lens behaviour in such waveguide can be obtained.

When the 4—element lens which is optimized on isotropic material is used on anisotropic material, even though the waist size analysis by raytracing (in section II.5.1.) shows sensitivity of waist size and position of focal plane to incident angle,

the Huygens– Fresnel analysis shows that spot size becomes a little wider and the sidelobes rises but the focal surface still keeps plane. The spot size is still acceptable, with the number of resolvable spots estimated to be about 1320 in the incident angle range of $\pm 5^0$, or 1060 in a range of $\pm 4^0$. The major drawback will be the higher background noise which will reduce the main lobe intensity and hence the signal– noise ratio.

The analysis shows that the single– element bi– aspherical lens, which has been reported as having good resolvable spot size [Tatsumi 1988], has a big aberration of field of curvature. The background noise is higher than that of the four– element lens.

A new design of one– element lens is proposed, allowing for anisotropic aberration. There is no aberration of field of curvature. The spot size can be held to 2.7μm over the incident angle range of $\pm 5^0$, equivalent to 1200 resolvable spots. But the background noise level is high. The SNR is just -5.7dB at an incident angle of 5^0. The optical performance is obviously worse than that of the four– element lens, but the single element lens can be readily fabricated to give highly efficient light transmission.

The lens with contour of $z_i(y)$, (i refers to the boundary number) can be magnified or reduced H times with geometrical similarity. The new lens contours are described as

$$z_i'(y') = H\ z_i(y'/H) \qquad (2-11)$$

The spaces between the surfaces should be multiplied by H at the same time. If the incident beam is also accordingly multiplied by H, then the all geometrical optics parameters will be multiplied by H but the relative aperture D/f will remain constant. Even though the geometrically calculated waist size will decrease by H if the lens

size is reduced by H, the reduction of the spot size will be limited by diffraction.

For larger lens with the same relative aperture D/f, the diffraction limitation does not increase but the angle resolution increases because of larger f, unlike the diffraction limitation, provided that the aberration remains small and the spot sizes are still in the range of diffraction limitation.

Table 2-1 Ordinary and extraordinary refractive index for substrate, low index waveguide, high index waveguide and effective ordinary and extraordinary refractive index for low and high index waveguide. λ=0.633μm.

	substrate n_s	low index waveguide n_l	high index waveguide n_h	low index waveguide effective $n_{l.eff}$	high index waveguide effective $n_{h.eff}$
n_o	2.287	2.287+0.008	2.287-0.040	2.2922	2.2451
n_e	2.201	2.201+0.010	2.201+0.131	2.2080	2.3293

Table 2-2 Spot sizes and resolvable spot number for 4-element lens [Laybourn 1988] on anisotropic material. D=A=6mm. Back focal length = 15.91mm.

θ^0	Yc(mm)	σ(μm) at -8.1dB	σ(μm) at -10.0dB	σ(μm) at -10.9dB	N σ=2.8μm	SNR -dB
0		2.8	3.0	3.1		10.9
±2	±0.793	2.8	3.0		566	10.0
±5	±1.847	2.8			1319	8.2
±8	±3.023	2.8			2159	8.1

Table 2-3 Spot sizes and resolvable spot number for 4-element lens [Laybourn 1988] on isotropic material. D=A=6mm. Back focal length = 14.87mm

θ^0	Yc(mm)	$\sigma(\mu m)$ at -10dB	$\sigma(\mu m)$ at -17.4dB	$\sigma(\mu m)$ at -20.3dB	$\sigma(\mu m)$ at -20.6dB	N $\sigma=2\mu m$	SNR -dB
0		1.6	2.0	2.1	2.1		20.6
±2	±0.691	1.6	2.0	2.1	2.1	691	20.6
±5	±1.732	1.7	2.0	2.1		1732	20.3
±8	±2.784	1.7	2.1			2784	17.4

Table 2-4 Spot sizes, back focal length and resolvable spot number for one-element lens [Tatsumi 1988] on isotropic material. D=A=3mm. $n_h/n_l=1.049$ Space between two surfaces: 4.5mm.

θ^0	Yc(mm)	$\sigma(\mu m)$ at -3dB	$\sigma(\mu m)$ at -9.2dB	$\sigma(\mu m)$ at -10.6dB	$\sigma(\mu m)$ at -20.0dB	N $\sigma=2\mu m$	b.f. (mm)	SNR -dB
0		1.2	1.9	2.1	4.0		9.98	20.0
±3	±0.64	1.9	2.9			640	10.10	9.2
±5	±1.09	2.2	3.6	3.8		1090	10.35	10.6
±7	±1.58	2.7	4.3				10.74	9.6

Table 2-5 Spot sizes, back focal length and resolvable spot number for one-element lens [Tatsumi 1988] on anisotropic material. D=A=3mm. n_h/n_l=1.049 Space between two surface: 4.5mm.

θ^0	Yc(mm)	$\sigma(\mu m)$ at -3dB	$\sigma(\mu m)$ at -4.8dB	$\sigma(\mu m)$ at -6.7dB	$\sigma(\mu m)$ at -12.1dB	N σ=2μm	b.f. (mm)	SNR -dB
0		1.8	2.2	2.6	3.2		10.71	12.1
±3	±0.647	2.0	2.8			647	10.89	4.8
±5	±1.115	2.3	2.7	3.1		1115	11.31	6.7

Table 2-6 Parameters for the one-element lens. Dimensions are in mm.

C1=0.500 C2=-0.711 K1=-1.05 K2=-1.18
Space between two surfaces: 10mm. n_h/n_l=1.0548.

Table 2-7 Spot sizes, back focal length and resolvable spot number for 1-element lens on anisotropic material Back focal length=14.041mm. f=18.94mm. D/f=0.317. D=A=6mm. n_h/n_l=1.0548.

θ^0	Yc(mm)	$\sigma(\mu m)$ at -3dB	$\sigma(\mu m)$ at -5.7 dB	$\sigma(\mu m)$ at -5.9dB	$\sigma(\mu m)$ at -10.3dB	N σ=2.7μm	SNR -dB
0		1.9	2.6	2.6	3.3		10.3
±3	±1.047	2.7	3.2	3.3		774	5.9
±5	±1.626	2.5	3.0			1200	5.7

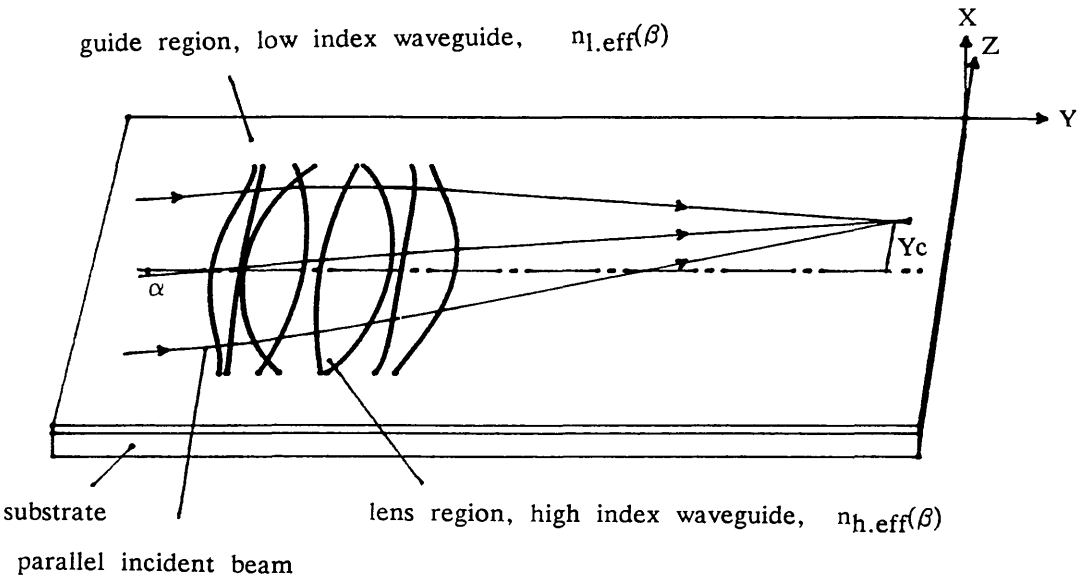

Figure 2−1. 4−element homogenous planar lens on x−cut $LiNbO_3$. The high index waveguide with the lens contour is inserted in a low index waveguide. The guided wave has effective refractive index $n_{l.eff}(\beta)$ and $n_{h.eff}(\beta)$ in guide region and lens region respectively, where β is the ray direction with respect to the Z axis. α is the incident off−axis angle. Yc is the distance between the focal spot and lens axis in the focal plan

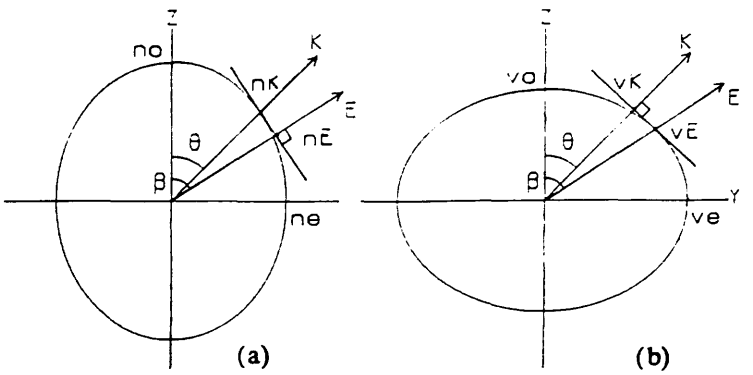

Figure 2—2. Elliptic sections of refractive index of wave normal K (a) and velocity of ray E (b) and relationship between K and E.

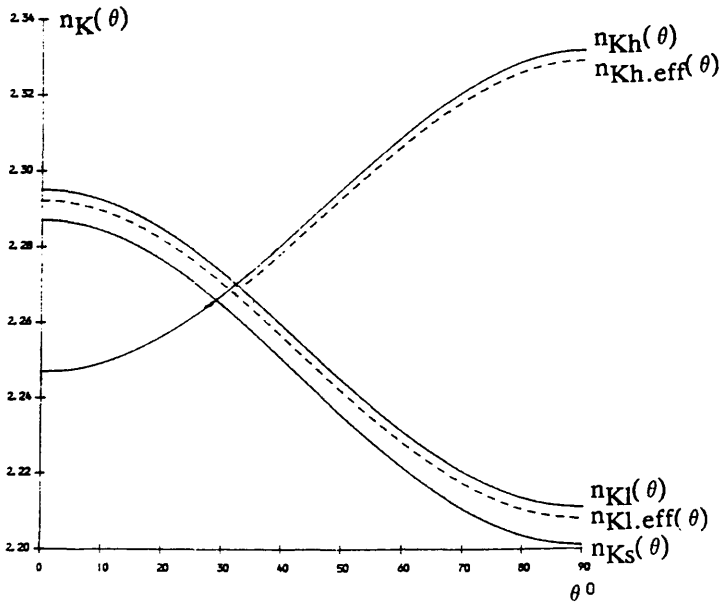

Figure 2—3 Refractive indices of $LiNbO_3$ substrate, TI waveguide and TIPE waveguide and effective refractive indices of low index and high index waveguide on x—cut $LiNbO_3$.

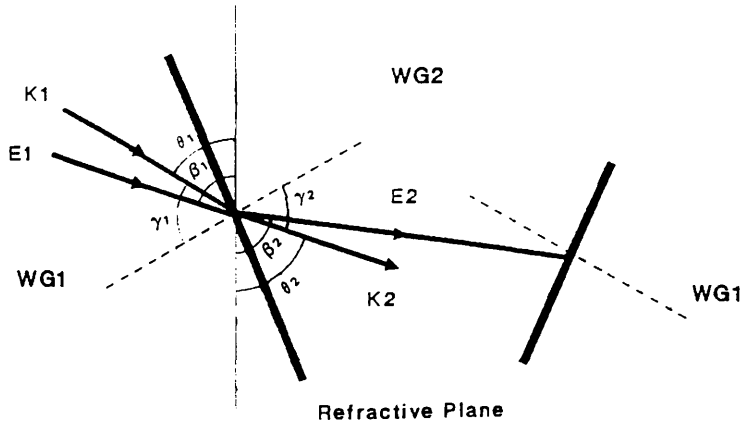

Figure 2— 4 Illustration of raytracing on anisotropic material.

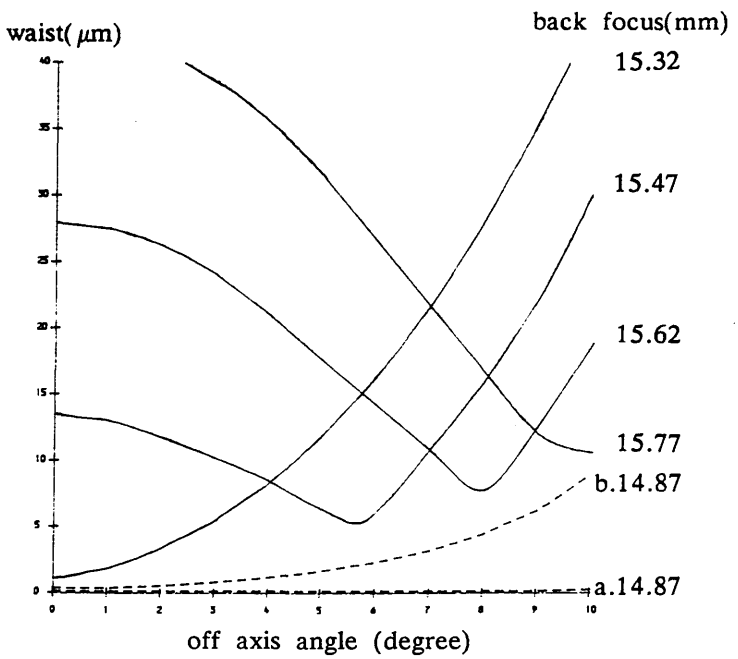

Figure 2— 5 Anisotropic aberration of 4— element lens. Waist size vs incident angle on different positions of focal plane. Beam wide 2mm. Dashed line: aberration on isotropic material for incident beam of 2mm(a) and 6mm(b) wide.

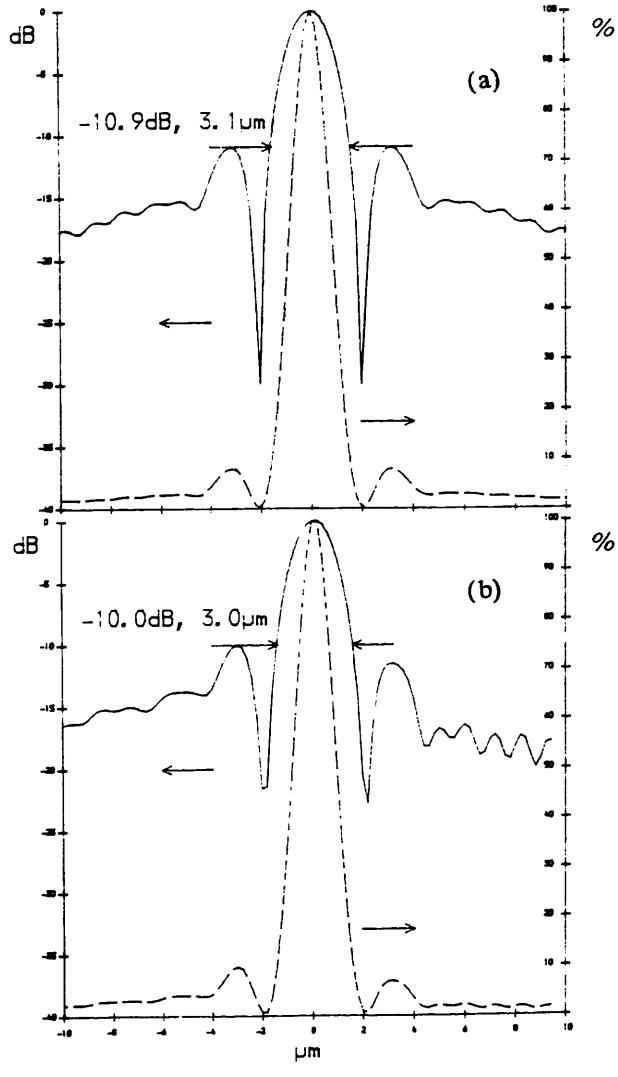

Figure 2−6. Calculated diffraction intensity profile for 4−element lens on anisotropic material. $\lambda = 0.633\,\mu m$. Incident beam D= 6mm wide with Gaussian width A= 6mm. Back focal length f= 15.91mm. Incident angle $\alpha = 0^0$(a), 2^0(b), 5^0(c) and 8^0(d). Dashed line is in percentage and solid line is in dB.

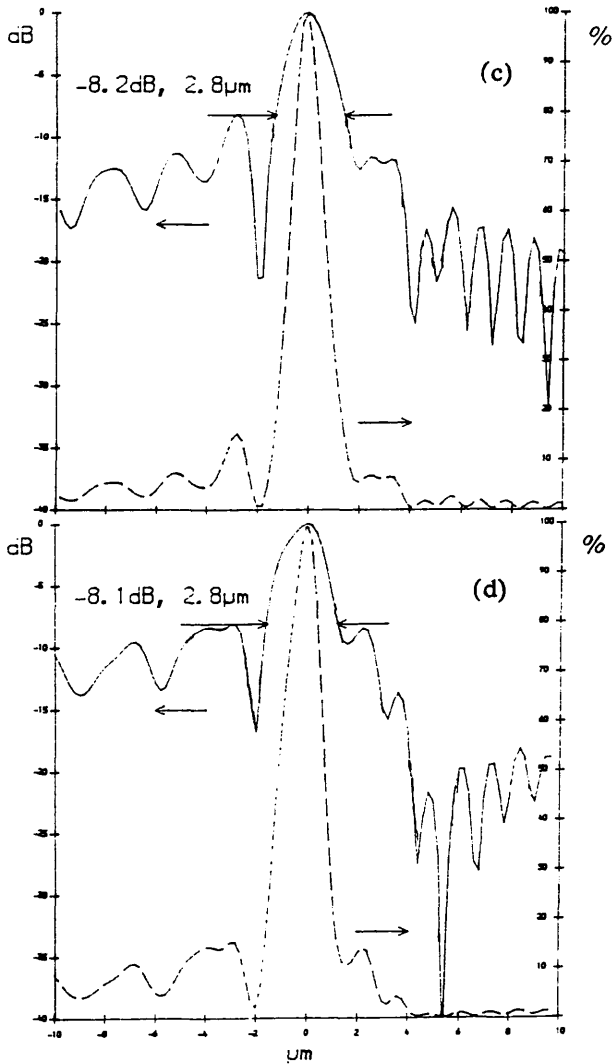

Figure 2−6. Calculated diffraction intensity profile for 4−element lens on anisotropic material. $\lambda = 0.633\,\mu m$. Incident beam D= 6mm wide with Gaussian width A= 6mm. Back focal length f= 15.91mm. Incident angle $\alpha = 0^0$(a), 2^0(b), 5^0(c) and 8^0(d). Dashed line is in percentage and solid line is in dB.

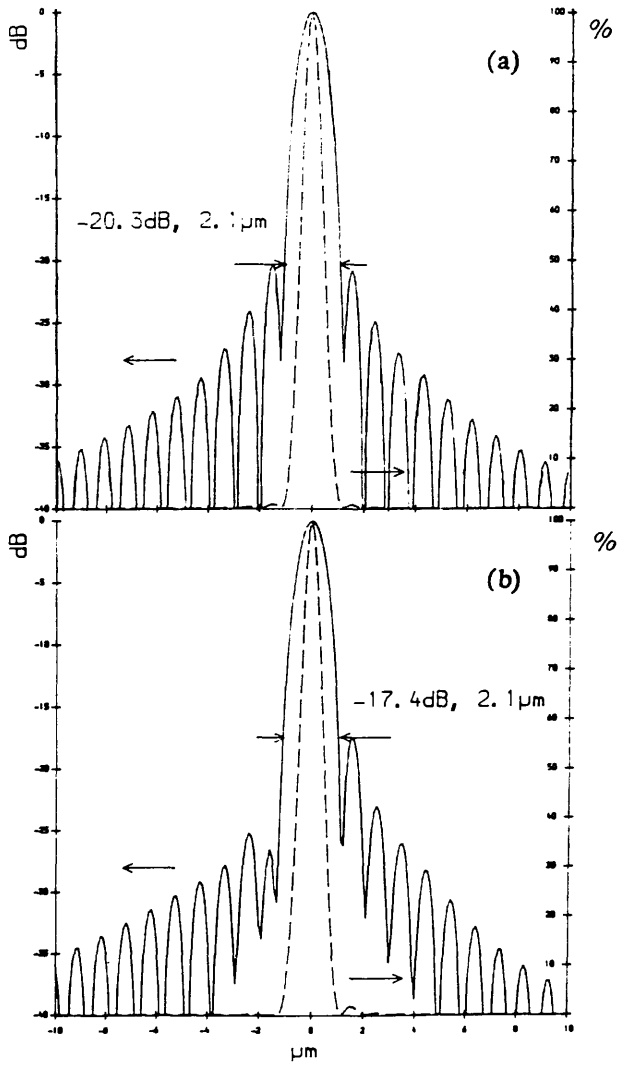

Figure2— 7. Calculated diffraction intensity profile for 4— element lens on isotropic material. $\lambda = 0.633\mu m$. Incident beam D= 6mm wide with Gaussian width A= 6mm. Back focal length f= 14.87mm. Incident angle $\alpha = 5^0$(a) and 8^0(b). Dashed line is in percentage and solid line is in dB.

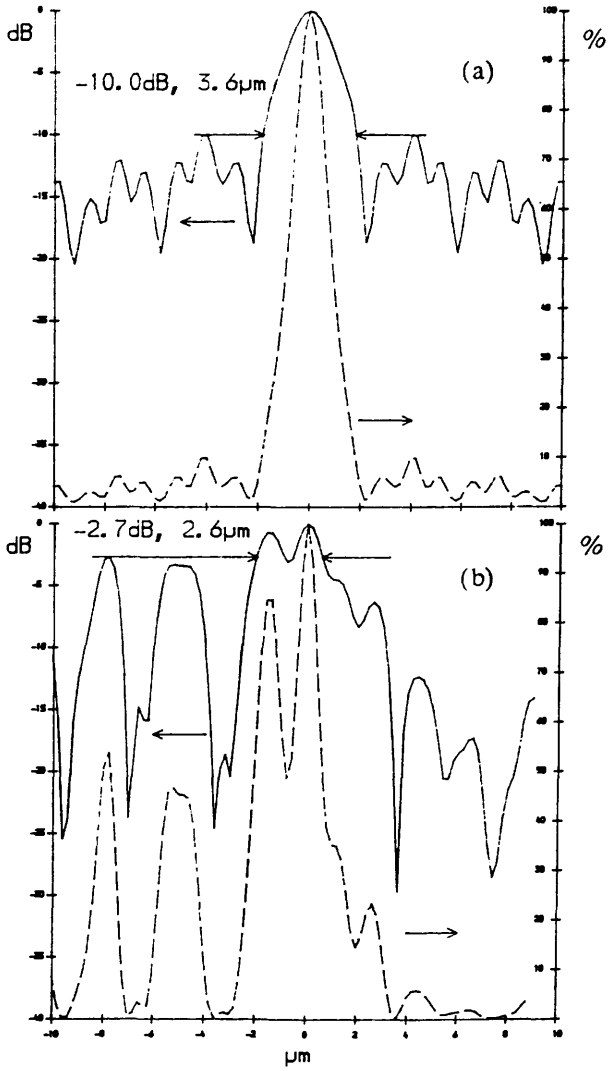

Figure 2−8. Calculated diffraction intensity profile for Elliptical−Hyperbolic lens on anisotropic material. $\lambda = 0.633\mu m$. Incident beam D= 6mm wide with Gaussian width A= 6mm. Back focal length f= 11.07mm. Incident angle $\alpha = 0^{0}$(a) and 2^{0}(b). Dashed line is in percentage and solid line is in dB.

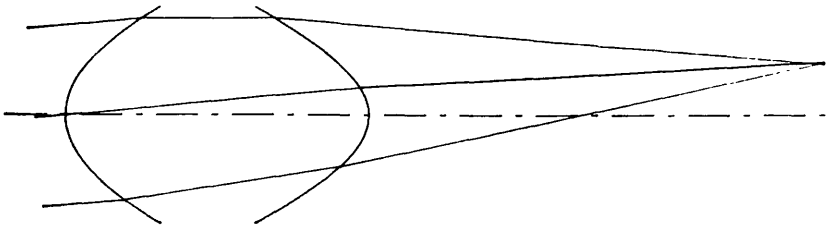

Figure 2−9. One element lens design.

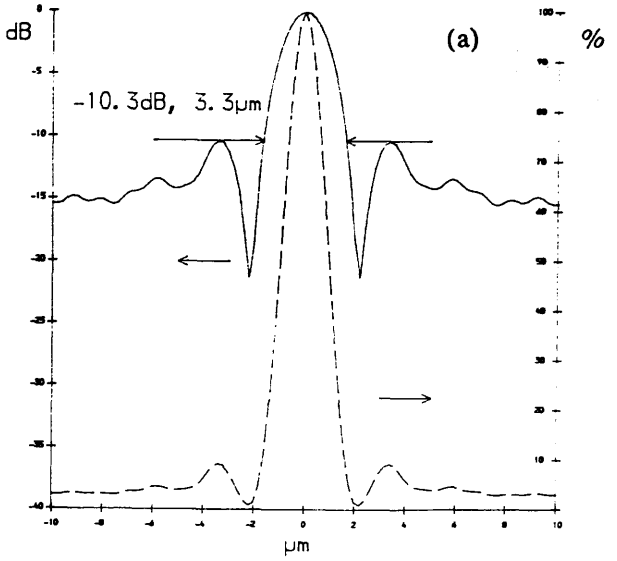

Figure 2−10. Calculated diffraction intensity profile for 1−element lens on anisotropic material. $\lambda = 0.633\,\mu m$. Incident beam D= 6mm wide with Gaussian width A= 6mm. Incident angle $\alpha = 0^0$(a), 3^0(b), 5^0(c). Dashed line is in percentage and solid line is in dB.

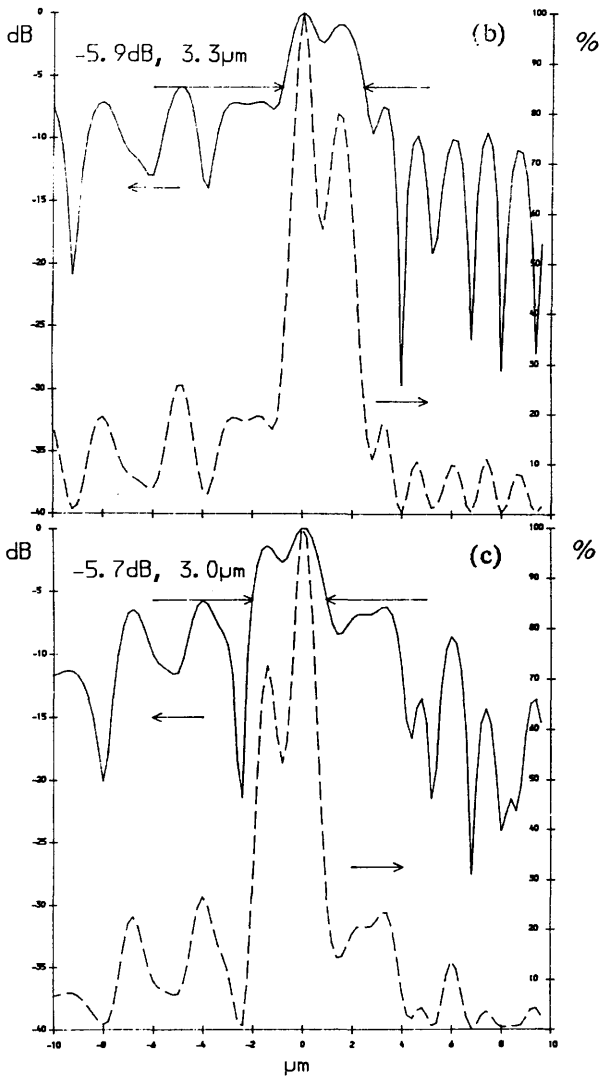

Figure 2−10. Calculated diffraction intensity profile for 1−element lens on anisotropic material. $\lambda = 0.633\,\mu m$. Incident beam D= 6mm wide with Gaussian width A= 6mm. Incident angle $\alpha = 0^0$(a), 3^0(b), 5^0(c). Dashed line is in percentage and solid line is in dB.

CHAPTER THREE: COUPLING EFFICIENCY ON THE BOUNDARY OF TWO WAVEGUIDES

III.1. Introduction

The power transmission efficiency is clearly important for optical elements. Boundary loss degrades the coupling efficiency of the guided wave on the boundary, and reduces the power transmission. Early multielement lens designs [Laybourn 1986] using circular lens boundaries required of the order of 30 elements (and 60 boundaries) – coupling efficiency η would have to be very close to 100% at each boundary, while for a 4–element lens [Laybourn 1988] a coupling efficiency of 92% is required on each boundary to achieve an overall transmission efficiency of 50% or –3dB.

The boundary losses come from mismatch between the modes in the two waveguides, reflection from the boundary interface and scattering on the boundary.

In homogenous lenses, light is confined in a high refractive index layer as guided wave. The guided wave has a certain electric field profile or optical intensity profile in depth. The guided wave must have different optical intensity profiles in the lens region waveguide and the surrounding waveguide because these two waveguides have different structures. The power from the guided wave in one waveguide could not be fully coupled into another waveguide when crossing the boundary because of mismatch of the two profiles, see figure 3–1. The coupling efficiency is normally expressed as the overlap integral of field profiles in the two waveguides.

Different order modes have different effective refractive indices, (so–called modal

dispersion). Only one guided mode is wanted and then the fundamental mode is the only candidate because it has the least attenuation. So it is clear that in order to reduce light in unwanted modes the low index waveguide at least should only support one mode. It will be shown later that the high index guide will inevitably be multimode for optimum coupling efficiency η between two fundamental modes. As well as by scattering out into the substrate, light power may be lost by coupling to modes other than the fundamental m= 0 mode in the second waveguide, when it is refracted at different angles because of different effective refractive indices as shown in figure 3– 2 and hence will constitute a background noise signal around the focused spot. It is self– evident that the higher the efficiency of coupling into the fundamental mode, the lower the efficiency of coupling into higher order modes. Any higher order modes excited in the high index lens region by coupling from the fundamental mode of the low index waveguide region, at low efficiency, will be recoupled at exit from the lens region at equally low efficiency to the fundamental guide mode, and although mis– focused, should not present significant background noise if η is high. If however higher modes were supported in the guide region there could be significant coupling of light to them from higher modes in the lens region.

In the conventional optical lens, the only power loss comes from reflection on the boundary of the lens and the surrounding materials. In the case of waveguide lenses, the difference of waveguide indices is small (e.g. 2.208 for Ti indiffusion (TI) low index waveguide and 2.330 for proton exchange (PE) high index waveguide) and then the reflection is comparably small. Even for very large incident angle the power reflection coefficient is much less than 1% [Zhou 1990]

Imperfections of the boundary scatter the guided wave, either transversely (in– plane) or into substrate and all other modes, and hence decrease the coupling efficiency.

The expression for the overlap integral of TE modes has been proposed but that for TM has not. So in section III.2. a general expression for the overlap integral of TE and TM modes is proposed. In section III.3., various refractive index profiles are considered for the two guiding layers and overlap integrals between two modes in the waveguides with those index profiles are calculated. In section III.4., there are presented the experimental results of investigating overlap integral of optical intensity profiles for glass waveguide system, TIPE $LiNbO_3$ waveguide system and double PE $LiNbO_3$ waveguide system. In the section III.5., it will shown how the boundary scattering degrades the coupling efficiency.

III.2. Overlap Integral of Two Modes in Different Waveguides

The overlap integral η between two guided waves of TE modes with electric field profiles $E_l(x)$ and $E_h(x)$ is expressed as [Hunsperger 1977]

$$\eta = \left[\frac{\beta_l \, \beta_h}{\omega \, \mu_0 \, (\beta_l + \beta_h)} \int_{-\infty}^{\infty} E_l(x) \, E_h(x) \, dx \right]^2 \qquad (3\text{-}1)$$

where β is the propagation constant, ω is the frequency, μ_0 is the permeability, and where the l and h subscripts refer, respectively, to the two different waveguides. This is an approximate result. More generally, the overlap integral for TE modes, η_E, is expressed as

$$\eta_E = \frac{\left[\int E_{ly}(x) \times H_{hx}(x) \, dx \right] \left[\int H_{lx}(x) \times E_{hy}(x) \, dx \right]}{\left[\int E_{ly}(x) \times H_{lx}(x) \, dx \right] \left[\int H_{hx}(x) \times E_{hy}(x) \, dx \right]} \qquad (3\text{-}2)$$

The two upper terms are the overlap integrals of the two modes and the two lower

terms are the normalization integrals. For a TE mode $E_{ly}(x)=E_{1y}(x)$, $H_{lx}(x)=-i(\partial E_{ly}(x)/\partial z)/(\omega \mu_0)=-\beta_1 E_{1y}(x)/(\omega \mu_0)$ and $E_{hy}(x)=E_{hy}(x)$, $H_{hx}(x)=-i(\partial E_{hy}(x)/\partial z)/(\omega \mu_0)=-\beta_h E_{hy}(x)/(\omega \mu_0)$. Then, with x and y subscripts ignored

$$\eta_E = \frac{\left[\int E_1(x) \times E_h(x)\, dx \right]^2}{\left[\int E_1^2(x)\, dx \right] \times \left[\int E_h^2(x)\, dx \right]} \qquad (3\text{-}3)$$

Following the same procedure [Hunsperger 1977] and putting it into a more general form, the overlap integral for TM modes η_M is expressed as

$$\eta_M = \frac{\left[\int H_{ly}(x) \times E_{hx}(x)\, dx \right] \left[\int E_{lx}(x) \times H_{hy}(x)\, dx \right]}{\left[\int H_{ly}(x) \times E_{lx}(x)\, dx \right] \left[\int E_{hx}(x) \times H_{hy}(x)\, dx \right]} \qquad (3\text{-}4)$$

For TM mode $H_{ly}(x)=H_{1y}(x)$, $E_{lx}(x)=i(\partial H_{ly}(x)/\partial z)/(\omega \epsilon)=\beta_1 H_{1y}(x)/(\omega \epsilon)$ and $H_{hy}(x)=H_{hy}(x)$, $E_{hx}(x)=i(\partial H_{hy}(x)/\partial z)/(\omega \epsilon)=\beta_h H_{hy}(x)/(\omega \epsilon)$ where $\epsilon(x)=n^2(x)$ is dielectric constant and n(x) is the index profile. Then, with x and y subscripts ignored

$$\eta_H = \frac{\int \frac{H_1(x)\, H_h(x)}{n^2{}_1(x)}\, dx \int \frac{H_1(x)\, H_h(x)}{n^2{}_h(x)}\, dx}{\int \frac{H_1{}^2(x)}{n^2{}_1(x)}\, dx \int \frac{H_h{}^2(x)}{n^2{}_h(x)}\, dx} \qquad (3\text{-}5)$$

III.3. Computer Modelling

III.3.1. Overlap Integral of TE Modes

The coupling efficiency, η, between two TE modes at a boundary between two dissimilar planar waveguides can be expressed as the overlap integral of the transverse electric field profiles as (3-3). The electric profile E(x) in a planar waveguide is a solution of the wave equation:

$$\frac{d^2E(x)}{d^2x} + k^2 \times [\, n^2(x) - n_e{}^2 \,] \times E(x) = 0 \qquad (3\text{-}6)$$

where n(x) is the refractive index profile; n_e is the waveguide effective index, β/k; k $= 2\pi/\lambda_0$; and λ_0 is the free-space wavelength. Calculations and measurements have been made with $\lambda_0 = 633$ nm.

The wave equation of the step-index planar waveguide is simply solved, yielding the effective index n_e, and the transverse field is written as [Yariv, 1973]:

$$E(x)=\begin{cases} \exp(x \times R) & x<0 \text{ (superstrate:air)} \\ \cos(x \times Q) + \dfrac{R}{Q} \sin(x \times Q) & 0 \leqslant x<d \\ [\cos(d \times Q) + \dfrac{R}{Q} \sin(d \times Q)] \times \exp[P \times (d-x)] & d \leqslant x \end{cases} \qquad (3\text{-}7)$$

d is the waveguide thickness, while

$$R = k \times (n_e{}^2 - 1)^{1/2}$$

$$Q = k \times (n_1{}^2 - n_e{}^2)^{1/2}$$

$$P = k \times (n_e{}^2 - n_2{}^2)^{1/2}$$

n_1 and n_2 are the waveguide and substrate refractive indices, respectively.

For gradient index profile planar waveguides with a known index profile n(x), E(x) may be written as:

$$E(x) = \begin{cases} E_1(x) = \exp(x \times R) & x < 0 \text{ (air)} \\ E_2(x) & x > 0 \end{cases} \qquad (3\text{-}8)$$

where $R = k \times (n_e^2 - 1)^{1/2}$. $E_1(x)$ is assumed the exponential form because the expression of (3−8) should be valid for step−like index profile waveguide which has an exponential form of electric field profile in air region as shown in (3−7). From the requirement that E_y and H_z be continuous at x= 0, there are:

$$E_2(0) = E_1(0) = 1 \qquad (3\text{-}9)$$
$$E_2'(0) = E_1'(0) = R$$

Rewriting (3−6) in the form of differential difference equation

$$\frac{E((I+1)\triangle x)-2E(I\triangle x)+E((I-1)\triangle x)}{\triangle x^2}+k^2\{n^2((I)\triangle x)-n_e^2\}E((I)\triangle x)=0 \qquad (3\text{-}10)$$

I=1, ...

Then we obtained

$$E(I+1) = \{\triangle x^2\, k^2\, (n_e^2 - n^2(I)) + 2\}\, E(I) - E(I-1) \qquad (3\text{-}11)$$

E(x) is divided into 6001 E(I)s in the range of $-0.3\mu m \leqslant x \leqslant 11.7\mu m$ with $\triangle x = 0.002\mu m$ and is expressed as

$$
\begin{cases}
E(I) = E_1(I) = \exp((-0.302 + I\,\triangle x)\,R) & \\
\qquad I=1,150; \qquad -0.3\mu m \leqslant x < 0.0\mu m \quad (air) & \\
E(151) = E_2(151) = 1 \qquad\qquad x=0.0\mu m & \\
E(152) = E_2(152) = 1 + \triangle x\,R \quad x=0.002\mu m & \\
E(I) = E_2(I) = \{\triangle x^2\,k^2\,(n_e^2 - n^2(I-1)) + 2\}\,E(I-1) - E(I-2) & \\
\qquad I=153,6001;\ 0.004\mu m \leqslant x \leqslant 11.7\mu m \text{ (guiding layer and substrate)} &
\end{cases}
\qquad (3\text{-}12)
$$

$\triangle x = 0.002\mu m$

Using regression numerical method and assuming a value for n_e, the resulting electric field profile $E_2(x)$ can be calculated numerically from the air/guide interface down into the graded index guiding region by using equation (3−12) over successive increments of x. It is found that only when the true solution for n_e is taken does $E_2(x)$ approach zero for x very large ($10\mu m$ proved to be large enough in our calculations while the calculation was going to about $12\mu m$). Then the corresponding electric field profile is also known. Mathematically, the expression (3−10) holds good for $\triangle x \to 0$. Our calculation shown that it made no significant difference whether $\triangle x$ was assumed to be $0.005\mu m$ or $0.002\mu m$. So $\triangle x = 0.002\mu m$ was thought small enough. The method has shown to be in good agreement with known solutions of planar waveguides.

Having calculated the electric field profiles E_ℓ and E_h in two adjacent waveguide sections, with low and high refractive indices, the overlap integral across the interface is numerically calculated by using equation (3−3).

III.3.2 Results of Calculation

(i) Step − step index profile

Both waveguide regions, with low and high indices, are assumed to possess step refractive index profiles: the refractive index is constant across the waveguide region. Figure 3−3 shows the overlap integral η as a function of the depth of the high

index guide for a particular low− index guide depth d_ℓ of 2.2144 μm, in a waveguide system where the substrate index n_2 = 2.202, and the guide indices are n_ℓ = 2.212, n_h = 2.322.

The high− index waveguide is multimoded around the depth d_h for optimum coupling efficiency, and the cut− off depths for modes m = 5, 6, 7 are shown on the graph. The optimum coupling efficiency is seen to occur for d_h around 2.68μm, slightly deeper than the low− index guide. Figure 3− 4 is a plot of such optimum efficiencies as a function of the low− index guide depth, where it is seen that increasing d_ℓ continues to increase the overlap integral. However, the guide region in an optical signal processor should be single− mode, so that the optimum low− index guide depth will be just below the cut− off depth for m= 1 (shown in figure 3− 4). In the following cases the low− index guide depths are also selected to be just below the cut− off depth for m= 1 mode.

Figure 3− 5 shows the electric field profiles of the modes in the two coupled waveguides, with η maximised at 99.1% for the particular refractive indices chosen.

The optimum value of d_h, the high index waveguide depth, is plotted against the low index guide depth d_ℓ in figure 3− 6, from which it is clear that $d_h > d_\ell$ for optimum coupling efficiency. The point m = 1 is the single− mode limit of d_ℓ.

(ii) Gaussian − step index profiles

The Gaussian refractive index profile (normally used to model TI waveguide) is expressed as

$$n(x) = n_2 + \triangle n \times \exp\{-(x/d)^2\} \qquad (3-13)$$

where d is the $1/e^2$ depth and $\triangle n$ is the increase in surface refractive index over

that of the substrate. The low index waveguide is approximated by the Gaussian profile, the high index waveguide by the step index profile, modelling Ti− indiffused and proton exchanged regions. For given refractive indices, waveguide depths have again been optimised, and an example is shown in figure 3−7, modelling the TIPE system. Because the electric field distributions are a relatively poor match, the overlap integral can only predict a maximum η of 95.6%.

(iii) Gaussian − Gaussian index profiles

In this and the following two examples various graded index approximations were used to simulate silver and potassium ion−exchanged glass waveguides.

If both high and low index guiding regions are Gaussian in refractive index distribution, the fundamental modes can be well matched, as shown in figure 3−8. An optimised coupling efficiency of 99.6% was predicted. However, the high index waveguide depth is then about 12μm, and the waveguide supports 27 modes. Even though it might be possible to achieve such a depth, transverse diffusion would be going on simultaneously, degrading the lens boundary definition between the two waveguides.

(iv) Exponential − exponential and erfc − erfc index profiles

The exponential index profile may be expressed as:

$$n(x) = n_2 + \triangle n \times \exp(-x/d) \qquad (3-14)$$

while the complementary error function (erfc) profile is:

$$n(x) = n_2 + \triangle n \times \mathrm{erfc}(x/d)$$

$$= n_2 + \triangle n \times (1 - \frac{2}{\sqrt{\pi}} \int_0^{x/d} e^{-x^2} dx) \qquad (3\text{-}15)$$

Figure 3−9 and figure 3−10 show optimised electric field profiles. Again, high maximum coupling efficiencies are predicted, but the optimum high index waveguide depths are now 70μm and 60μm respectively, outside the limits of good waveguide fabrication. With these three highly overmoded graded index profiles, it is clear that the fundamental mode is confined to the region of highest refractive index, very near to the waveguide surface, and the large diffusion depth is needed to extend the electric field profile sufficiently to match the wider−spread low index field profile.

III.3.3. Overlap Integral of TM Modes and the Results of Calculation

For TE modes, $E_y(x)$ and $H_z(x)= i\ (\partial E_y(x)/\partial x)/(\omega\ \mu_0)$ are continuous at the waveguide boundaries, but for TM modes, they are $H_y(x)$ and $E_z(x)= -i\ (\partial H_y(x)/\partial x)/(\omega\ \epsilon)= -i\ (\partial H_y(x)/\partial x)/(\omega\ n^2(x))$. Because n(x) is normally discontinuous, e.g. at interface of air and guide layer, $\partial H_y(x)/\partial x$ is not continuous. In the section III.3.1. we used (3−8) and (3−9) as an expression of transverse electric field and the continuity conditions for TE mode. Now for TM modes the expression of transverse magnetic field and the continuity conditions should be

$$H(x)= \begin{cases} H_1(x) = \exp(x \times R) & x<0 \text{ (air)} \\ H_2(x) & x>0 \end{cases} \qquad (3\text{-}16)$$

$$H_2(0) = H_1(0) = 1 \qquad (3\text{-}17)$$

$$H'_2(0)/n^2(0) = H'_1(0)/\ n_0^2 = R/n_0^2$$

where n(x) is the index profile of the waveguide and $n_0= 1$ is the index of air. As in III.3.1. for E(x), the profile of magnetic field H(x) can be solved from the wave equation with any given index profile n(x), using the transverse magnetic field expression and continuity conditions (3−16) and (3−17). $H_1(x)$ still has the

exponential form and $H_2(x)$ is the solution of wave equation as (3−6). But because of the different continuity conditions, H(I) should be written as

$$
\begin{cases}
H(I) = H_1(I) = \exp((-0.302 + I\,\triangle x)\,R) \\
\qquad I=1,150; \qquad -0.3\mu m \leqslant x < 0.0\mu m \quad (air) \\
H(151) = H_2(151) = 1 \qquad\qquad x=0.0\mu m \\
H(152) = H_2(152) = 1 + \triangle x\, R\, n^2(0) \quad x=0.002\mu m \\
H(I) = H_2(I) = \{\triangle x^2\, k^2\, (n_e^2 - n^2(I-1)) + 2\}H(I-1) - H(I-2) \\
\qquad I=153,6001;\ 0.004\mu m \leqslant x \leqslant 11.7\mu m \ \text{(guiding layer and substrate)} \\
\triangle x = 0.002\mu m
\end{cases}
\tag{3-18}
$$

Then the overlap integral can be obtained from (3−5).

The general results for TE modes in III.3.2. still exist for TM modes: the overlap integral between two waveguides with the same type of index profile (both are step−like, or Gaussian distribution et al) can be >99%; if both low and high index waveguides have gradient index profiles such as Gaussian, exponential and error function, the depth of the high index waveguide required to obtain optimal matching will have to be so large that it is technically impractical (for the Gaussian profile the depth of the high index waveguide will be about 10μm, for exponential profile about 65μm and for the error function profile about 55μm); for a certain depth of low index waveguide, there is an optimum depth for high index waveguide at which the overlap integral reaches maximum and this maximum overlap integral increases with the depth of low index waveguide. Keeping the low index waveguide mono−mode, the optimum depth for low index waveguide is just below the cut−off of first order mode.

Using the same refractive indices of substrate, low index waveguide layer and high index waveguide layer as in III.3.2. for TE mode analysis, the low index waveguide starts to guide the first order TM mode at a greater depth than that for the TE mode. The Table 3−1 gives the depths of low and high index waveguides and

overlap integrals for the specified waveguide structures, compared with that of TE mode. The results are very close for TM and TE modes except that the optimum depths and overlap integrals are slightly larger for a TM mode than for a TE mode.

III.4. Experimental Results

III.4.1. Optical Intensity Profile Measurement and Overlap Integral Calculation

Two substrate materials have been considered as the basis for experimental lens preparation, soda–lime glass and single–crystal lithium niobate. It was hoped that the lens preparation on glass substrates would prove to be relatively straightforward, using silver and potassium ion exchange with the sodium in the glass to provide the high and low index waveguide regions [Chartier 1986], rather than the more involved but more useful lens production on lithium niobate by titanium indiffusion and proton exchange. It happens that the refractive index ratio between high and low index guides is similar in the two systems, allowing the same lens designs to be used, since the refractive index ratio is the only material parameter appearing in the designs [Laybourn 1988].

Measurements of electric field intensity profiles were carried out on waveguides fabricated on glass and lithium niobate substrates. One end of each sample was polished to optical quality. Light was coupled into the waveguide by prism coupler, to excite only the lowest order mode. A microscope objective (x40) was used to image the polished waveguide end face onto a Hamamatsu video camera, recording the near field intensity profile of the guided wave. The magnification of the system was fixed so that the recorded mode profiles of all samples were comparable. The intensity profile I(x) of the lowest order mode in each guide was sampled and stored by an associated computer as $I(x_i)$ $i=1...n$, and from pairs of intensity profiles

measured in low and high index guides on the same substrate material the predicted coupling efficiency was calculated using a numerical approximation of the overlap integral, equation(3−3),:

$$\eta = \frac{(\sum_i \surd(I_l(x_i) \times I_h(x_i)))^2}{\sum_i I_l(x_i) \quad \times \quad \sum_i I_h(x_i)} \qquad (3\text{-}19)$$

In the case of the TE mode there is no difficulty: what is measured is $I(x)=E_l^2(x)$ or $E_h^2(x)$. But for the TM mode what is measured is

$$I(x) = \frac{H_l^2(x)}{n^2_l(x)} \quad \text{or} \quad \frac{H_h^2(x)}{n^2_h(x)} \qquad (3\text{-}20)$$

Because the actual index profile of the low index waveguide was unknown, $H_l^2(x)$ and $H_h^2(x)$ could not be obtained directly, nor could equation (3−5) be used to calculate for TM modes. But theoretical model analysis showed that it made no significant difference if we ignored the index profiles. So the overlap integral was calculated using a numerical approximation of equation (3−19) for TM modes.

The range of samples was limited, and the position of the air−guide interface had to be estimated from the measured profiles. Examples of measured profiles are shown in figures 3−11 to 3−15, 3−18 and 3−20. In most cases there was a decaying oscillatory field outside the surface of the guide (probably due to the diffraction at the sample edge) − for the purpose of calculating the overlap this part of the measured profile was discounted, and the first minimum was taken as the position of the surface. The overlap integration started at this point.

III.4.2. Overlap Integral for Glass Waveguide System *

*: This part of the measurements was done by Mr. Weiping Zhang who was on leave from the Department of Electronics of Shandon University, P. R. China. He also prepared the masks of several lens designs. His contribution is greatly appreciated.

The ion exchange temperatures used were 375 °C for K^+ exchange and 225 °C for Ag^+ exchange. A diffusion time of 20 minutes was used for the potassium exchange, forming a single-mode waveguide. Different diffusion times were used to form various overmoded silver-exchanged guides, as shown in Table 3-2, in an attempt to produce a guide that would be deep enough to support a fundamental mode well-matched to the potassium-exchanged guide. Examples of measured optical field profiles in potassium and silver ion exchanged guides are shown in figure 3-11, where it can be seen that even with three hours of diffusion time, the depth of the fundamental mode in the high index guide is insufficient to match the mode profile in the low index guide. The computed overlap integral resulting from the measured mode profiles is shown in Table 3-2. It is apparent that the efficiency is rising very slowly with diffusion time.

The experimental results of mode profile measurements on glass ion exchanged waveguides may be compared with a Gaussian model for the profile [Ramaswamy 1988]. The electric field profiles of the low and high Gaussian refractive index profiles give a high theoretical optimum efficiency, calculated to be 99.6% for the particular waveguides considered. However, to achieve this optimum efficiency the high index waveguide profile has to be about 12μm deep and to support 27 modes. In the experimental Ag^+ exchanged guides the longest diffusion time of 12 hours only produced a guide supporting 11 modes, and consequently the best overlap integral calculated from measured field profiles was only 91.3%. Step index guides could be expected to result in better-matched mode profiles, and can be produced by electric-field-assisted ion exchange [Ramaswamy 1988]. In such a high-index guide the step index profile would result in a deeper fundamental mode profile, and

hence a shallower optimum guide depth. However, the added difficulties of electric field assistance make its use less desirable, while the guides produced by simple ion exchange do not seem to offer a good medium for experimental lens fabrication.

III.4.3. Overlap Integral for $LiNbO_3$ waveguide system

(a) TIPE system (TE mode)

Low-effective index waveguides were made by titanium indiffusion (TI) into lithium niobate. A 25 nm film of Ti was deposited on x-cut lithium niobate substrates. The samples were heated to 1000 °C for 4 hours in flowing wet oxygen, resulting in a single mode waveguide. TE propagation was used in the y direction. The effective mode index was measured to be 2.2065, while the substrate extraordinary index was 2.2015. The optical mode intensity profile was recorded as before.

One Ti-diffused sample was then subjected to proton exchange (PE) in benzoic acid at 236 °C for 3 hours. The sample was left to stabilise for 16 days [Jackel 1984], after which time the intensity profile of the fundamental mode was measured (figure 3-12). The sample was then annealed for 3 hour periods at 300 °C in wet oxygen, and the optical mode profile remeasured after each period of annealing (figures 3-13 to 3-15). After the first annealing period the profile was seen to match very well to the Ti-diffused low index profile. However, subsequent annealing degraded the good mode match. The calculated overlap integral, shown in Table 3-3, confirmed the matching properties of the waveguides.

The index profiles of the multimode proton-exchanged waveguides were calculated from the mode effective indices measured before and after each annealing step (and plotted in figure 3-16), and are shown in figure 3-17. After annealing the proton-exchanged region assumed an index profile very close to rectangular, with the 3-hour-annealed guide showing a good mode profile match to the Ti-diffused

guide. Further annealing, although not changing the refractive index profile greatly, evidently had sufficient effect on the mode intensity profile of the proton-exchanged guide to reduce significantly the match between the high and low index guides and the resulting computed overlap integral. The optimum coupling efficiency is much better than would have been expected from the theoretical modelling of the Ti-indiffused waveguide by a Gaussian profile and the proton-exchanged waveguide by a step profile, as discussed in section III.3. This could be partly referred to the fact that the index increases of TI and PE are additive [De Micheli 1983], and therefore the index profile of TIPE waveguide is the sum of the index profiles of TI waveguide (Gaussian profile) and PE waveguide (step-like profile), which is consequently a gradient one.

(b) TIPE system (TM mode)

Optical intensity profiles of TM mode were measured and overlap integrals calculated. A 30nm Ti film was deposited on z-cut $LiNbO_3$ substrates, and the samples were annealed at 1000 °C for four hours in flowing wet oxygen, resulting in a single mode waveguide just below the cut-off of first order mode. One TI sample was then proton exchanged in benzoic acid, forming a TIPE waveguide. The exchange rate is much smaller on z-cut $LiNbO_3$ than on x-cut material, so a higher temperature, 255 °C, was used to enhance the exchange rate. Figure 3-18 shows the optical intensity profiles of TM modes on TI waveguide and TIPE waveguide after proton exchange for six hours, from which the calculated overlap integral was 96.0%. To optimise the overlap integral, the TIPE sample was annealed at 300 °C for 20min, after which the optical intensity profile was measured and plotted in the figure 3-18, and the overlap integral rose up to 98.3%. Figure 3-19 shows the index profile of the TIPE sample after proton exchange and annealing, calculated by the IWKB method.

(c) Double proton exchange system

Matching between fundamental modes of a dilute melt proton exchange (DPE) waveguide and a PE waveguide is more complicated because the index profile of DPE waveguide changes during subsequent processing at elevated temperatures including proton exchange for the lens region. Annealing the sample at a higher temperature can stabilise the waveguide structure.

Some z− cut $LiNbO_3$ samples underwent DPE in 1% lithium benzoate acid diluted benzoic acid at 210 °C for 16− 60min and annealed at 380 °C for 12min. All samples supported a single mode. The optical intensity profiles are plotted in figure 3− 20. After 16min and 25min DPE, the samples failed to support any guided mode. After annealing, the optical intensity profiles were broad because of the small index increase and consequent weak guiding. The DPE samples which underwent long exchanges (50min and 60min) supported a single mode. After annealing the waveguides were still single moded and just below the cut− off of first order mode. The power was still strongly confined and can be well matched by the optical intensity profiles of the TIPE and TIPE plus annealing waveguides of figure 3− 18. The PE rate is greater on a virgin sample than on a TI sample so the proton exchange time required for the waveguide to match the DPE waveguide should be shorter than that required to match TI waveguide.

An experiment was done to see how annealing affected the index profile of a DPE waveguide. Some multi− mode waveguides were made, effective indices were measured and the index profiles were calculated by IWKB method. Then various annealing conditions were used and the index profiles were worked out as before. Figure 3− 21 shows some examples, where the z− cut $LiNbO_3$ was proton exchanged in pure benzoic acid at 235 °C for 90 minutes and then annealed at 320 °C and 380 °C for 10 minutes. The index profile became a little lower and wider but still close to step− like. The depths increased from 1.2 μm to 1.8 μm and from 1.4 μm to 1.9 μm, respectively. They did not convert into a smooth gradient, this, however,

could be due to the fact that for the thicker PE waveguide, a longer annealing time is required to convert the step-like index profile into a gradient profile [Goto 1989]. The waveguide mentioned in the last paragraph was very thin (to get a single-mode waveguide) and it was therefore expected to be more easily affected by annealing and converted into a gradient profile, in which case the waveguide has a weak confinement and has a broad electromagnetic field profile.

III.5. Coupling Efficiency Measurement from m-line

As mentioned above, mode mismatch leads to power loss when a guided wave propagates across the boundary of two waveguides. The imperfections of the boundary scatter the guided wave, either transversely or into the substrate and all other modes. In addition, as will be found in the next chapter, if the sample has an out-diffusion mode after Ti indiffusion, the power will be partially coupled or scattered into the out-diffusion modes. As a consequence, the coupling efficiency will be smaller than that calculated from the overlap integral of the electromagnetic field profiles or optical intensity profiles. The coupling efficiency could be defined and measured in another way, as illustrated in figure 3-22. A laser beam is coupled into the low index single-mode waveguide by a prism and propagates across the boundary into the high index multi-mode waveguide and then is coupled out by another prism and gives a m-line. Assuming that the incident power is totally redistributed into all modes in the high index multi-mode waveguide and that the power distribution among the modes in the m-line is identical to that in the high index waveguide, then measuring the power percentage of the fundamental mode over all modes in the m-line gives the coupling efficiency of the fundamental mode across the boundary. Only the concentrated spots in the m-line will propagate in the expected direction and then the coupling efficiency is defined as the ratio of the power in the concentrated spot of the fundamental mode to all the collected power. This coupling efficiency takes into consideration mode mismatch and boundary

scattering, and the power of each mode can be measured using a photodetector plus a slit.

The coupling efficiency measurement from the m− line showed that for the samples for which an overlap integral of 99% was obtained from the measured optical intensity profiles, the coupling efficiency was degraded to about $\eta = 75\%$.

Figure 3− 23(a) shows the m− line of a z− cut $LiNbO_3$ sample which was proton exchanged in 1% diluted benzoic acid at 210 °C for 50 minutes and annealed at 320 °C for 10 minutes to form the low index waveguide and then in pure benzoic acid at 235 °C for 3 hours with half of the waveguide surface covered by a SiO_2 film to form the high index half of the waveguide region. For the DPE waveguide annealed at 320 °C for 10 minutes before PE, it was difficult for the PE waveguide to match, and much stronger PE (255 °C for 6 hours) was needed for the high index waveguide to match because the DPE waveguide was too deep and probably had a gradient index profile. As explained in section III.4.3., low coupling efficiency between such a waveguide and a step− like PE waveguide was expected (as shown in III.3.2.). That is why figure 3− 23(a) gives poor coupling: much of the power is in the highest order mode. Figure 3− 23(b) shows the m− line of a sample of which the processing was the same as the sample of figure 3− 23(a) except that no annealing was done. Most power was concentrated in the fundamental mode.

III.6. Discussion and Summary

The overlap integral between two waveguides with the same type of index profile (both are step− like, or Gaussian distribution etc.) can be $> 99\%$; if both low and high index waveguides have gradient index profile such as Gaussian, exponential and error function, the depth of the high index waveguide required to obtain optimal matching will have to be so large that it is technically impractical. For a certain

depth of low index waveguide, there is an optimum depth for high index waveguide at which the overlap integral reaches a maximum and this maximum overlap integral increases with the depth of low index waveguide. Keeping the low index waveguide mono-mode, the optimum depth for low index waveguide is just below the cut-off of the first order mode.

Even though the boundary continuity conditions are different for TE modes and TM modes, it makes no significant difference in the field profile and overlap integral. So we can use same waveguide structure for either TE or TM guided waves to get similar coupling efficiency; however the fabrication parameters may differ because of different material and processing performances.

Experimentally, optical intensity profiles had overlap integrals of about 99% for TE mode on x-cut and TM mode on z-cut TIPE $LiNbO_3$. Annealed DPE waveguide has a broad intensity profile which is difficult to match to that in PE waveguide.

The experiments that have been performed on glass and lithium niobate optical waveguides suggest that while the TIPE double waveguide system might be used to produce homogeneous refracting thin-film lenses for signal-processing applications, simple ion exchange on a soda-lime glass substrate will not model the lithium niobate lens system well, notwithstanding a similar effective index ratio. It seems that the problem with high effective index graded-index waveguides is a concentration of the electric field at the peak of the index profile, restricting the width of the fundamental mode profile and producing a poor match to a mode in a low-effective-index guide.

Boundary scattering was shown to be a major problem, decreasing the coupling efficiency. Even though the match of the intensity profile could be excellent, the coupling efficiency will be finally limited to about 75% by boundary scattering, and after passing 8 boundaries there would be only 10% power left. In our attempt to

fabricate 4— element lenses, the overall transmission of the guided wave power was poor, the main contributor being boundary scattering losses. For a single element lens the overall transmission comes to be about 56% or −2.5dB which may be acceptable and is readily achievable.

Table 3-1 The optimum depths of low and high index waveguides and coupling efficiencies for TE and TM modes

low and high index waveguide have step-like index profile $n_{sub}=2.202, n_l=2.212, n_h=2.322$		low index waveguide has Gaussian index profile, $n(x)=2.202+0.01\times\exp(-(x/a)^2)$, high index waveguide has step-like index profile, $n_{sub}=2.202$, $n_h=2.322$	
TM mode	TE mode	TM mode	TE mode
$d_l=2.2550\mu m$	$d_l=2.2144\mu m$	$a=2.05\mu m$	$a=2.00\mu m$
$d_h=2.7296\mu m$	$d_h=2.6768\mu m$	$d_h=2.68\mu m$	$d_h=2.60\mu m$
$\eta=99.10\%$	$\eta=99.09\%$	$\eta=95.66\%$	$\eta=95.63\%$

Table 3-2 Coupling efficiency between K^+ exchanged waveguide (20 minutes at 375°C) and Ag^+ exchanged waveguide (at 225°C)

Ag^+ exchange time (hrs)	3	6	10	12
number of modes	5	8	10	11
η (%)	90.9	86.3	91.2	91.3

Table 3-3 Coupling efficiency between TI waveguide (25nm Ti, 4hrs at 1000°C) and annealed TIPE waveguide (Benzoic acid, 3hrs at 236°C, annealing at 300°C)

annealing time(hrs)	0	3	6	9
number of modes	7	10	10	10
η (%)	93.4	99.1	95.5	96.5

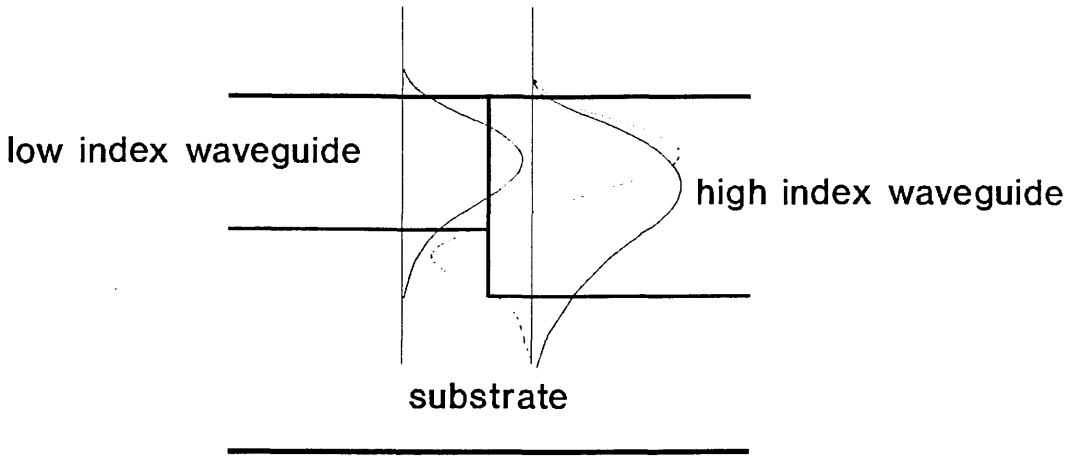

Figure 3−1. Modes match between two electromagnetic field profiles.

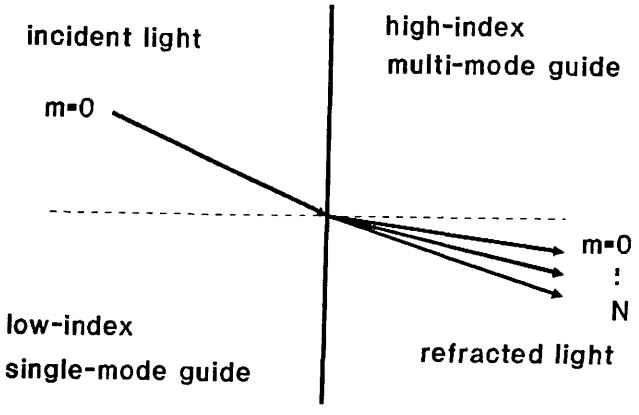

Figure 3−2. Refraction from a fundamental mode in a low index single mode waveguide into all modes in a high index multi−mode waveguide

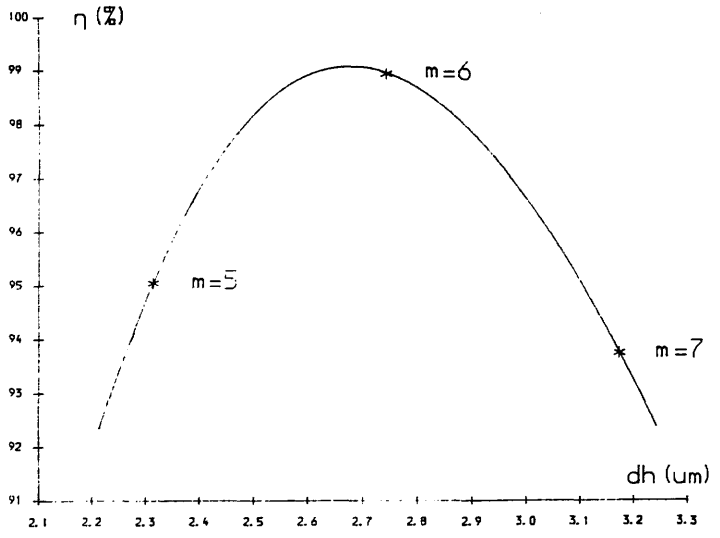

Figure 3−3 Overlap integral vs high index waveguide depth. $n_l = 2.212$, $n_h = 2.322$, $n_2 = 2.202$, $d_l = 2.2144\,\mu m$.

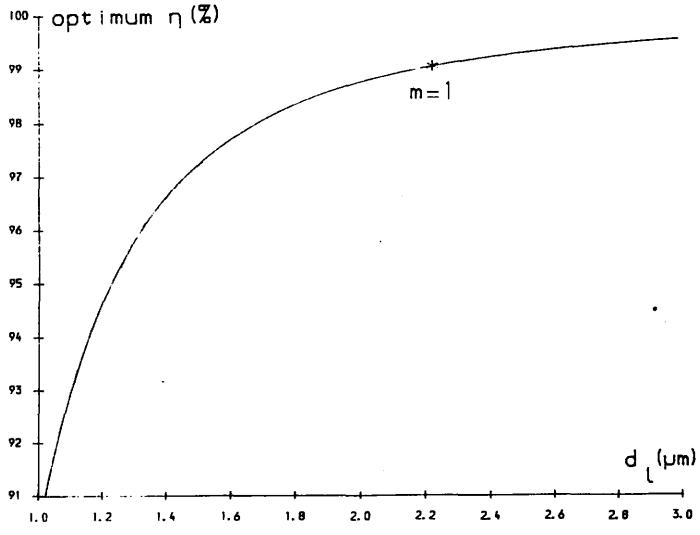

Figure 3−4 Optimum efficiency vs low index waveguide depth. $n_l = 2.212$, $n_h = 2.322$, $n_2 = 2.202$.

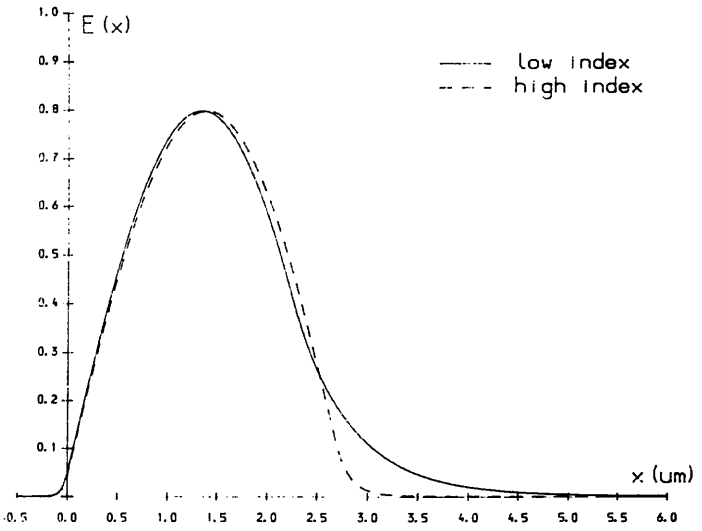

Figure 3– 5 Electric field profiles. $n_l = 2.212$, $n_h = 2.322$, $n_2 = 2.202$, $d_l = 2.2144\,\mu m$, $d_h = 2.677\,\mu m$, $\eta = 99.1\%$.

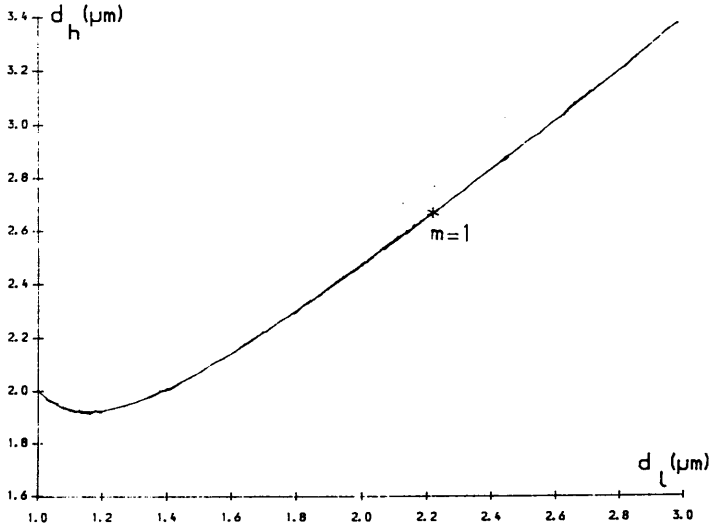

Figure 3– 6 d_h vs d_l, for d_l η is optimised at d_h. $n_l = 2.212$, $n_h = 2.322$, $n_2 = 2.202$.

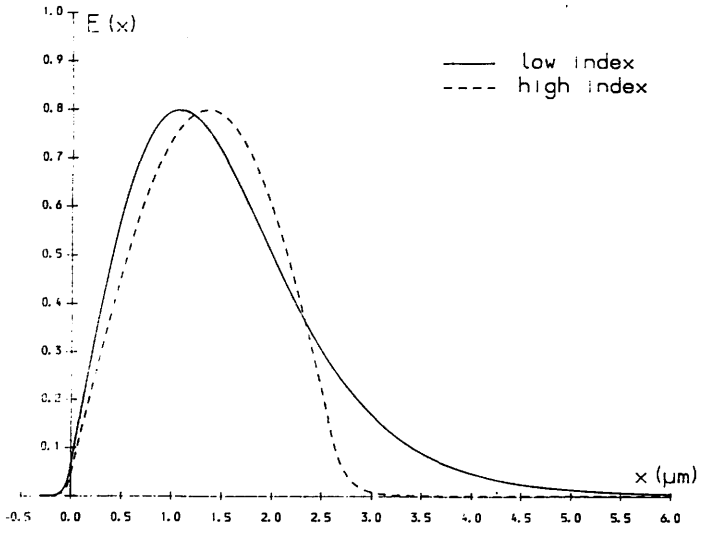

Figure 3－7 Electric field profiles. $n_l = 2.202 + 0.01 \times \exp(-(x/2.0)^2)$, $n_2 = 2.202$, $n_h = 2.322$, $d_h = 2.609\,\mu m$, $\eta = 95.6\%$.

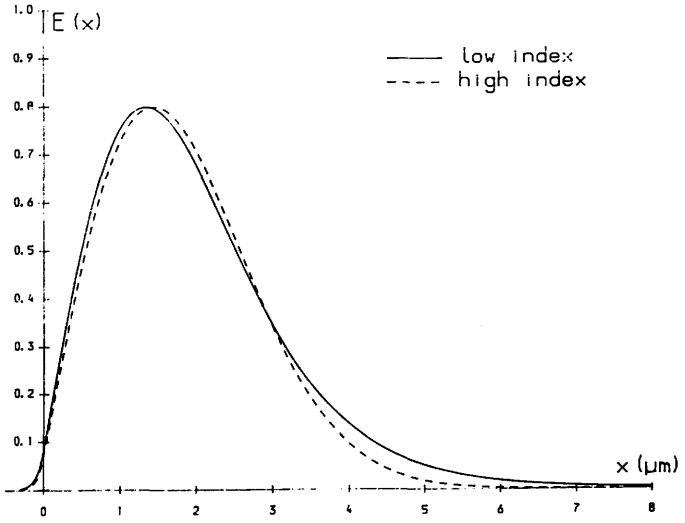

Figure 3－8 Electric field profiles. $n_l = 1.512 + 0.009 \times \exp(-(x/2.0)^2)$, $n_h = 1.512 + 0.100 \times \exp(-(x/12.37)^2)$, $\eta = 99.6\%$.

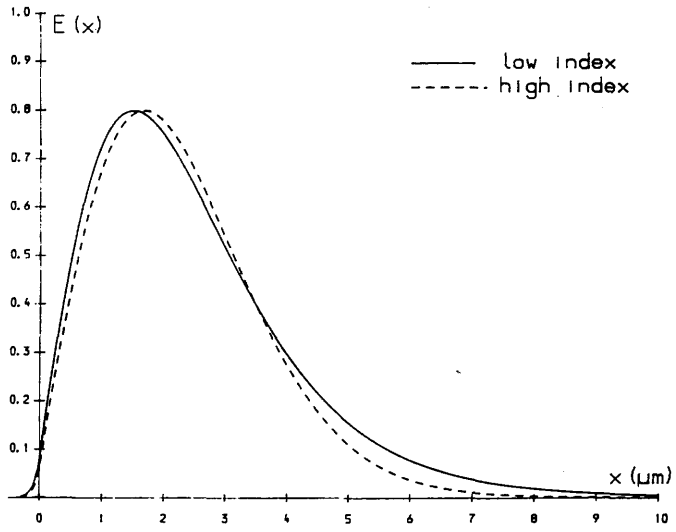

Figure 3－9 Electric field profiles. $n_l = 1.512 + 0.009 \times \exp(-x/1.8)$, $n_h = 1.512 + 0.100 \times \exp(-x/71.63)$, $\eta = 99.4\%$.

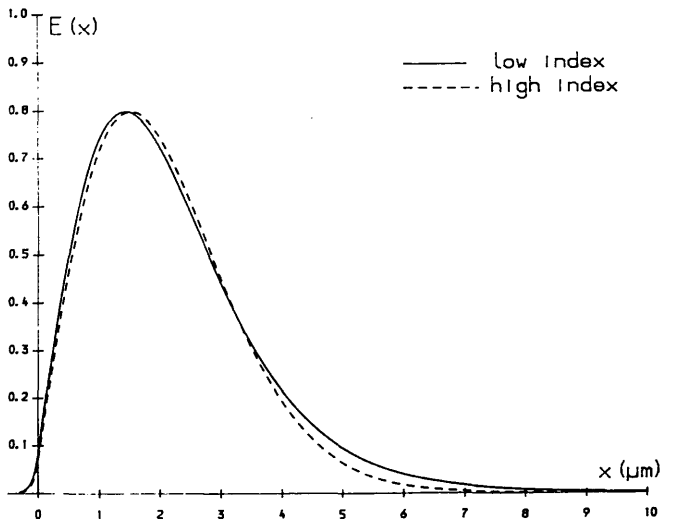

Figure 3－10 Electric field profiles. $n_l = 1.512 + 0.009 \times \mathrm{erfc}(x/3.5)$, $n_h = 1.512 + 0.100 \times \mathrm{erfc}(x/62.75)$, $\eta = 99.7\%$.

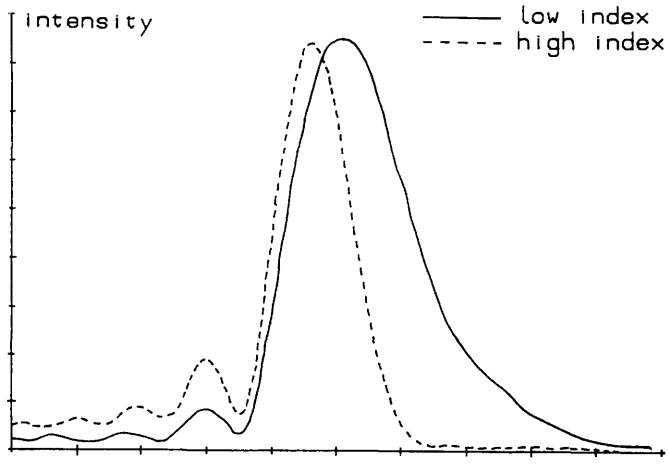

Figure 3–11 Measured optical intensity profiles. $\eta = 90.9\%$. Low index waveguide: K^+ exchange, 20 minutes at 375 °C; high index waveguide: Ag^+ exchange, 180 minutes at 225 °C.

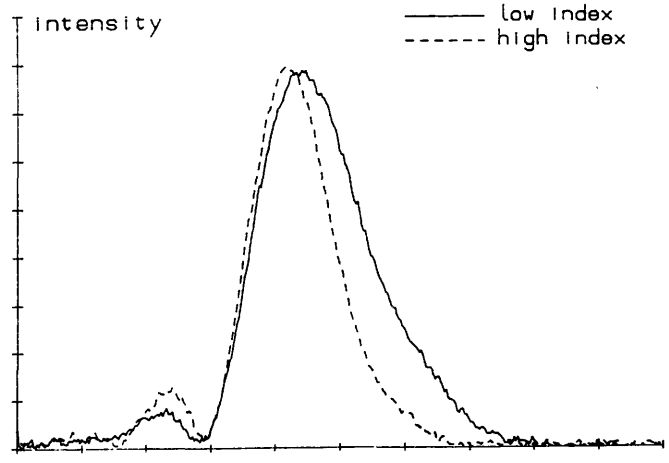

Figure 3–12 Measured optical intensity profiles. $\eta = 93.4\%$. Low index waveguide: 25nm Ti, 1000 °C, 4 hours; high index waveguide: proton exchange in benzoic acid, 236 °C, 3 hours.

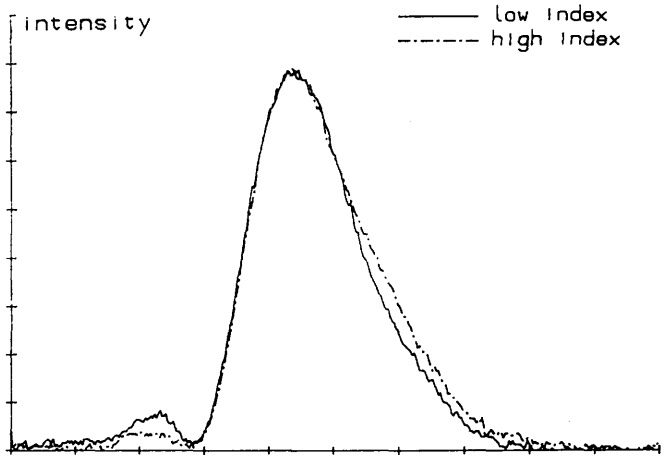

Figure 3–13 Measured optical intensity profiles. $\eta = 99.1\%$. Low index waveguide: 25nm Ti, 1000 °C, 4 hours; high index waveguide: proton exchange in benzoic acid, 236 °C, 3 hours; annealing, 300 °C, 3 hours.

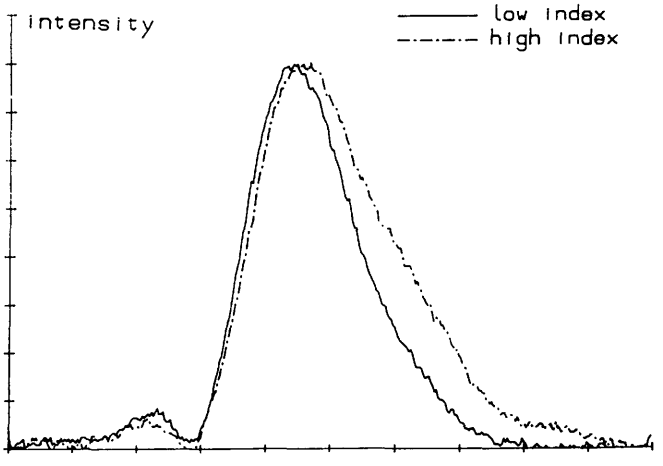

Figure 3–14 Measured optical intensity profiles. $\eta = 95.5\%$. Low index waveguide: 25nm Ti, 1000 °C, 4 hours; high index waveguide: proton exchange in benzoic acid, 236 °C, 3 hours; annealing, 300 °C, 6 hours.

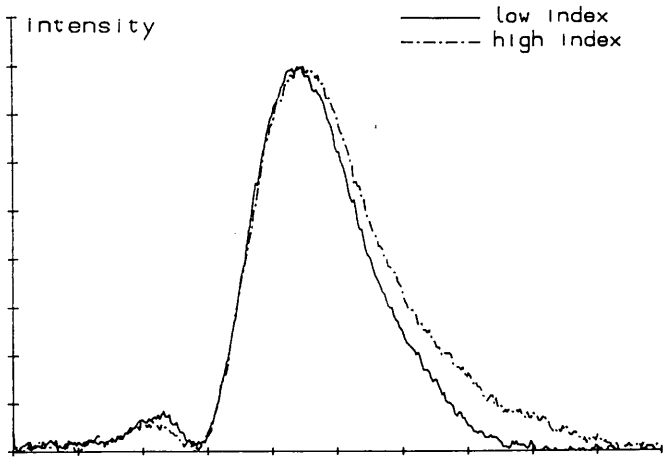

Figure 3−15 Measured optical intensity profiles. η= 96.5%. Low index waveguide: 25nm Ti, 1000 °C, 4 hours; high index waveguide: proton exchange in benzoic acid, 236 °C, 3 hours; annealing, 300 °C, 9 hours.

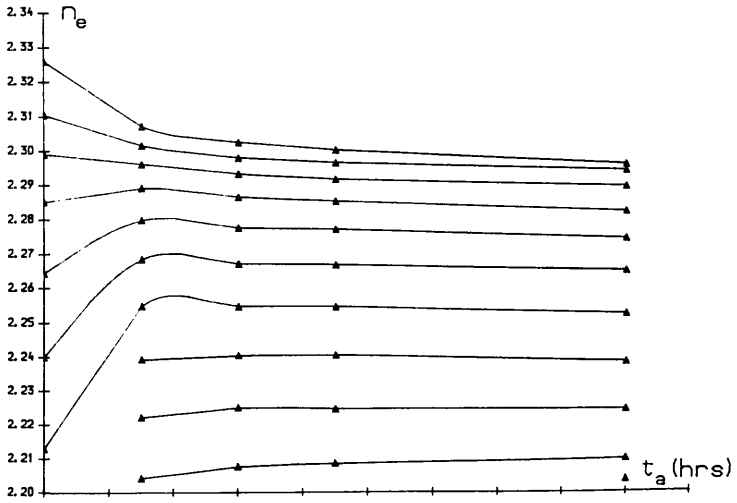

Figure 3−16 Effective index vs annealing time. x−cut $LiNbO_3$. TI: 25nm Ti, 1000 °C, 4 hours; PE: benzoic acid, 236 °C, 3 hours; annealing temperature 300 °C.

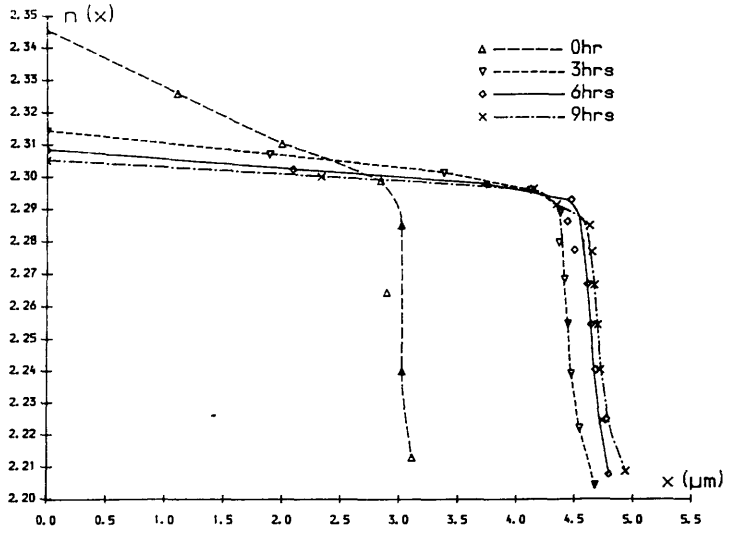

Figure 3—17 Variation of index profile vs annealing time, the same sample as in figure 3—16.

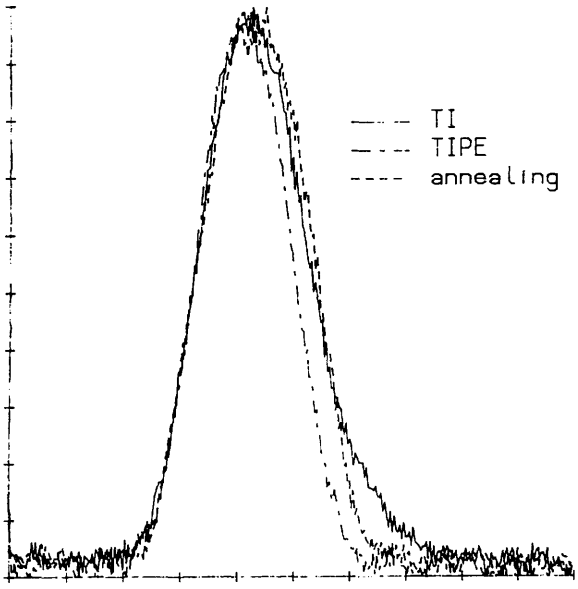

Figure 3—18 Measured optical intensity profiles of TM mode on z—cut $LiNbO_3$. Low index waveguide: 30nm Ti, 1000 °C, 4 hours; high index waveguide: proton exchange in benzoic acid, 255 °C, 6 hours, η= 96.0%, annealing, 300 °C, 20 minutes, η= 98.3%.

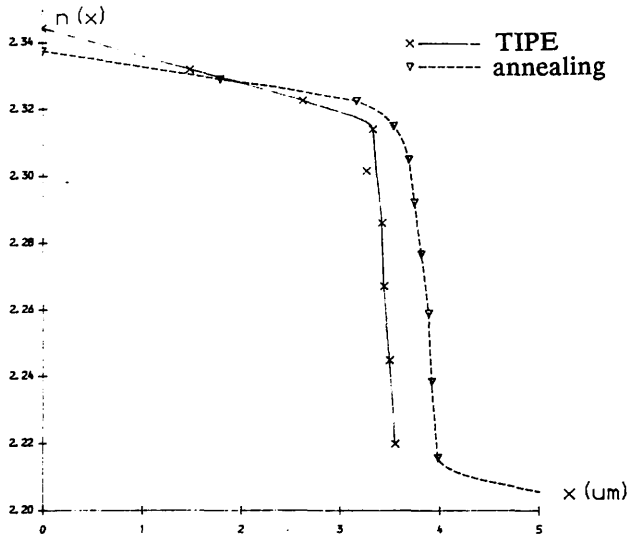

Figure 3－19 Index profile vs annealing time. z－cut $LiNbO_3$, 30nm Ti, 1000°C, 4 hours, benzoic acid, 255°C, 6 hours, annealing 300°C, 20 minutes.

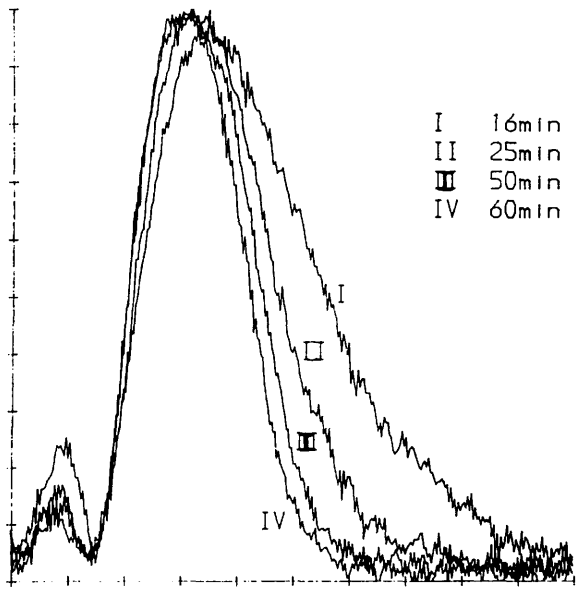

Figure 3－20 Measured optical intensity profiles of TM mode on z－cut $LiNbO_3$. DMPE in 1% diluted benzoic acid, 210°C, 16－60 minutes, annealing at 380°C, 12 minutes.

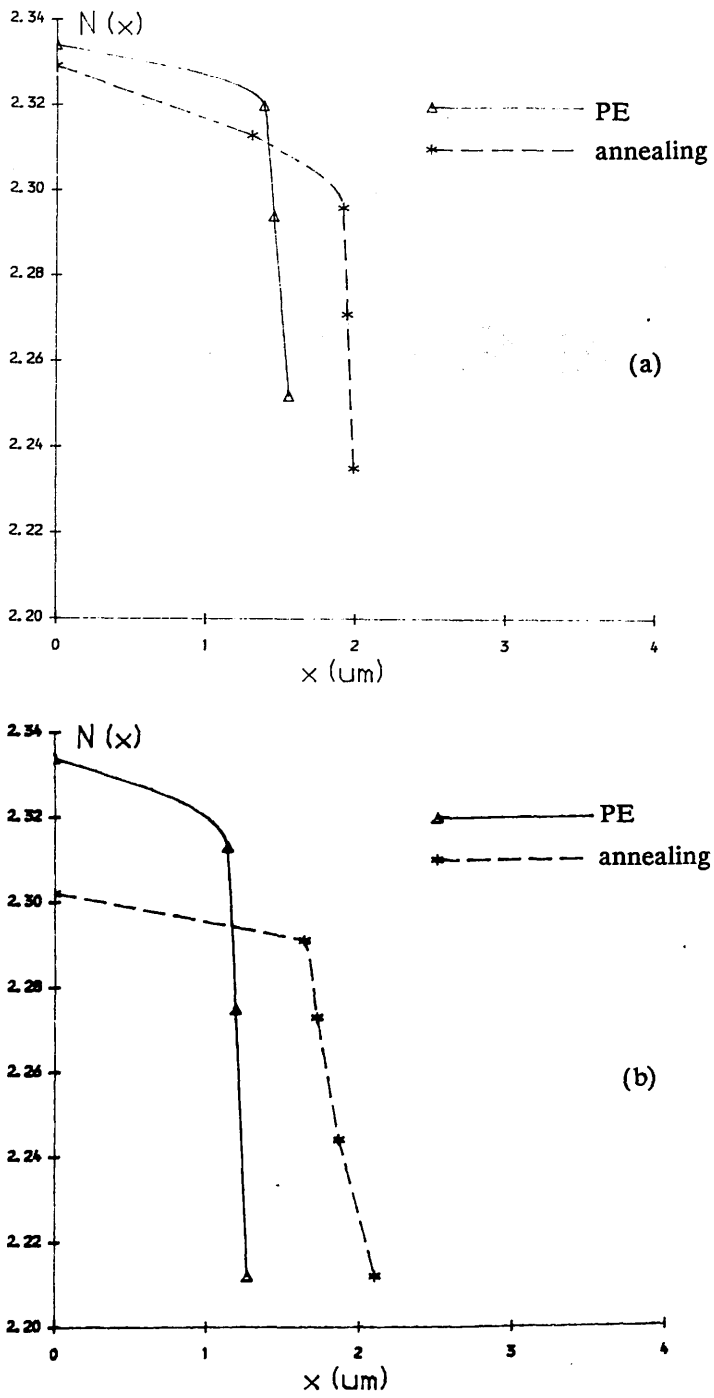

Figure 3—21 Index profiles before and after annealing. PE: benzoic acid, 235 °C, 90 minutes; annealing: 10 minutes at (a)320 °C and (b)380 °C

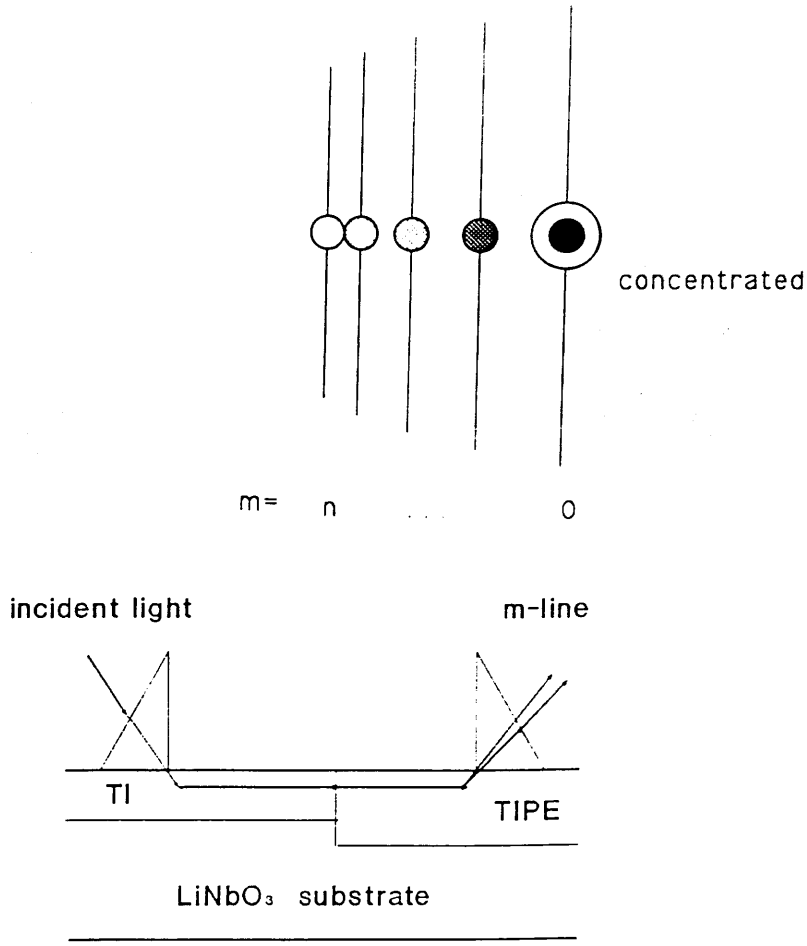

Figure 3– 22 Arrangement of coupling efficiency measurement.

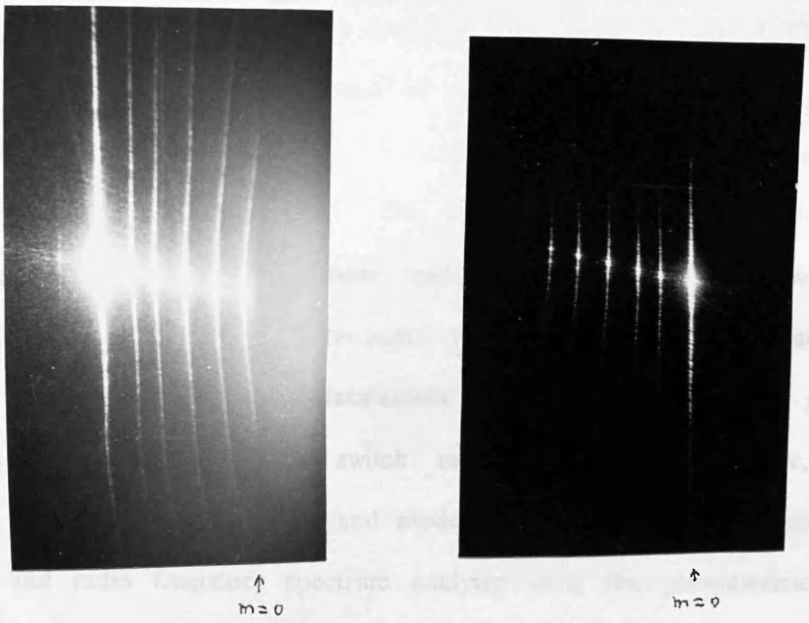

(a) (b)

Figure 3−23 (a): Coupling from a fundamental mode in DPE waveguide into the modes in PE waveguide. DPE: 1% dilute benzoic acid, 210 °C, 50 minutes; annealing: 320 °C 10 minutes; PE: 235 °C, 3 hours. (b): same as (a) but without annealing.

CHAPTER FOUR: $LiNbO_3$ WAVEGUIDE TECHNOLOGY

IV.1. Introduction

Lithium niobate ($LiNbO_3$) has been for many years a favourite with scientists because of its acousto–optic, electro–optic, piezoelectric and non–linear properties. Since the availability of waveguide fabrication on $LiNbO_3$ came true a great variety of devices have been invented, switch matrices, frequency shifters, computing processors, A/D and D/A converters and modulators using its electro–optics property, correlators and radio frequency spectrum analyser using the piezoelectric effect and acousto–optic properties, wavelength multiplexers and demultiplexers using its non–linearity property, and various kinds of sensors. Its connection with optical fiber is attractive for the future communication system. Many reviews have dealt with the device application of $LiNbO_3$ [Neyer 1990, Taylor 1987, Tsai 1988, Verber 1984 and Voges 1987].

$LiNbO_3$ waveguide can be easily made by allowing Li_2O out–diffusion from the surface at high temperature ($>800\,^0C$) forming an index–increased layer [Kaminow 1973]. The out–diffusion waveguide has an increased extra–ordinary refractive index which, along with the depth of the waveguide, increases with annealing time as $t^{1/2}$ [Kaminow 1973]. Metal atom in–diffusion can increase refractive index, larger than out–diffusion [Schmidt 1974]. The increase of refractive index is proportional to the original metal film thickness and the depth increases with annealing time. So both parameters can be controlled separately. Many metals have been found to yield good waveguides when indiffused, e.g. Au^-, Ag^-, Fe^-, Co^-, Nb^-, Ge^-, V^-, Ni^- and Ti^- [Schmidt 1974], but finally Ti^- was chosen as the standard technique. Titanium in–diffusion (TI) takes place

at a high temperature, normally round 1000 °C and the maximum increase of refractive index is about 0.02.

Another $LiNbO_3$ waveguide fabrication technique is proton exchange (PE) [Jackel 1982a]. Proton–exchange takes place at about 200–240 °C and the increase of refractive index is about 0.12–0.13. Benzoic acid [Jackel 1982a], pyrophosphoric acid [Goto 1989] and adipic acid [Pun 1991] etc. have been used to provide protons. Ti–indiffusion and proton–exchange can be combined as a TIPE technique [Micheli 1982]. Ti indiffusion (TI), proton–exchange (PE) and TIPE are now standard techniques for $LiNbO_3$ integrated optics devices.

In the next section there will be some description of TI technique and the emphasis will be on Li_2O out–diffusion because it has been a controversial problem. Section IV.3. is about the PE technique. Section IV.4. discusses the combination of TI and PE technology, so called TIPE. Section IV.5. and IV.6. are about buried TIPE waveguide polariser and erbium doping in $LiNbO_3$, which are interesting even though they do not find use in the thin film lenses.

IV.2. Titanium In–Diffusion (TI) on $LiNbO_3$

TI waveguide is preferred as the low index waveguide of the lens because of its good stability. Once it is formed it will not be affected by subsequent proton exchange and annealing processes which will be used to form high index waveguide. The attenuation of TI waveguide is smaller than that of PE waveguide, although there were some reports of very low attenuation dilute proton exchange (DPE) waveguide [Loni 1988]. Another advantage of using TI waveguide is its higher electro–optic coefficient accompanied by the acousto–optic effect, resulting in large Bragg diffraction [Davis 1984], while the disadvantage is its poorer photorefractive threshold [Becker 1983].

IV.2.1. TI on $LiNbO_3$

The diffusion of Ti^- into $LiNbO_3$ increases the refractive index. TI processing is done as follows: deposition of high purity Ti metal film on the optical quality $LiNbO_3$; annealing the sample at about 1000 °C to allow the metal to be fully in− diffused.

The control of Ti film thickness must be addressed because it determines the index increase. The thickness monitor has proved to be unreliable because the relative positions of the sensor and the sample differs from time to time, so every time after deposition the thickness should be checked by TalyStep (RANK TAYLOR HOBSON) which has an accuracy of 1% down to 1nm. If the thickness is wrong, etch away Ti film in $HF:H_2O = 1:26$ for half minute and deposit again. The nonuniformity of Ti of about 10% can be achieved over the 10mm substrate [McLachlan 1981]. The sample for planar waveguide lenses should be more than 35mm long and the nonuniformity will be bigger than 10%. Sputter deposition can give a larger area of more uniform film thickness, an estimated nonuniformity of 5% in 50mm [McLachlan 1981], but unfortunately such a system was not available.

The arrangement of Ti diffusion is shown in figure 4−1. The sample is put on a Pt foil above a quartz boat. Such an arrangement is intended to hold some $LiNbO_3$ powder in the quartz boat to suppress Li_2O out− diffusion [Esdaile 1978]. Water vapour is normally used to reduce Li_2O out− diffusion [Jackel 1982b] and has been shown to improve waveguide quality. The water column used to saturate the flowing gas is heated to 90 °C before inserting the sample in the furnace and is kept at constant temperature during annealing. Either oxygen or argon bubbles through the water column and bringing the water vapour into the furnace tube. When the sample is heated up to 1000 °C, the time is noted. When annealing is finished, the furnace is switched off but the hot water vapor is passed until the sample is cooled

down to about 500 °C. If the there were still water vapour in the tube at lower temperature, the vapour would condense on the tube wall and then fall down on to the sample and the sample would be broken. The boat is then drawn out to the tube end and, after it reaches room temperature, the sample is taken out.

IV.2.2. Li_2O Out–Diffusion

Li_2O out–diffusion occurs when a $LiNbO_3$ sample is heated up to above 800 °C, introducing a spurious waveguide and resulting in an index profile which is a combination of the index profile of out–diffused waveguide and that of TI or TIPE waveguide. There might be some guided modes additional to the pure TI or TIPE modes. When the light beam crosses the boundary of two waveguides some power will inevitably be coupled into the out–diffused guide, and this has been observed in the m–lines of a prism coupler as shown in figure 4–2, even though the loss was small in some cases. In a 4–element planar lens light was coupled into out–diffusion modes at every boundary as shown in figure 4–3, decreasing the signal level and introducing noise. Figure 4–3(b) shows a computer model of such out–diffusion mode refraction.

Several techniques have been suggested for the suppression of lithium oxide out–diffusion. Carrying out the Ti indiffusion in a flowing atmosphere containing water vapour seems to reduce the mobility of Li and Ti by occupying some of the vacancies with H^+ ions [Jackel 1982b]. Out–diffusion cannot be suppressed completely by this mechanism because some Li^+ escapes before the H^+ occupation. But if the out–diffusion can be reduced sufficiently, and out–diffused layer may be too shallow to support a guided mode, the out–diffusion can be considered to be suppressed. On the other hand, if the out–diffusion is to such an extent that the mode confined in the TI layer and the modes in the TI plus out–diffusion layer are mismatched with each other, the excited TI mode is hardly coupled into out–diffusion modes at the boundary of two different waveguides. This phenomenon

was observed by a colleague* where on some TI strip waveguide samples, in which no major defects had been produced during processing which would scatter guided light into out−diffusion modes, a pure TI strip mode was seen by suitably adjusting the incident light angle even though there was an out−diffusion waveguide all over the sample. Here the water vapour was thought to be good to improve the boundary quality, instead of completely suppressing the Li out−diffusion, and hence reduced the scattering into out−diffusion modes (then no out−diffusion mode could be seen). Some authors found the absence of an out−diffusion mode on the sample just by using a dry oxygen and argon atmosphere [Fouchet 1987], without using any water vapour or $LiNbO_3$ powder. In such a case the out−diffusion should not have been suppressed. By saturating the atmosphere in which the diffusion is carried out with Li_2O vapour, out−diffusion may be fully suppressed: indeed, lithium in−diffusion has been reported by this means [Burns 1978], provided the Li vapour pressure is high enough. But care should be taken to guarantee surface quality; the $LiNbO_3$ powder which was used to provide the Li_2O atmosphere will stick on the sample surface. If the atmosphere is closed and of small enough volume the substrate itself may be able to supply the saturated vapour pressure without the generation of an out−diffused layer capable of supporting a mode [Esdaile 1978 and Neyer 1987]. But the reproducibility of the first system [Esdaile 1978] was found questionable later, and the author of the second paper [Neyer 1987] later found that their system's "reproducibility in the visible to the near infrared range remains critical" [Neyer 1990]. Some groups found that the result varied with the sample batches, under the same waveguide fabrication processing condition.

In a first series of experiments, as arranged in figure 4−1, out−diffusion modes were always found by prism coupling in slab waveguide samples processed at 1000 °C for 4h or longer in flowing wet oxygen. The oxygen was bubbled at 1.0 to 1.5ℓ/minute through a 15cm high water column at >90 °C. In a second series of experiments the sample was placed polished face up on a bed of $LiNbO_3$ powder, to provide a local atmosphere rich in Li_2O vapour. The quartz boat containing the sample and

the powder was covered with platinum foil, and either dry or wet oxygen flowed through the furnace tube. In some cases no out-diffusion mode was seen but then the crystal surface was damaged and the TI waveguide mode suffered from scattering. In the third experiment a platinum box [Neyer 1987] containing a sample was buried in $LiNbO_3$ powder, to fully seal off the box, and annealed at 1000 °C for 4 hours. An out-diffusion mode was still found.

For a fourth series of experiments, in an attempt to provide a local atmosphere saturated with Li_2O vapour, two samples were placed face-to-face and buried in $LiNbO_3$ powder while being annealed in air at 1000 °C for 4 hours. The arrangement is depicted in figure 4-4. It was expected that such an arrangement would provide a very controlled environment for the sample surface. Out-diffusion modes could not be observed in a pair of virgin samples but were seen in a pair of TI samples (with Ti film). In an ideal circumstance with two face-to-face samples tightly bound together and buried in $LiNbO_3$ powder, the surfaces are surrounded by the same material as within bulk material. There is no way for the Li_2O to diffuse out. If the areas of two samples are big enough the practical case could be thought of as an ideal one, which might be the reason of that the virgin samples were free of out-diffusion mode. For the TI samples, the Ti film will abstract oxygen from $LiNbO_3$ for its oxidization and the TiO forms islands on the surface, which separate the two samples and give way for Li_2O to diffuse out, even though the outlet could be imagined as very limited.

* Mr. Dejie Li was on leave from Tsinghua University of P. R. China

IV.2.3. Single Mode TI Waveguide

For the purpose of making a thin-film lens, a single mode waveguide should be

formed in the low index region of the lens, and it should satisfy the following conditions:

1) will support only the fundamental mode and is near the cutoff of the 1st mode as required in Chapter Three;

2) should have low loss, because the light will have a path of several centimeters in an integrated optical spectrum analyser device and will be scattered too much if the loss is too high;

3) the depth should not be too large, because otherwise it would be very difficult for a high index waveguide to match it well.

There are three parameters in TI processing: thickness of Ti film, temperature and time of annealing. There are two parameters which characterize the waveguide: depth a and index increase $\triangle n$. Here a Gaussian index profile is assumed [McLachlan 1981]:

$$n(x) = n_2 + \triangle n \times \exp(-(x/a)^2) \qquad (4\text{-}1)$$

$$\triangle n = C \times d \div a \qquad (4\text{-}2)$$

$$a = 2 \times (D \times t)^{1/2} \qquad (4\text{-}3)$$

$$D = D_0 \times \exp(-T_0/T) \qquad (4\text{-}4)$$

where n_2 denotes substrate index, d Ti film thickness, t diffusion time, T diffusion temperature, D diffusion coefficient, D_0, T_0 and C constants. T and T_0 should be expressed in Kelvin (K).

Once n_2, D_0, T_0 and C are determined the index profile is known as function of T, t and d. Then the relationship between single mode waveguide parameters a and Δn and processing parameters T, t and d can be found. This would be helpful to find the suitable processing parameters for single mode waveguide satisfying conditions described previously.

a) x−cut $LiNbO_3$ at T=1038 °C

Experiments on x−cut $LiNbO_3$ at T=1038 °C were carried out. The Ti film thickness and diffusion time were set as follows:

t(hr)	3	5	7	9	12	15	18
d(μm)							
0.025	V	V	V	V	V	V	
0.040			V	V	V	V	V
0.060			V	V	V	V	V
0.080		V	V	V	V	V	V
0.100				V	V	V	V

Using the IWKB method, we obtained the surface index $n_{surface}$ and depth a of the waveguide after measuring the mode effective indices. By plotting a vs $\sqrt{t}$, as in figure 4−5, we get the slope of the straight line $a = 2 \times \sqrt{(D \times t)}$, giving $D(T=1038\,^{\circ}C) = 0.47\,\mu m^2/hr$. By plotting $n_{surface}$ vs d, as in figure 4−6, we get the slope of the straight line $n_{surface} = C \times d \div a$. With a calculated from (4−3), C = 1.072. By averaging more than 30 measurements, the average substrate index $n_2 = 2.2009$. So (4−1) is re−written as

$$n(x) = 2.2009 + 1.072 \frac{d}{2 \times \sqrt{(0.47t)}} \exp\left(-\left(\frac{x}{2 \times \sqrt{(0.47t)}}\right)^2\right) \qquad (4\text{-}5)$$

From figures 4−5 and 4−6, it is seen that the results were fairly scattered and

would have introduced a large error in extrapolation. This may have been due to errors in the Ti film thickness. It was later found that, by checking the thickness with TalyStep, the monitor reading varied from time to time, because of the change of distance between sample and the crystal detector.

From (4−5), we can find the conditions under which the waveguide can guide only a single mode. Figure 4−7 shows the boundary conditions. In the region M=0, the waveguide made with the corresponding values of d and t guides only the fundamental mode. Below this region, the waveguide is cut−off. Above this region, the sample will support more than one mode.

b) x−cut $LiNbO_3$ at T=1000 °C

At T=1038 °C, D=0.47 μm^2/hr, and fabrication of a waveguide with a=2 μm takes only 2hrs. Because of the thermal inertia of the diffusion oven, the control of the process will be easier if the diffusion time could be longer. So we have deduced the result of lowering T from 1038 °C to 1000 °C.

Using (4−4) and D(T=1038 °C)=0.47 μm^2/hr, and quoting the data of $T_0 = 2.9 \times 10^4 K^0$ from [McLachlan 1981], we get $D_0 = 1.9 \times 10^9 \mu m^2$/hr. Then we obtain D(T=1000 °C) = 0.24 μm^2/hr. Figures 4−8 and 4−9 show the single−mode waveguide condition as a function of d, t and d, a respectively.

It was estimated [Canali 1984] that it will take 0.015hr for complete indiffusion of every angstrom of Ti film at a temperature of 1000 °C. This gives a requirement of diffusion time needed to completely indiffuse a certain thickness of Ti film. This requirement is drawn as straight line L1 in figure 4−8, the slope of which is 0.0066 μm/hr. In [Canali 1984], the experiments showed that there existed a diffusion time at which the loss of waveguide reached minimum. On y−cut $LiNbO_3$, a 0.025 μm Ti film needed a diffusion time about 9hr and a 0.055 μm film needed

about 16hr at 1000 °C. We could link these points using a straight line slope of 0.003 μm/hr which is drawn in figure 4−8 as L2. The point at the intersection of L2 and the upper boundary of M= 0 region represents a waveguide of a= 2.4 μm. This depth should be reasonable. Now the waveguide represented by the points both on the straight line L2 and near the upper boundary will be satisfactory.

As an example, we pick up two points A and B as our selection of single mode waveguides as shown in figure 4−8 and 4−9. The point A represents a single mode waveguide near the cut−off of the second mode on x−cut $LiNbO_3$, made with a 15nm Ti film and annealed at 1000 °C for 5 hours, giving an index increase of 0.0073 and depth of 2.2 μm. The point B represents a similar waveguide made with a 17nm Ti film and annealed for 5.5 hours, giving an index increase of 0.0079 and depth of 2.3 μm.

c) z−cut $LiNbO_3$ at T= 1000 °C

The same experimental procedure was carried out on z−cut $LiNbO_3$ at T= 1000 °C. The Ti film thickness and diffusion times were taken as follows:

t(hr)	9	13	15	18
d(μm)				
0.025	V	V	V	V
0.050	V	V	V	V
0.065	V	V	V	V
0.080	V	V	V	V

The average refractive index of the substrate is n_s= 2.2022. The empirical expression for waveguide index profile is

$$n(x) = 2.2022 + 1.56 \frac{d}{2 \times \sqrt{(0.38t)}} \exp\left(-\left(\frac{x}{2 \times \sqrt{(0.38t)}}\right)^2\right) \qquad (4\text{-}6)$$

Figures 4−10 and 4−11 show the conditions for making a single mode TI waveguide on z−cut $LiNbO_3$. In figure 4−10, the straight line L represents the time requirement to get a fully indiffused and low loss waveguide. The experimental data is not available and here a somewhat larger slope of 0.004 μm/hr is used because the indiffusion rate on z−cut $LiNbO_3$ is bigger than on the x−cut sample. The point A represent a single mode waveguide near the cut−off of the second mode on z−cut $LiNbO_3$, made with 12nm Ti film and annealed at 1000 °C for 3 hours, giving an index increase of 0.0088 and depth of 2.1 μm.

IV.3. Proton Exchange (PE) on $LiNbO_3$

Exchange of some elements with the elements in the solid may increase the refractive index of the solid, as exemplified by potassium and silver in exchange with sodium ions in soda−lime glasses and proton (H^+) in exchange with lithium ions in $LiNbO_3$. The reaction of proton exchange takes place in the range of 150−300 °C and is represented as [Loni 1989]:

$$LiNbO_3 + xH^+ \rightarrow Li_{1-x}H_xNbO_3 + xLi^+ \qquad (4-7)$$

Such an exchange causes an increase of extraordinary refractive index about 0.12−0.14 and a decrease of ordinary refractive index about 0.04 [De Micheli 1982], which means that only TE modes are guided in x−cut and y−cut waveguides and TM modes on z−cut waveguides.

IV.3.1. Pure Proton Exchange on $LiNbO_3$

Proton−exchage is the only way at present to produce a high index increase in $LiNbO_3$. The diffusion rate of proton−exchange at 235 °C is about 0.4 μm/hr on an

x− cut and 0.3 μm/hr on a z− cut TI waveguide. The diffusion rate is greater on a virgin sample than on the TI waveguide sample, and is greater on an x− cut sample than on a z− cut sample.

IV.3.2. Dilute Melt Proton Exchange (DPE)

There are some advantages in using DPE waveguide as the low index waveguide in thin film lens fabrication. The threshold of photorefractive damage is higher than that of TI waveguide [Becker 1983]. This is important in thin film lenses where the light power density is very high in the beam focus region. If a 1mm wide incident beam is focused into a 1 μm wide spot with 3dB(50%) loss through the lens, the light power density at the focus is 500 times that of incident beam. A DPE waveguide can be made shallower than a TI waveguide, which is important for high frequency SAW applications [Tsai, 1979]. Calculation in chapter III shows that if both low and high index waveguides have step− like index profiles, by means of DPE and PE, respectively, the coupling efficiency is much better than that if the low index waveguide has a gradient index profile while the high index waveguide has a step− like index profile, by means of TI (or annealed DPE) and TIPE, respectively. A disadvantage of DPE waveguide is its higher scattering loss, especially for un− annealed samples. On the un− annealed DPE sample the scattering can be easily seen on the waveguide surface. It has been reported that annealed DPE sample can have very low attenuation [Loni 1988].

IV.3.3. Proton Exchange Plus Annealing

The protons will re− distribute at enhanced temperature, 250− 400 ^{0}C, and then the index profile is modified. Annealing also changes other parameters, such as electro− optic coefficient and attenuation [Loni 1989]. It has been reported that annealing improved waveguide quality on y− cut [Varasi 1987] and x− cut [Loni 1988] but worsened it on z− cut [Loni 1988]. In our experiment, no decrease of

attenuation on DPE z− cut sample was observed upon annealing. As seen in the chapter III, annealing makes it difficult for the low index DPE waveguide to match high a index PE waveguide.

IV.4. TIPE Waveguide on $LiNbO_3$

Proton− exchange may also take place on TI waveguides, forming so called TIPE waveguide but the exchange rate is reduced [De Micheli 1982]. If a mask is used to block the proton exchange on some region of the TI waveguide and allows the unmasked area to be proton exchanged, the TIPE waveguide can be used as high index waveguide while the TI waveguide (masked area) remains low index waveguide.

The index increases by Ti− indiffusion and proton− exchange are additive [De Micheli 1982]. It was reported that the index increase by proton− exchange in pure benzoic acid was about 0.11 and by Ti− indiffusion and proton− exchange was about 0.12, while that by Ti− indiffusion was about 0.014 [De Micheli 1982]. In our experiments, the index increase by proton− exchange in pure benzoic acid is about 0.13 and that by Ti− indiffusion and proton− exchange is about 0.14, while that by Ti− indiffusion is about 0.01 to 0.02.

Figure 4− 12 shows the index increase profiles of a TI waveguide and an out− diffusion waveguide, both samples were x− cut and underwent the same annealing processing and then should have the same out− diffusion waveguide structure. In the figure 4− 12, the index increase profile, $\triangle n(x)$, of TE mode in TI waveguide (TE:TI) is the sum of that of TM mode in TI waveguide (TM:TI) and that of TE mode in out− diffusion waveguide. The out− diffusion does not increase the ordinary refractive index and therefore the TM:TI index profile has no such a tail as TE:TI index profile. This result shows that the index increase is the sum of that by

Ti indiffusion and that of by out−diffusion. Because proton−exchange has very similar characteristics as out−diffusion, this phenomenon should happen for TIPE waveguide, i.e. the index increase is the sum of that by Ti indiffusion and of that by by proton exchange.

If the PE waveguide is deep enough, much more than TI waveguide, the low ordinary index layer can act as a substrate upon which there is an index−increase layer by Ti indiffusion, as shown in figure 4−13. Then there is a waveguide for the ordinary refractive index. Guided waves in such waveguides have been found in our experiments. By combination of proton exchange and annealing, the decrease of the ordinary index is adjustable in the range of 0 to 0.04, while the effective index for the ordinary modes is also adjustable. This phenomenon has been used for controlling birefringence [Hinkov 1986]. In this way, two waveguides can be formed: TI waveguide with high ordinary index and TIPE waveguide with low ordinary index, of which the index difference is about 0.04. These two waveguides have same index profiles, as shown in figure 4−13, with slightly different substrate indices, and therefore will have perfect mode match. If TI waveguide is still required as the surrounding area, because of its lower attenuation than TIPE waveguide, the TIPE lens region waveguide has to be a low index one. That means a concave lens. The index difference is too small for the homogenous refracting lenses but it is big enough for Fresnel's lens. Such a concave Fresnel's lens has been developed on glass waveguide [Pitt 1988]. There is at least one advantage for deploying such waveguide system: TM mode is to be used on x−cut or y−cut $LiNbO_3$, which is related to ordinary refractive index and is completely isotropic.

IV.5. Buried Titanium Indiffusion Waveguide and Polariser *

*:In addition to the main object of waveguide lens study, some work on other integrated optical devices was carried out and is described in this section and next

section. This work was done in cooperation with Dr. Feng Zhou in this department. He did double proton exchange in an attempt to bury waveguide, proton exchange waveguide on Er:$LiNbO_3$, measurement of photo-luminescence spectrum of Er:Ti doped waveguides and end-fire coulping of buried waveguides. His co-work is greatly appreciated.

Burying a waveguide is attractive in reducing surface scattering loss and modifying the mode profile to suit optical fibre coupling. Since buried waveguide on $LiNbO_3$ has lower propagation losses and a more symmetric intensity profile than surface waveguide, it may be useful for integrated optical devices such as miniature solid-state waveguide lasers and polarisers which have been formed in surface waveguide [Ctyroky 1986, Stock 1988 and Han 1991]. Recently buried PE waveguide has been reported [Jackel 1991], but when the same procedure was repeated no clear evidence of the waveguide's being buried was observed. Buried TIPE waveguides have also been demonstrated, but the refractive index profile was asymmetric, just as for surface waveguide [De Micheli 1983]. Buried $LiNbO_3$ waveguides can also be made by ion-implantation but again the index profile tends to be asymmetric [Chandler 1990].

Ti indiffusion increases both the ordinary (n_o) and the extraordinary (n_o) refractive indices, and hence TI waveguide can guide both TE and TM modes on x, y and z-cut $LiNbO_3$. The TE mode in such guides is subject to the ordinary refractive index on z-cut $LiNbO_3$ and, when propagating along the y direction, the extraordinary refractive index on x-cut $LiNbO_3$. The TM mode will be subject to the ordinary refractive index on x-cut $LiNbO_3$ and extraordinary refractive index on z-cut $LiNbO_3$. Subsequent stages of proton exchange will increase the extraordinary refractive index and decrease the ordinary refractive index. A shallow PE layer will reduce the ordinary refractive index of a TI waveguide near the surface but leave the index profile beneath unchanged, thus forming a buried waveguide. The increased extraordinary index layer can still guide a wave at the surface of the substrate and

this wave can be retarded by an additional cladding layer.

IV.5.1. Experiment

An x−cut $LiNbO_3$ substrate with a Ti film 100nm thick deposited on its surface was annealed at 1000 °C in a wet oxygen atmosphere for 15 hours. A z−cut $LiNbO_3$ substrate with a Ti film 65nm thick was annealed under the same conditions but for 13 hours. The index profiles were calculated from the measured effective refractive indices using the IWKB method and are shown in figures 4−14 and 4−15. A wavelength of 0.633 μm was used.

The samples were then immersed in pure benzoic acid at 235 °C for 40 minutes for the x−cut sample and 60 minutes for the z−cut sample to allow proton exchange to take place. After proton exchange the effective extraordinary indices of the waveguide modes were measured and the index profiles calculated, and are also shown in figures 4−14 and 4−15. No mode related to the ordinary refractive index (ordinary mode) was seen from prism coupling since, owning to the reduction of the ordinary refractive index near the surface, the waveguides were well buried. When end−coupling was utilised it was confirmed from observing the waveguide output that there were still guided ordinary polarisation modes on both samples. After annealing at 380 °C for 2 hours, to adjust the index profile, the effective extraordinary guided mode refractive indices were measured and the index profiles calculated (see figures 4−14 and 4−15), while the ordinary modes (single −moded) were still seen by end−coupling. The index profile could not be calculated for the buried ordinary modes, because the modal effective indices could not be measured. But the ordinary polarisation index profile could still be deduced from the extraordinary refractive index profile, for which the effective indices are always measurable. The maximum increase of extraordinary refractive index obtainable by benzoic acid proton exchange has been quoted as 0.11 and the maximum decrease of ordinary refractive index by proton exchange has been quoted

as 0.04 [De Micheli 1982], while in our experiment the maximum increase of extraordinary index by the proton–exchange process was about 0.13. The index increase for TI waveguide and for PE waveguide are additive [De Micheli 1983], so the index increase of TIPE waveguide is the sum of index increase for TI waveguide and for PE waveguide. The actual decrease of ordinary refractive index produced by proton–exchange in a TI waveguide can be taken as 0.04/0.11 times the actual increase of extraordinary refractive index by proton–exchange.

IV.5.2. Discussion

The progression of index profiles after processing by TI, PE and annealing are shown in figures 4.14 and 4.15 for the x–cut and z–cut $LiNbO_3$ samples respectively. Proton–exchange led to a step–like profile for both the extraordinary and ordinary indices, while the buried ordinary refractive index profiles (TM mode on x–cut and TE mode on z–cut material) were strongly asymmetric. Post–annealing changed the PE index profile into a Gaussian profile and the buried ordinary index profile turned into a nearly symmetrical one. The combination of different parameters for the TI, PE and annealing processes can give a variable index profile.

Mode profiles were measured using a video camera and a monitor, then fed into a computer. The dashed line in figure 4–16 is the measured optical intensity profile of a buried TM mode in an x–cut sample and is clearly quite symmetric. Figure 4–16 shows a computer model for a single ordinary TM mode buried waveguide on x–cut $LiNbO_3$. It has been assumed that titanium indiffusion produces a Gaussian profile increase in refractive index, while annealed proton–exchange produces a near Gaussian profile *decrease* in refractive index. The final buried index profile is then the sum of the two profiles. In figure 4–16(a), the parameters of the depth and index increase on the surface were obtained from fitting a Gaussian index profile to the ordinary index profile of TI waveguide in figure 4–15(a) and were estimated to be $\triangle n_1 = 0.013$ and $d_1 = 5.0 \mu m$, which gave

$$n_1(x) = 2.285 + 0.013 \times \exp(-(x/5.0)^2) \qquad (4\text{-}8)$$

where the substrate index was taken as 2.285. After Ti indiffusion, proton-exchange and annealing, a decreased ordinary Gaussian index profile was assumed to be superimposed on the TI waveguide ordinary index profile. From figure 4-15(a), the surface index had been reduced to the refractive index of the substrate, implying an overall decrease in the surface index of $\Delta n_2 = -0.013$. The depth of this decreased Gaussian index profile was assumed to be the same as that of the increased extraordinary index profile in figure 4-15(b) and was estimated to be 4.3μm. Then the final buried refractive index profile was the sum of the increased ordinary Gaussian index profile and the decreased ordinary Gaussian index profile:

$$n_2(x) = 2.285 + 0.013 \times \exp(-(x/5.0)^2) - 0.013 \times \exp(-(x/4.3)^2) \qquad (4\text{-}9)$$

Figure 4-16 also shows that the intensity profile of the TM mode has a nearly symmetrical shape in the buried waveguide. The distance between the peaks of the intensity profiles of the buried and unburied waveguides is about 3μm. In the experiments, we observed that, after proton-exchange and annealing, the position of incident light beam needed to excite a guided mode in the buried waveguide (TM mode on x-cut $LiNbO_3$ and TE mode on z-cut sample) was further away from the substrate surface than that needed to excite a mode in the surface waveguide (TE mode on x-cut sample and TM mode on z-cut sample), which is further evidence of the waveguide being buried. In figure 4-16, are also shown profiles of refractive index and intensity of surface TI waveguide.

The extraordinary mode will remain guided near the surface and it might be undesirable in some applications. It is quite possible to eliminate it by, for example, providing a surface index matching material or absorbing material (such as a metal electrode [Stock 1988], and in this case the buffer layer is not required) or by

deliberately roughening the surface.

The intensities of the TE and TM polarised modes were measured. Either the TE or the TM mode was excited by end–fire coupling. The intensities of the two modes were measured separately by changing the direction of a polarizing filter (without changing the incident intensity and end–fire coupling arrangement). On a 5mm long z–cut sample (where the TE mode is buried), it was found that the intensity of TM mode was lower than that of TE mode by 2dB. The higher loss for the surface TM mode can be attributed to the surface scattering and lower coupling efficiency at the waveguide ends due to mode mismatch (a strong asymmetry in waveguide index profile). After deposition of a 200nm thick aluminum layer on the surface, the TM mode was effectively absorbed and the extinction ratio was greater than >25dB (50dB/cm) under the same experimental conditions.

Because the prism coupling was no longer valid for the buried waveguide, optical loss was measured by cutback method on two 30mm long z–cut samples. One sample underwent Ti indiffusion only and held surface TM and TE modes. Another underwent Ti indiffusion, proton exchange and annealing and held surface TM modes and a buried TE mode. The measurement showed an optical loss for the buried TE mode of less than 1dB/cm compared with that for Ti indiffused surface TE mode of about 1.5dB/cm. The streak of light on the surface was obviously weaker for the buried waveguide mode.

IV.6. Erbium Indiffusion in $LiNbO_3$

Er is an important material in laser technology because it emits light at $\lambda = 1.5\mu m$ at which the optical fiber has minimum absorption, and therefore is useful in optical communications. Integration of laser and other components such as modulators

provides compactness, high speed and high efficiency for optical communications. Waveguide laser has recently been developed on $LiNbO_3$. The guided wave on these materials has a similar dimension as that in optical fiber and, specially in the buried waveguide as described in last section, provides good matching with optical fiber.

Er doped $LiNbO_3$ waveguide has been reported [Brinkmann 1991]. Because the diffusion coefficient of Er in $LiNbO_3$ is very small, it took about 80 hours for the 10nm thick Er to fully indiffuse in to the substrate 5μm deep at 1060 ^{0}C on z−cut $LiNbO_3$ (which has bigger Ti indiffusion rate than x−cut sample). Either titanium indiffusion or proton exchange can produce a waveguide subsequently, and in an ideal case it is expected that the Er is distributed to the same depth as the waveguide. In this section, an alternative method of Er diffusion is discussed.

The idea of this method is that if an alloy of Er and Ti is deposited on the $LiNbO_3$ surface and heated, the indiffusion of Ti *may* enhance the Er indiffusion.

Very recently similar work, which was done simultaneously with ours, was reported [Gill 1992] which demonstrated an approximately 15−fold increase in the diffusivity of Er into $LiNbO_3$ by co−diffusion with Ti and such an improvement was attributed to the increased partition coefficient of Er^{3+} when Ti^{4+} is available as a charge compensation mechanism. In their experiment, they used a temperature of 1050 ^{0}C and an annealing time of 20 or 40 hours.

The Er:Ti alloy is not available but a multi−layer structure was used for the same purpose. The structure and the thickness of each layer is shown in figure 4−17, which included 35nm Ti and 10nm Er. The measured thickness from the TalyStep was 48nm. After depositing the multi−layer on a x−cut $LiNbO_3$, the sample was annealed at 1000 ^{0}C in a water vapour environment as described in the section IV.2. for four hours. This processing was used to produce a single mode TI slab waveguide at 633nm wavelength, and also produced a single mode for this Er:Ti

co− indiffusion.

The sample ends were polished and the absorption spectrum and photo− luminescence spectrum were measured. The absorption spectrum showed some Er doping dependent features, however the features were somewhat masked by Ti dependent features and as yet it is not possible to obtain an accurate estimate of Er concentration from the absorption spectrum. The luminescence was excited using the 488nm line of an Argon ion laser and some care was taken to eliminate luminescence from anywhere other than the slab waveguide. Figure 4−18 shows the spectrum of photo− luminescence of the Er:Ti indiffusion sample (Er:Ti:$LiNbO_3$), and as comparison also shown are the spectrum from a Ti− indiffusion $LiNbO_3$ waveguide sample (Ti:$LiNbO_3$) and a waveguide sample which was bulk Er− doped at 0.2% mole and proton exchanged (Er:PE:$LiNbO_3$). The Er:PE:$LiNbO_3$ sample showed a peak between 1.45μm and 1.63μm. The Ti:$LiNbO_3$ sample showed a broad peak between 0.6μm and 1.3μm. The Er:Ti:$LiNbO_3$ sample showed a peak between 1.45μm and 1.63μm with a sharp peak at 1.52μm, associated with Er and a broad peak between 0.65μm and 1.3μm as associated with Ti, though a little narrower.

IV.7. Discussion and Summary

The controversial results imply that complete suppression of out− diffusion is very difficult. In some applications, e.g. strip waveguide, out− diffusion may not incur trouble. But in the case of a multi− element lens, there are 2m boundaries for an m− element lens and the power will be coupled from the fundamental mode into out− diffusion modes at every boundary, as shown in figures 4−2 and 4−3. So the coupling into out− diffusion mode must be minimised. From the review of previous work and experiment, it seems that the material of $LiNbO_3$ itself plays some role. On the waveguide lens samples, very weak out− diffusion modes were found sometimes.

From experiments, the relationship between the refractive index profile and processing parameters, Ti thickness d and annealing time t, was obtained assuming a Gaussian profile. By waveguide analysis, the relationship between single mode waveguide and processing parameters was obtained as well. Taking into consideration that the waveguide should have low loss and proper depth, we finally get a limited region in which the waveguides would satisfy the conditions needed to make thin-film lens.

Un-annealed DPE has high attenuation, while annealed DPE waveguide has a spread-out index profile and is difficult for the high index waveguide to match. TI waveguide has low attenuation and is stable afterwards. So TI waveguide is chosen as low index waveguide in waveguide lens fabrication even though the TI waveguide has lower optical damage threshold than DPE waveguide.

Ordinary polarization waveguide modes in TI waveguide can be effectively buried by proton-exchange. The index profile can be adjusted readily by annealing. The buried guide produced had reduced surface roughness scattering losses and provided a nearly symmetric optical intensity profile. The cladding layer attenuated the surface TM mode strongly and led to a high extinction ratio TE mode polarizer. In contrast to the PE waveguide polarizer, the buried TI waveguide polarizer holds the mode polarized with its main electric field component perpendicular to the optical axis on $LiNbO_3$ single crystals.

The enhancement of Er indiffusion by the presence of Ti is very interesting. In our experiment, the annealing temperature was lower, and the annealing time was much shorter than that used in [Brinkmann 1991 and Gill 1992] but an effective Er:Ti:$LiNbO_3$ waveguide was still obtained. The mechanism of such diffusion has not been well understood. There is a possibility that the indiffusion and oxdization of Ti changed the structure in $LiNbO_3$ crystal and left some spaces for the Er to come in. More experiments and theoretical analysis are required.

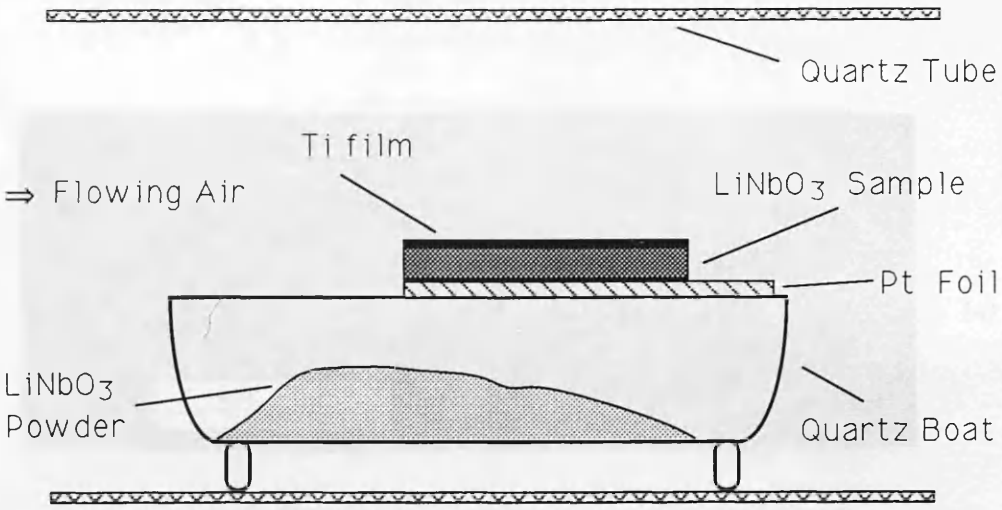

Figure 4-1. The arrangement of Ti indiffusion.

Figure 4-2. Coupling from TI mode into out-diffusion mode in the m-line from prism (shown by arrow) at a single boundary of TI waveguide and TIPE waveguide

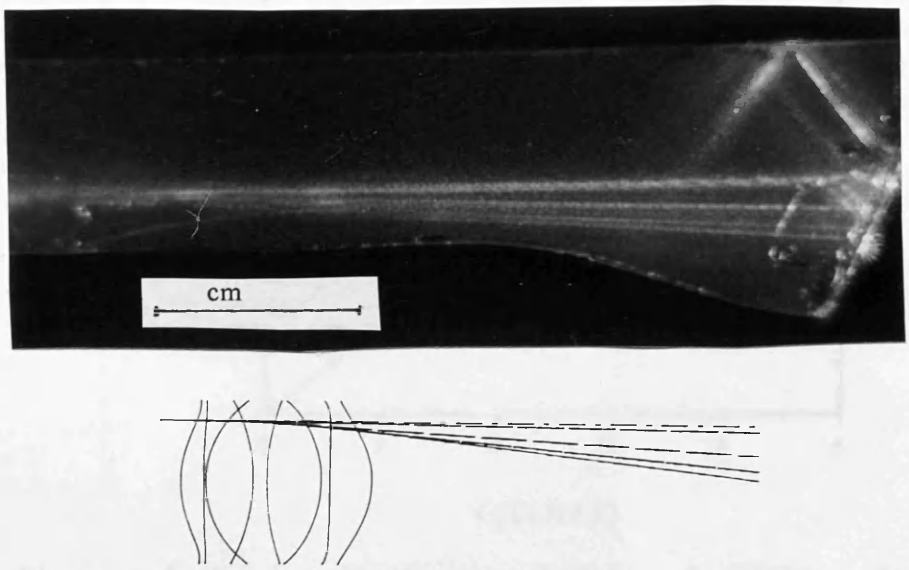

Figure 4-3. Coupling into out-diffusion modes at the boundaries of 4-element lens. (a):experimental result; (b): computed model. The fundamental mode has effective index n_h = 2.2904 in lens region and n_l = 2.2000 in waveguide region and is partially coupled into out-diffusion mode (n_o=2.2004) on every boundary.

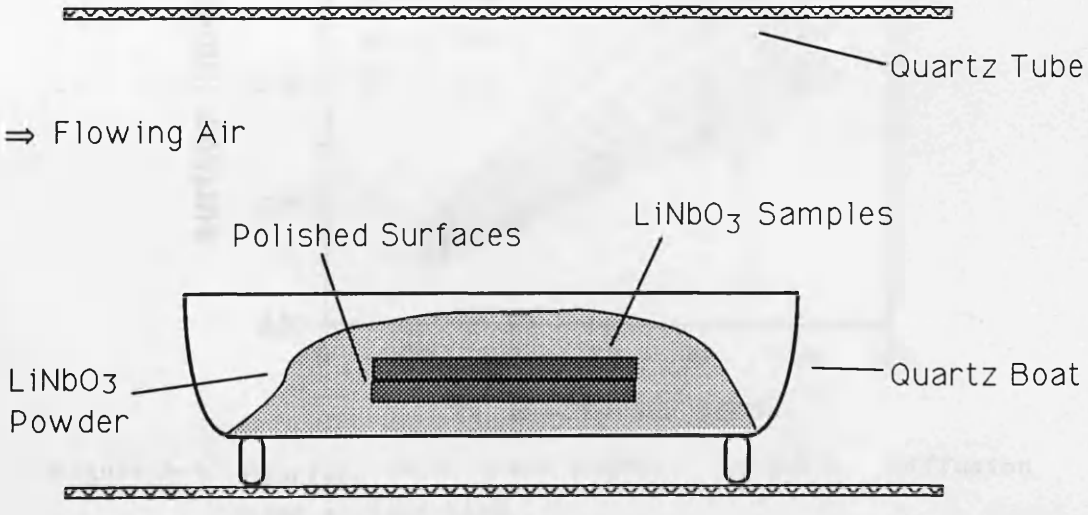

Figure 4-4. Arrangement of face-to-face diffusion.

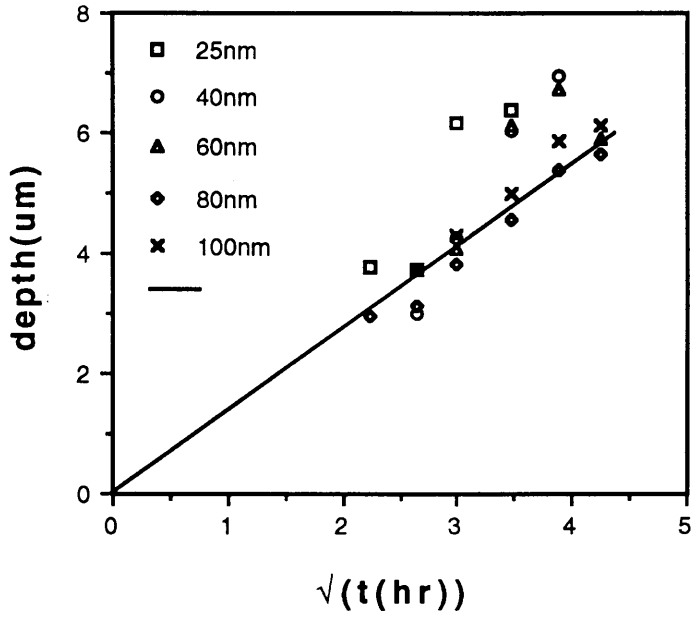

Figure 4-5. Depth a vs √t. x-cut $LiNbO_3$. T=1038°C. Ti film thickness as indicated. The slope of the straight gives a diffusion constant of 0.47μm^2/hr.

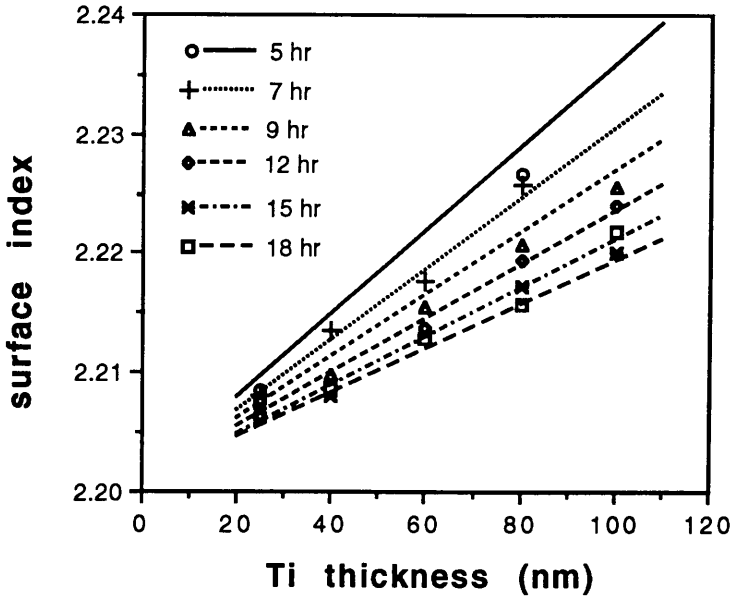

Figure 4-6. $n_{surface}$ vs d. x-cut $LiNbO_3$. T=1038°C. Diffusion time as indicated.

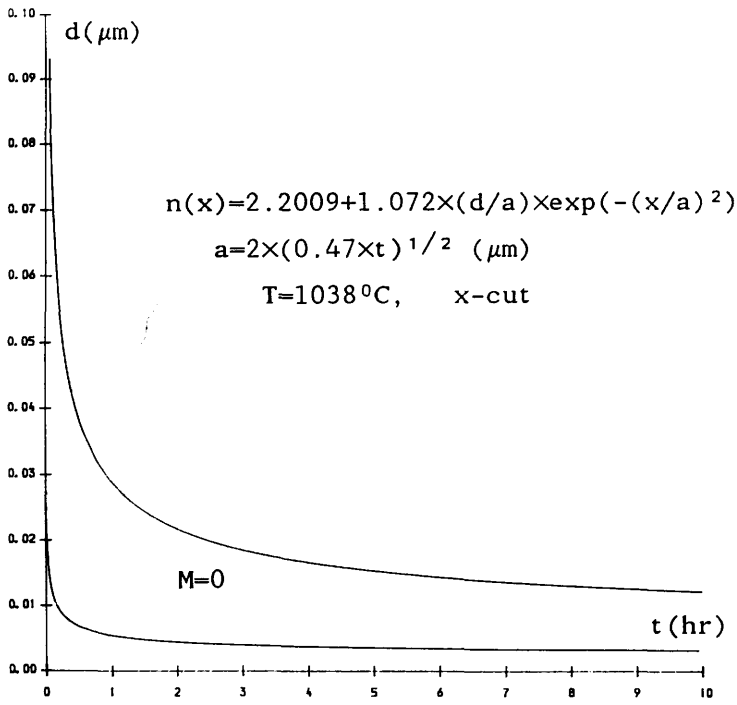

Figure 4-7. Single mode TI waveguide on x-cut $LiNbO_3$, vs Ti film thickness d and annealing time t at T=1038°C.

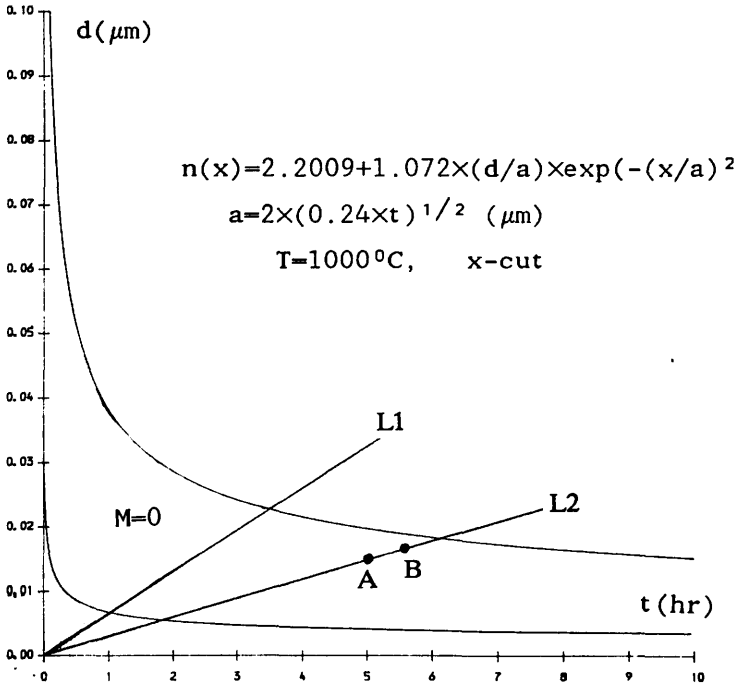

Figure 4-8. Single mode TI waveguide on x-cut $LiNbO_3$, vs Ti film thickness d and annealing time t at T=1000°C.

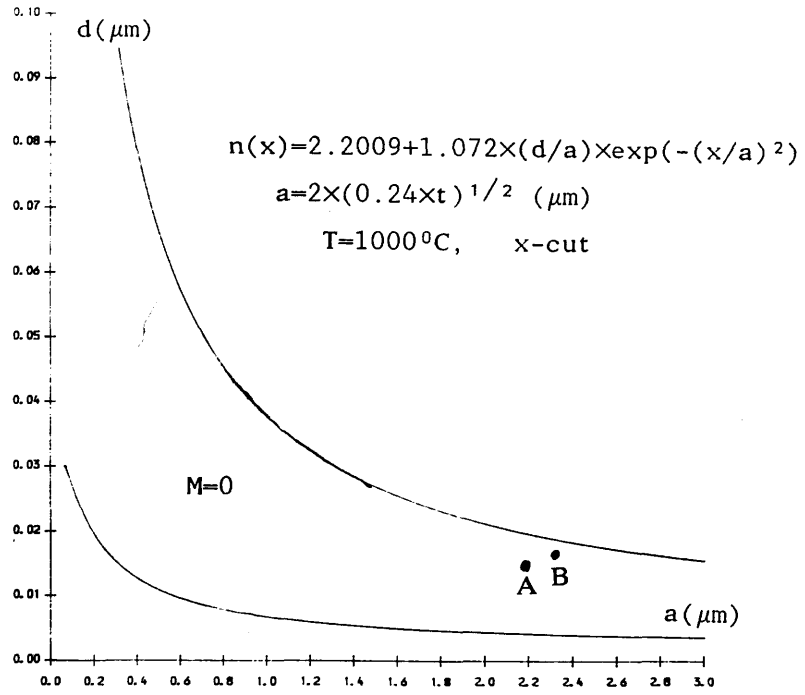

Figure 4-9. Single mode TI waveguide on x-cut $LiNbO_3$, vs Ti film thickness d and waveguide depth a at T=1000°C.

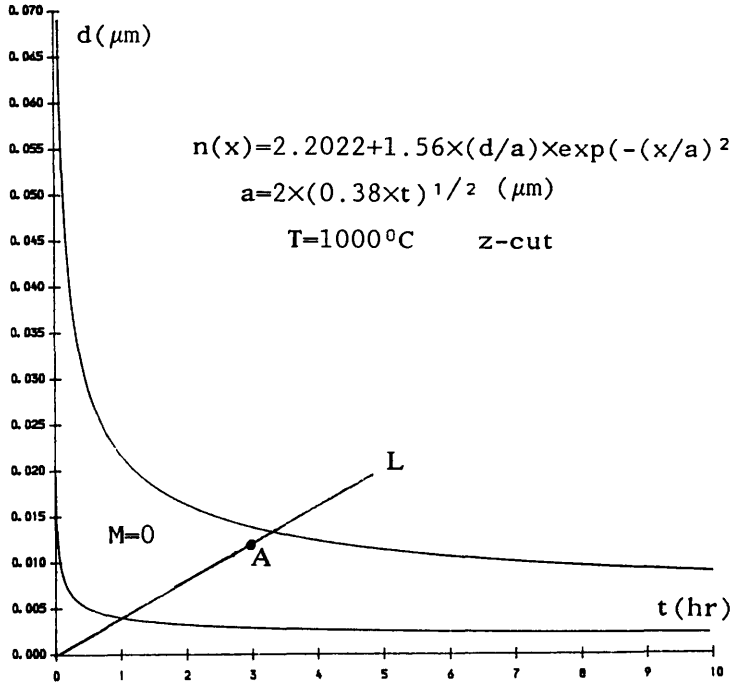

Figure 4-10. Single mode TI waveguide on z-cut $LiNbO_3$, vs Ti film thickness d and annealing time t at T=1000°C.

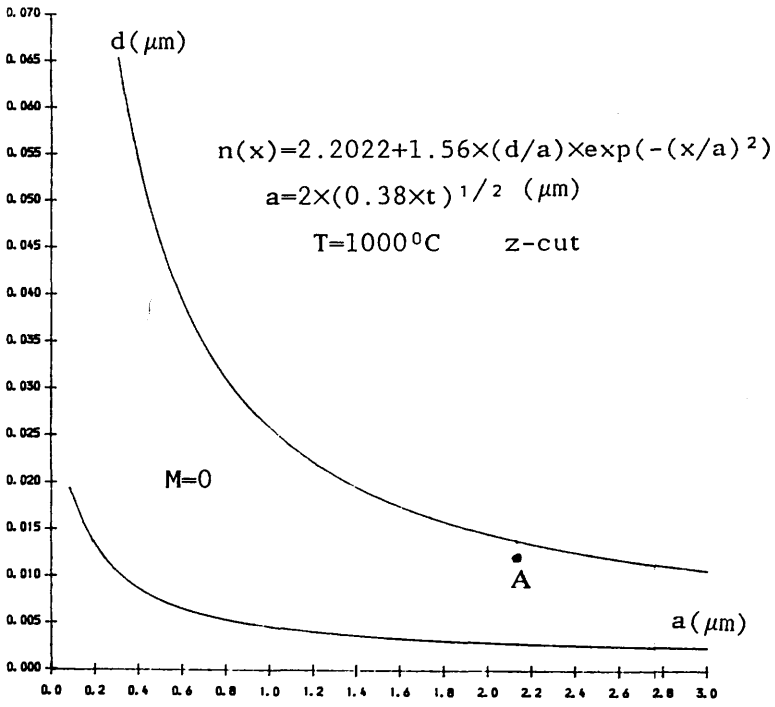

Figure 4-11. Single mode TI waveguide on z-cut $LiNbO_3$, vs Ti film thickness d and waveguide depth a at T=1000°C.

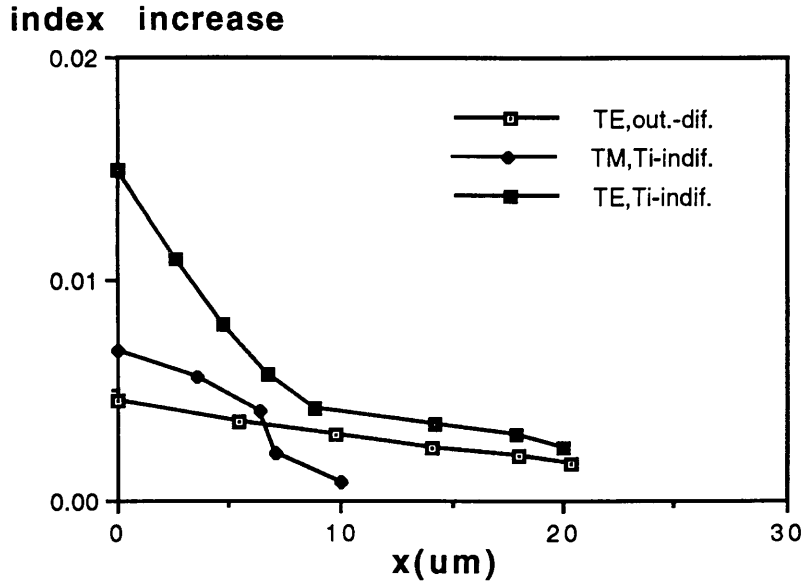

Figure 4-12. Index profile of TI waveguide and out-diffusion waveguide.

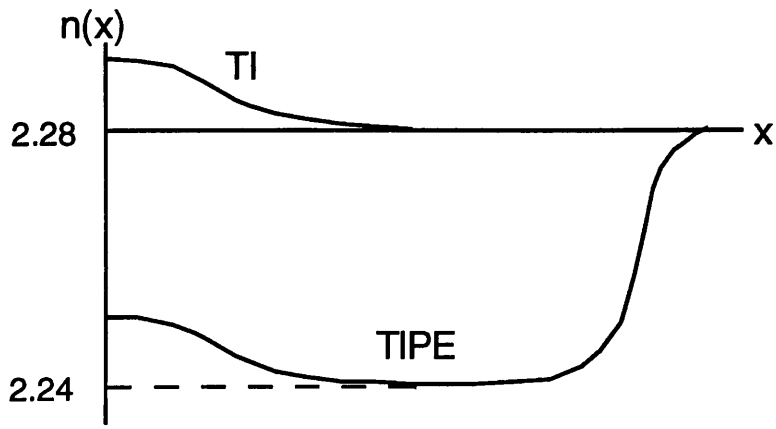

Figure 4-13. A TI waveguide with PE waveguide as the substrate.

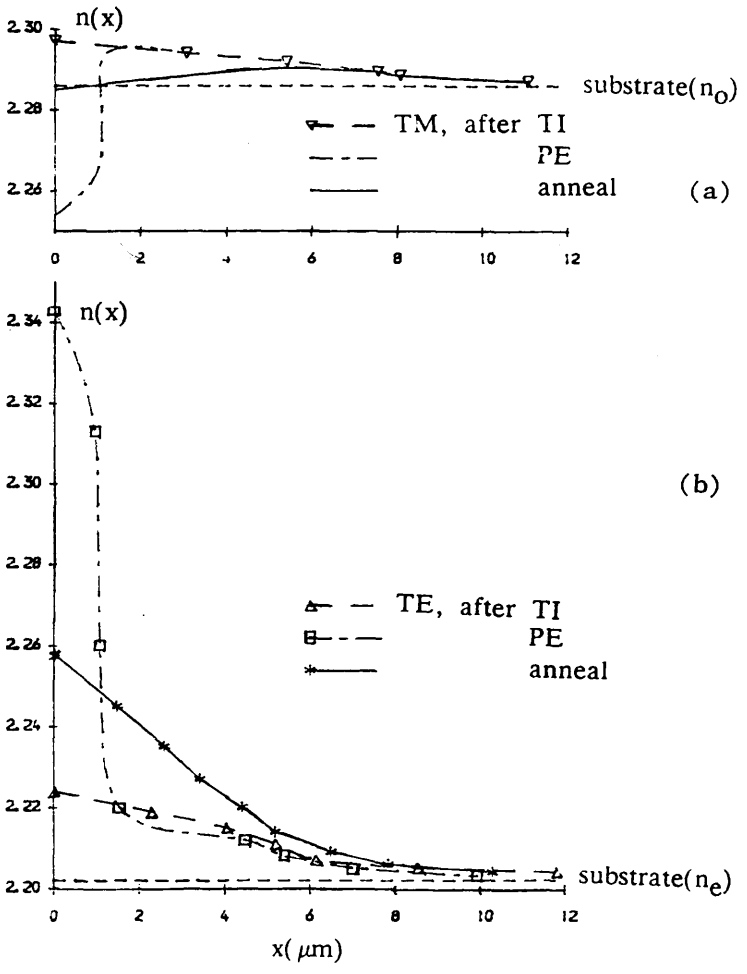

Figure 4-14. Measured profiles of (a): ordinary (TM mode) and (b): extraordinary (TE mode) refractive index on x-cut $LiNbO_3$. The sample undergoes Ti indiffusion, proton-exchange and annealing.

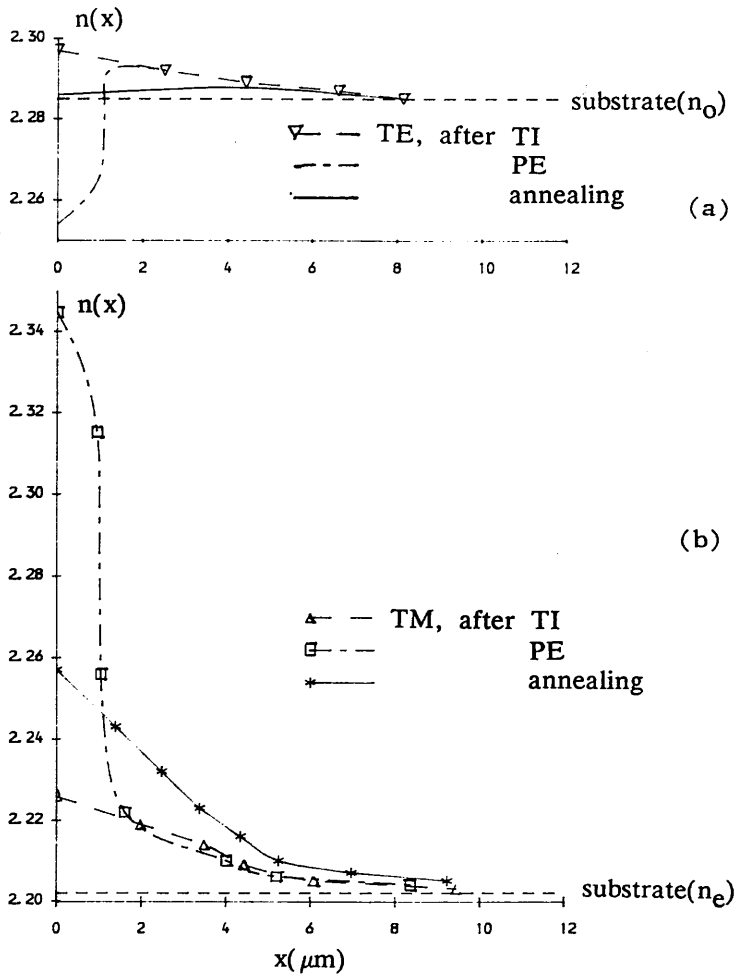

Figure 4-15. Measured profiles of (a): ordinary (TE mode) and (b): extraordinary (TM mode) refractive index on z-cut $LiNbO_3$. The sample undergoes Ti indiffusion, proton-exchange and annealing.

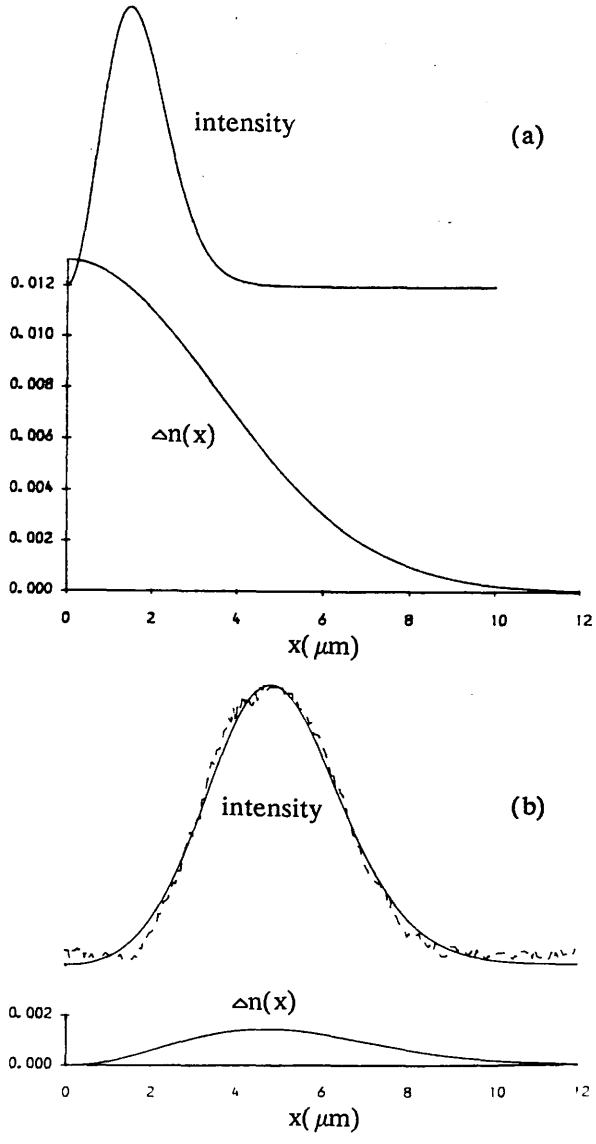

Figure 4-16. Intensity profiles of TM modes and profiles of ordinary refractive index (index increase $\Delta n(x)$)for:

(a) surface TI waveguide with

$$n_1(x)=2.285 + 0.013 \times \exp(-(x/5.0)^2)$$

(b) buried waveguide with

$$n_2(x)=2.285 + 0.013 \times \exp(-(x/5.0)^2) - 0.013 \times \exp(-(x/4.3)^2)$$

The dashed line in (b) is the measured optical intensity profile of the TM mode on x-cut $LiNbO_3$.

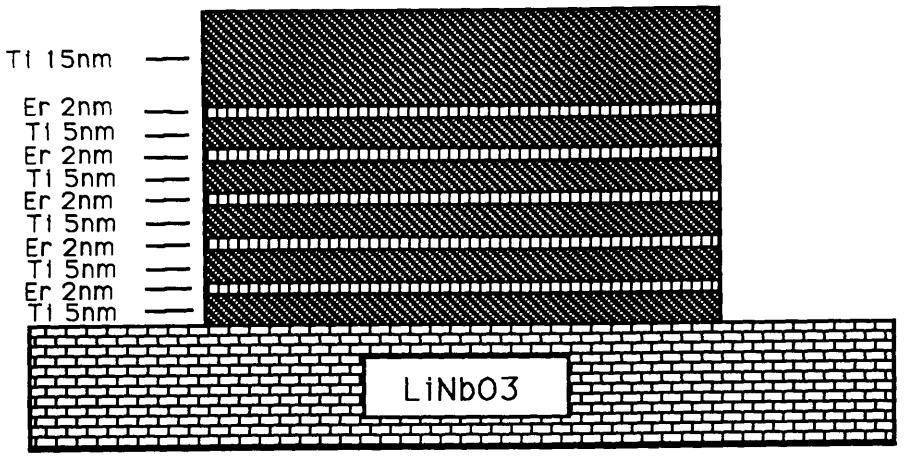

Figure 4-17. The structure and thicknesses of multi-layer Er:Ti for co-diffusion of Ti and Er.

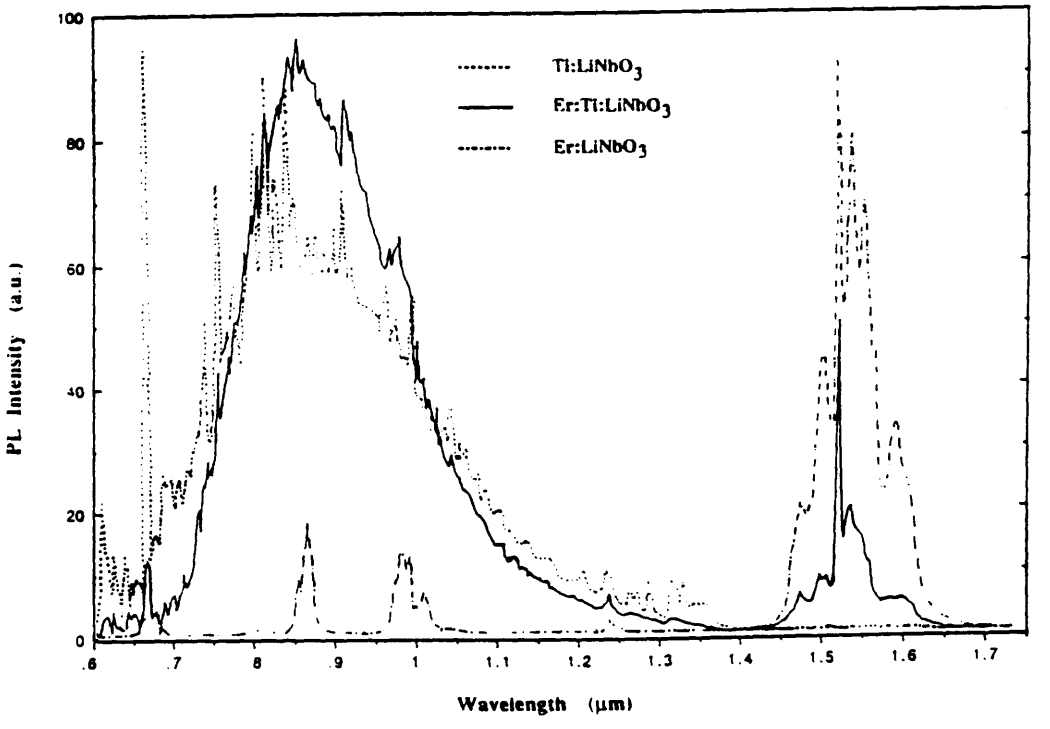

Figure 4-18. Photo-luminescence spectrum of Er:Ti:$LiNbO_3$, Ti:$LiNbO_3$ and Er:PE:$LiNbO_3$ samples.

CHAPTER FIVE: FABRICATION OF HOMOGENOUS PLANAR LENS

V.1. Introduction

The high index waveguide and low index waveguide are to be separated in some way to form the lens region and surrounding waveguide region. At the beginning of the development of waveguide lenses, the high index waveguide was formed by a top cladding layer or surface curvature in addition to the low index waveguide. The problem of this technology was that accurate control of the cladding layer or surface curvature was not easy and complicated and expensive facilities had to be used. The difficulty of fabrication also limited lens design because there were only limited lens contours possible for fabrication. Planar technology was introduced in waveguide lens fabrication [Zang 1983] soon after the technology of fabricating two different waveguides became feasible [De Micheli 1982]. This technology has been well developed for integrated circuits. By photolithography, the high index waveguide can be easily separated from the low index waveguide for the purpose of high index waveguide lens region fabrication. There is no limitation on the lens contour, and therefore any lens design can be realised. Not only homogenous refracting lenses but also Fresnel's lenses, which have very complicated contours, can be fabricated. Similar procedures of waveguide lens fabrication were used [Zang 1983, Suhara 1986 and Tatsumi 1988] and will be discussed in this chapter.

In next section, there will be a description of the waveguide lens fabrication procedure, using the standard planar technology. Section V.3. describes experiments in choosing masking layers for blocking proton–exchange. Section V.4. gives experimental results of the fabrication of waveguide optical components, lenses and prisms. In the section V.5., there is some discussion about fabrication tolerances as

they affect the lens performance.

V.2. Fabrication Procedure

A computer generated lens pattern was photo-reduced to form a mask-plate which was to be used to duplicate the lens pattern on the sample. As depicted in figure 5-1(a), the low index slab waveguide was made first, either by titanium indiffusion or dilute proton exchange as described in Chapter IV. A masking layer was then deposited on the waveguide surface, figure 5-1(b), to block proton exchange where needed. The photoresist was spun on the completely cleaned sample, at 4000rpm for 20 second giving about 1 μm thick uniform photoresist, figure 5-1(c). The sample was then baked in an oven at 90 ^{0}C for 30 minutes to drive off any remaining solvent. The mask-plate-covered sample was exposed under ultra-violent light for 5 minutes. The lens region was exposed and then the photoresist in this region was developed away afterwards, figure 5-1(d). A higher temperature post-baking at about 120 ^{0}C for about 30 minutes was found necessary for good boundary quality. The masking layer in the open window was etched away, figure 5-1(e). At this stage the sample should be carefully looked after and the etch bath slightly stirred, otherwise there might be some bubbles appearing as a result of chemical reaction, sticking on the edge of the boundary and preventing the area underneath from being further etched. The remaining photoresist was then removed and the sample cleaned ready for proton exchange, figure 5-1(f). The $LiNbO_3$ surface in the lens region was now open for proton exchange and the remaining area was still covered by the masking layer and prevented from being proton exchanged.

After proton exchange in benzoic acid, the remaining benzoic acid could be cleaned in acetone. After removing the remaining masking layer, the sample was ready for test, figure 5-1(g).

V.3. Masking Layers for Blocking Proton Exchange

V.3.1 Choice of Masking Material

Masking layers should be effective to block proton exchange, easy to process, and be low-cost; examples are Si_3N_4 [Zang 1982] and Al [Reid 1989]. Al is cheaper and easy to process. Al, Si_3N_4 and SiO_2 were tried in the experiment.

To check if the masking layer had effectively blocked the proton exchange, either the TI sample or virgin sample was covered with the masking layer and immersed in benzoic acid at about 236 ^{0}C temperature for up to 3 hours which were required to produce effective waveguide. Then the masking layer was removed and prism coupling was used to check if the effective index was increased and the waveguide had deteriorated on the TI sample or if there was a guided wave on the virgin sample. If the tests were negative it was thought the proton exchange was fully blocked.

A 200nm Al film was used as a mask and proton exchange was carried out at 236 ^{0}C in the following experiments. For proton exchange less than 30 minutes, strong in-plane scattering was observed in the prism output m-line even though the effective index was not found to have increased, which was thought to be because of the incomplete blocking and therefore the formation of some small high index islands by proton exchange. For proton exchange between 30 minutes and 3 hours, no increase of effective index was observed but light coupling into or out of the waveguide by prism was very poor in most cases; the waveguide had deteriorated after processing. Post-annealing in oxygen ambient at 300 ^{0}C for 3hrs partially restored the waveguide in some cases, as evidenced by the improvement of light coupling, even after proton exchange for 3hrs, but scattering was strong. Slightly increasing the mask thickness did not improve the situation and a much thicker film

was difficult to fabricate and process.

No increase in effective index was measured after proton exchange at 236 °C for 3hrs on the sample covered with 60nm Si_3N_4, but strong scattering was observed. With a thicker masking film of 200nm, the waveguide improved, but post-annealing was needed to improve light coupling.

A 60nm thick SiO_2 film prevented an increase in effective index after proton exchange at 236 °C for 3hrs, but scattering was still obvious. With a SiO_2 film 200nm thick, no deterioration was found after proton exchange at 236 °C for 3 hours and no post-annealing was necessary.

Proton exchange in $LiNbO_3$ leads to an increase in infrared (IR) absorption at wavenumber 3505cm^{-1} due to free OH groups [Loni 1989]. Infrared spectra were recorded using a Perkin-Elmer 983 spectrometer and data station. Two samples were half-covered, one with 200nm Al and another with 200nm Si_3N_4, and were immersed in benzoic acid at 235 °C for 2 hours. After removing the remaining masking layers, the IR spectra were measured on the covered and uncovered areas. Figure 5-2 shows the results. The relative heights of the absorption peaks of the covered area and that of the uncovered ares was 0.36 for Al-covered sample and 0.30 for the Si_3N_4-covered sample, indicating stronger proton exchange in the Al covered sample. Figure 5-3 shows the IR spectra of two samples, one of which was covered with 300nm Al and another with 100nm SiO_2 and which were immersed in benzoic acid at 235 °C for 3 hours. The Al-covered sample had the greater IR absorption. These results indicate that an Al film has poorer quality in blocking proton exchange than SiO_2.

V.3.2 SiO_2 Deposition

It was found that after plasma deposition of SiO_2 and removal in $HF:H_2O = 1:10$, the

surface scattering increased. Annealing in air at 500 °C for 2 hours improved the waveguide. This degradation was supposedly due to damage by the plasma during the deposition, as previously reported [Suhara 1986].

An interesting thing happened. If the SiO_2 was etched away, in $HF:H_2O=1:10$, before annealing, and was proton exchanged, in pure benzoic acid at 235 °C for four hours, normal bright TIPE modes were seen from prism coupling. If the TI sample was annealed with the SiO_2 covered and afterwards the SiO_2 was etched away, then after the proton exchange the guided waves were vague. Some times the number of modes was smaller and the modes were weak compared with normal TIPE modes, and sometimes only a TI mode was observed as if the sample did not undergo PE at all. No more explanation is available but it is supposed that there must be some interface layer formed during plasma deposition and subsequent annealing, between the $LiNbO_3$ substrate and the SiO_2 film.

Special care should be taken during SiO_2 deposition. When the sample was heated up to 300 °C, required for SiO_2 to stick on the substrate, it charged up on the surface and was attractive to the residual dusts in the deposition chamber which may come from the gas tube. As the result there were some holes in the SiO_2 film. If the deposition was done after an overhaul of the system there were very few holes, otherwise a lot of holes were seen. This was more severe for z−cut than for x−cut, because of bigger r_{33} coefficient and therefore stronger electric charging. Using a thin metal film (for example 20nm Ti) either discharged the sample surface or prevented the damage from the plasma. The SiO_2 film could stick on Ti and NiCr films but not on Al film. Ti can be etched in the same etchant as for SiO_2 and therefore they can be etched in a single process.

V.4. Waveguide Optical Components

Figure 5－4(a) shows a photograph of a waveguide triangle prism formed on x－cut $LiNbO_3$ by Ti indiffusion and proton exchange. The deflection is not clear in the photograph but figure 5－4(b) is a sketch from the original picture. The deflection angle θ was deduced from figure 5－4(b) and was about 3.2^0. It is small because of the small difference of effective indices.

Figure 5－5 shows a 4－element waveguide lens made on z－cut $LiNbO_3$ by Ti indiffusion and proton exchange. The Ti film was 32nm thick and the sample was annealed at 1000^0C for 3.5 hours. The effective index of the fundamental mode was 2.2059. 300nm thick SiO_2 was used and proton exchange was carried out at 235^0C for 7 hours. There were 8 modes in the TIPE area and the waveguide depth was calculated by the IWKB method to be about 3.2μm. The effective index of the fundamental TIPE mode was 2.3273. The ratio of high and low effective indices was 1.0550. The coupling efficiency measured from the m－line as described in the section III.5. was about 75% which means an overall power transmission of 10% through the lens. The final focal spot was very weak because of the boundary losses after the light beam had passed eight boundaries.

Figure 5－6 shows a one－element waveguide lens formed on z－cut $LiNbO_3$ by Ti indiffusion and proton exchange with incident beam angle of 0^0, 3^0 and 5^0. The Ti film thickness was 30nm and the sample was annealed at 1000^0C for 3 hours. The effective index of the fundamental mode was 2.2097. 300nm thick SiO_2 was used as a mask and proton exchange was carried out at 235^0C for 5 hours. There were 8 modes in the TIPE area and the waveguide depth was calculated to be about 3.0μm. The effective index of the fundamental TIPE mode was 2.3326. The ratio of high and low effective indices was 1.0556. The coupling efficiency was about 88% which means an overall power transition of 77% through the lens. After passing two boundaries, the intensity of the light beam was still strong.

V.5. Fabrication Tolerances

The optical performance of the lenses is mainly affected by the ratio of effective indices in the high and low index waveguides and lens contours. The waveguide structure will affect not only the effective index, hence the index ratio, but also the coupling efficiency. The lens contours affect the optical path of the light beam.

V.5.1. Effect of Titanium Indiffusion on Effective Index in Low Index Waveguide

There are several parameters affecting the effective refractive index in a TI waveguide: the thickness of the Ti film, and the temperature and time of annealing. Equation (4−6) in section IV.2.3. expresses the extraordinary refractive index profile of z−cut $LiNbO_3$, assuming the temperature of 1000 °C, as a function of Ti film thickness, temperature and annealing time and is rewritten here:

$$n(x) = 2.2022 + 1.56 \frac{d}{2 \times \sqrt{(0.38t)}} \exp\left(-\left(\frac{x}{2 \times \sqrt{(0.38t)}}\right)^2\right) \qquad (5\text{-}1)$$

The effect of these parameters on the index profile and hence on effective index can be analysed.

Figure 5−7 shows the relationship between the effective index of the fundamental TM mode in a TI waveguide vs the thickness of the Ti film, for a fixed annealing time of 4 hours. It is linear and has a slope of 0.000498/nm. This means that an inaccuracy of 1nm in Ti film thickness will result in an effective index change of 0.00050. Figure 5−8 shows the relationship of the effective index vs the annealing time for a fixed Ti film thickness of 30nm. The curve can be approximately fitted by a straight line with a slope of −0.000955/hour. This means that an inaccuracy of 1 minute in annealing time will result in an effective index change of 0.000016.

The effect of temperature can be taken into consideration. Using equation (4−4) of the dependence of diffusion coefficient on temperature and quoting $D_0 = 1.9 \times 10^9$ $\mu m^2/hr$ and $T_0 = 2.9 \times 10^4$ ^0K [McLachlan 1981], figure 5−9 shows the relationship of the effective index vs temperature with fixed Ti film thickness of 30nm and annealing time of 4 hours, which has a slope of −0.0000846/degree. This means that an inaccuracy of $1\,^0C$ in annealing temperature will result in an effective index change of 0.000085.

The thickness of the Ti film could be checked with the Talystep which has an accuracy of ±1nm. The timing could be controlled with 1 minute. The oven can be well controlled to within $\pm 1\,^0C$. The inaccuracy of effective index as the results of inaccuracy of Ti film, annealing time and temperature is then estimated as bigger than 0.000498+ 0.000016+ 0.000085, i.e. > 0.0006. The major inaccuracy comes from the Ti film thickness. The nonuniformity of the Ti film will also bring inaccuracy but the variation of the film thickness is too complex and difficult to analyse.

V.5.2. Effect of Proton Exchange and Post−Annealing on Effective Index in High Index Waveguide and on the Ratio of High and Low Effective Indices

The maximum refractive index by proton exchange is about 2.34. The effective index of the fundamental mode obtainable by proton exchange is 2.33 with reasonable waveguide depth and temperature, while the effective index of the low index single−mode TI waveguide is about 2.208. The ratio of these two is normally a little more than 1.055. If a smaller ratio is used in the lens design as done in the Chapter II, then the index ratio should be properly adjusted to that value. Post annealing can adjust not only the effective index of the high index waveguide and hence the index ratio, but also the mode match as discussed in Chapter III. After Ti indiffusion and proton exchange, the effective indices of low and high index waveguides are measured and the index ratio calculated which is normally larger than

1.055. Then post annealing is applied to adjust the index ratio and mode match.

After some time of proton exchange, say one hour, the surface index has reached the maximum, and afterwards the fluctuation in temperature and time will only affect the diffusion coefficient, and in turn the depth of the waveguide and hence the effective index. The waveguide depth a is related to the diffusion constant D:

$$a = 2 \surd (D t) \qquad (5\text{-}2)$$

With fixed temperature and known time, the effective indices were measured and index profile was calculated by the IWKB method and the waveguide depth could be obtained. The diffusion constant D could then be calculated from (5−2). After more than 20 measurements at temperature of T= 235 ^{0}C, an average diffusion constant for z− cut $LiNbO_3$ was obtained as D= 0.464 μm^2/hr.

Figure 5−10 shows the relationship between the effective refractive index of the fundamental mode and the proton exchange time at a temperature of T= 235 ^{0}C and fixed waveguide index of 2.34 and substrate index of 2.20. The tangent at t= 4hr has a slope of 0.000661/hour which implies an inaccuracy in effective index of 0.000011 for an inaccuracy in proton exchange time of one minute.

The diffusion constant has a relationship with temperature given by Arrhenius law;

$$D = D_0 \times \exp(-Q/RT) \qquad (5\text{-}3)$$

where Q is active energy in $kJ.mol^{-1}$, R is the universal constant $8.314 J.K^{-1}.mol^{-1}$, T is the temperature in K and D_0 is a constant. Quoting the value of Q_z= 81.2$kJ.mol^{-1}$ for z− cut $LiNbO_3$ [Loni 1989] and our experimental results of diffusion constant D= 0.464 μm^2/hr for z− cut $LiNbO_3$ at 235 ^{0}C, the D_0 is worked out as $D_0 = 1.038 \times 10^8 \mu m^2$/hr. Now the dependence of effective index on

proton exchange temperature can be analysed.

Figure 5−11 shows the relationship between the effective index of fundamental mode and proton exchange temperature, with fixed proton exchange time of 4 hours and fixed waveguide and substrate indices as before. The tangent at T=235 ^{0}C has a slope of 0.000096/degree, which means an inaccuracy in effective index of 0.0001 for an inaccuracy in temperature of 1 ^{0}C. The oil bath used for proton exchange can be controlled to ±0.25 ^{0}C [Loni 1989], which means an inaccuracy of effective refractive index of 0.000048.

During annealing, the refractive index decreases and the waveguide depth increases at same time. So the analysis is complicated. Rigorous analysis of such a process with varying time and temperature needs resolving the solution of the diffusion equation. A simple model exists [Goto 1989]. Assuming a step−like index profile, the increase in refractive index $\triangle n$ and the depth of the waveguide d are related to annealing time t:

$$1/\triangle n - 1/\triangle n_0 = a\ t^b \qquad (5\text{-}4)$$

$$d - d_0 = p\ t^q \qquad (5\text{-}5)$$

where $\triangle n_0$ and d_0 are the index increase and waveguide depth after proton exchange, a, b, p and q are constants and are 1.7, 0.35, 0.78 and 0.15 respectively for proton exchange at 200 ^{0}c for 3.5hr and annealing at 300 ^{0}C. Assuming $\triangle n_0$= 0.14 and d_0= 3.0μm, the index increase $\triangle n$ and waveguide depth d can be calculated as functions of annealing time t, and then the relationship of effective index of fundamental mode and t can be obtained as shown in figure 5−12. The effective index decreases dramatically initially and levels out. The tangent at t= 3hr has a slope of − 0.0035/hr, which means an inaccuracy in effective index of 0.000058 for an inaccuracy of annealing time of one minute. This is beyond the effective

index measurement accuracy which is normally about 0.0002. The longer annealing time will allow better control. At lower annealing temperature, the waveguide index relaxation is slower and the control is easier, but the values of the constants a, b, p and q are not available so the problem can not be solved by this simple model.

A similar simple model of the relationship of index increase and waveguide depth with annealing temperature is not available. Any deviation of effective index after proton exchange from temperature fluctuation can be compensated by adjustment of annealing time. The effective index can be controlled independently by adjusting the annealing time if the effective index is monitored by withdrawing the sample from the oven at intervals.

There many other factors affecting effective index. The stoichiometry of the $LiNbO_3$ material and benzoic acid will affect the parameters. So in practice, the actual variation of effective index was apparently bigger than that estimated as above.

The ratio of the effective indices of high and low index waveguide rather than the absolute value of the indices decides the optical performance of a waveguide lens. After Ti indiffusion and proton exchange, the effective indices of the high index TIPE waveguide and the low index TI waveguide can be measured, and then annealing is applied to adjust the effective index of TIPE waveguide and therefore the index ratio. If the annealing process can be well controlled the effective index of the high index waveguide can be adjusted to within the measurement error, and then the index ratio can be reasonably good. Assuming the effective index of TI low index waveguide of 2.2080 and the effective index of TIPE high index waveguide of 2.3290 and an inaccuracy in effective index of 0.0002, the ratio of effective index will be 1.0548 ± 0.0001.

In principle, the inaccuracy of mode match may be also considered. Proper index profiles for low and high index waveguides can be chosen and controlled so that the

mode match and index ratio are satisfied at the same time. But even if the processing is well controlled, material imperfetions will induce losses. As seen in Chapter III, the main contribution to boundary losses was boundary scattering rather than mode mismatch. So a little mode mismatch will not significantly affect the total boundary losses. Therefore, the final stage of annealing should be used for the purpose of index ratio adjustment.

V.5.3. Effect of Lens Contours

Photolithography is one of the most tricky procedures in planar technology. The duplicate exactly the original pattern requires strict control of temperature, time and etchant quality. Even so, it is still quite possible that the pattern boundaries will have been expanded after etching. The expanded lens pattern will change the optical performance. It was reported that an expansion of 1 μm on all the lens boundaries extended the focal length by only 0.43 μm for the multi-element circular lens on an isotropic waveguide [Righini 1986]. This section analyses the effect of the expansion of lens contour on the optical performance for a one-element acircular lens on anisotropic waveguide.

The lens boundary is described by $z^m(y)$, as in figure 5-13, where m denotes the boundary number and the lens axis is along the z direction. Assuming that the lens boundaries are expanding along the normal direction a distance b, the point (y_0, z_0) will move to (y_1, z_1) and:

$$z_1 - z_0 = - (y_1 - y_0) / z'_y(y_0) \qquad (5\text{-}6)$$

$$(z_1 - z_0)^2 + (y_1 - y_0)^2 = b^2 \qquad (5\text{-}7)$$

The equations can be rewritten as

$$z_1 = z_0 + (-1)^m \times b \; / \sqrt{(1 + (z'_y(y_0))^2)} \quad (5\text{-}8)$$

$$y_1 = y_0 - z'_y(y_0) \times (z_1 - z_0) \quad (5\text{-}9)$$

The curves of (y_1^m, z_1^m) forms the new lens contours which have been expanded a distance b from the designed lens pattern $z^m(y)$. It can be shown that the direction of the normal at the point (z_1, y_1) on the new contour is in the same direction as the normal at the related point (z_0, y_0) on the designed contour.

Using programmes of raytracing and Huygens–Fresnel analysis as in Chapter II, the optical performance of the one–element lens based on an anisotropic waveguide described in the section II.7. was analysed. For an expansion of $1\mu m$, the optical intensity did not change significantly but the focal length increased. The changes in focal length were different for different incident angles but an acceptable focal plane was located about $3\mu m$ beyond the original one.

Distortion on the lens contour will affect the lens performance. Assuming a distortion of $d < 1\mu m$, feasible with present fabrication technology, the ray will change its optical path $d \times (n_{eff.h} - n_{eff.l}) < 1.0 \times 0.12\mu m \ll \lambda$. Such small change is acceptable in optical lens assessment.

V.5.4. Effect of Index Ratio

In section V.5.2., it was estimated that the index ratio can be controlled to ±0.0001. Similar analysis to that in last section showed that the spot size of an off–axis beam was sensitive to the index ratio. However the index ratio change of ±0.0001 in 1.0548 did not change the intensity profile dramatically but the focal length increased as the index ratio decreased, and *vice versa*, by about $30\mu m$.

V.5.5. Effect of Focal Plane

After fabrication, one side of the device will be cut and polished for the attachment of a photodetector. The end should be coincide with the focal plane, and is actually difficult to control. A simple geometrical optics analysis can give an estimation of the polish tolerance. The one–element lens has an aperture of 6mm and focal length of about 19mm, which means a cone of about 1/3. The shift of 3μm along optic axis will change the diameter of the cone by 1μm. Raytracing and Huygens–Fresnel analysis showed that the spot size and sidelobe height increased with focal plane shifting and we suggest that the polish should be controlled to within $\pm 3\mu$m.

V.6. Discussion and Summary

Experiments showed that SiO_2 (plasma deposited) gave better masking performance in blocking proton exchange than Si_3N_4 and Al. Clearly, the masking layer must be dense enough so that no leakage of H^+ and Li^+ occurs. There must be some imperfections such as holes in the films, especially for Al and Si_3N. Thicker film will reduce the risk of leakage.

An advantage of the SiO_2 masking layer, besides its better masking performance, is its ease of etching and removal in dilute HF without risk of damage on $LiNbO_3$ surface. A 200nm SiO_2 film can be etched away in $HF:H_2O = 1:10$ in 30 seconds, while no obvious damage was found on a $LiNbO_3$ surface which had been immersed in the same etchant for 10 hours.

Exposure to plasma creates some damage on the $LiNbO_3$ surface and annealing at 500^{0}C for 2 hours can improve the surface. Such annealing does not affect the TI

waveguide structure.

Waveguide optical components of prism and single element lenses can be fabricated by TIPE technology, while the boundary losses restrict the fabrication of multi– element components.

The tolerance of fabrication processing on lens performance was analysed. The inaccuracy of effective refractive index by Ti indiffusion was estimated to be about 0.0006, mainly from the inaccuracy of Ti film thickness.

The ratio rather than the absolute values of the effective indices of high and low index waveguide decides the optical performances of the waveguide lenses. After Ti indiffusion and proton exchange, the effective indices of the high index TIPE waveguide and the low index TI waveguide can be measured, and then annealing is applied to adjust the effective index of TIPE waveguide and therefore the index ratio. Assuming an inaccuracy in effective index of 0.0002, the inaccuracy of the ratio of effective index will be 0.0001.

The slight expansion of lens contour by photolithography results in the movement of focal plane. On anisotropic waveguide, the focal length of the one– element lens becomes about 3μm longer after 1μm expansion of the lens contour, while such an expansion in the multi– element circular lens on the isotropic waveguide extended the focal length only 0.43μm [Righini 1986].

The change of 0.0001 in the index ratio results in a change of focal length of about 30μm without much change in other optical parameters. The accuracy of the position of the focal should be controled to within 3μm so that the design performance can be achieved.

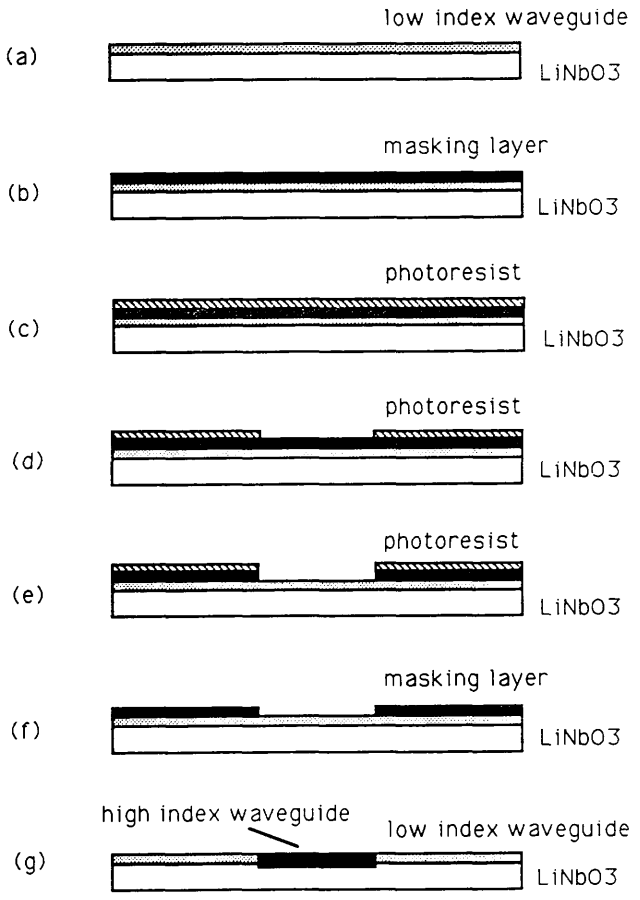

Figure 5—1. Procedure for the fabrication of planar thin film lens. (a) formation of low index waveguide; (b) deposition of masking layer; (c) coating photoresist; (d) photolithiography; (e) etching of masking layer; (f) removal of photoresist; (g) completion.

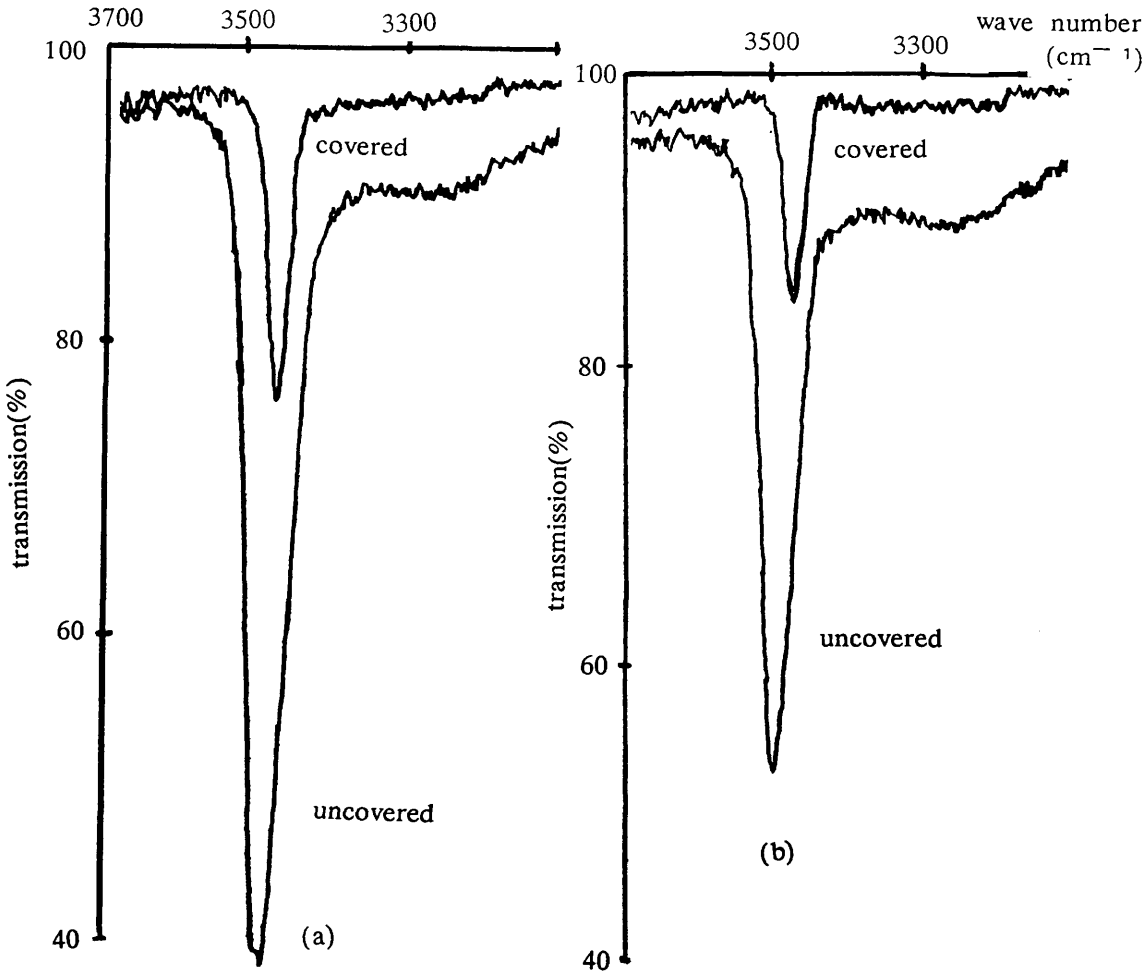

Figure 5-2. Infrared spectrum of (a) half-Al-covered sample and (b) half-Si_3N_4-covered sample.

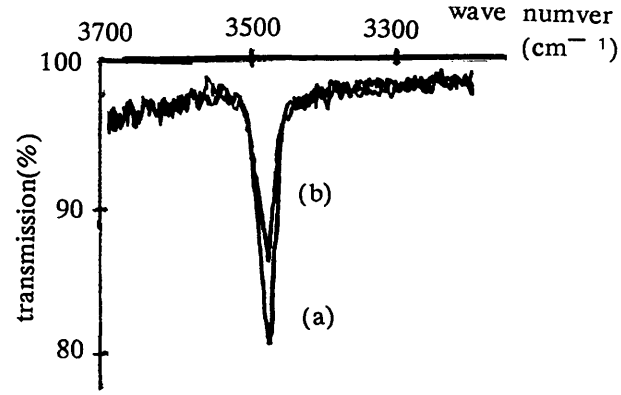

Figure 5-3. Infrared spectrum of (a) Al-covered sample and (b) SiO_2-covered sample.

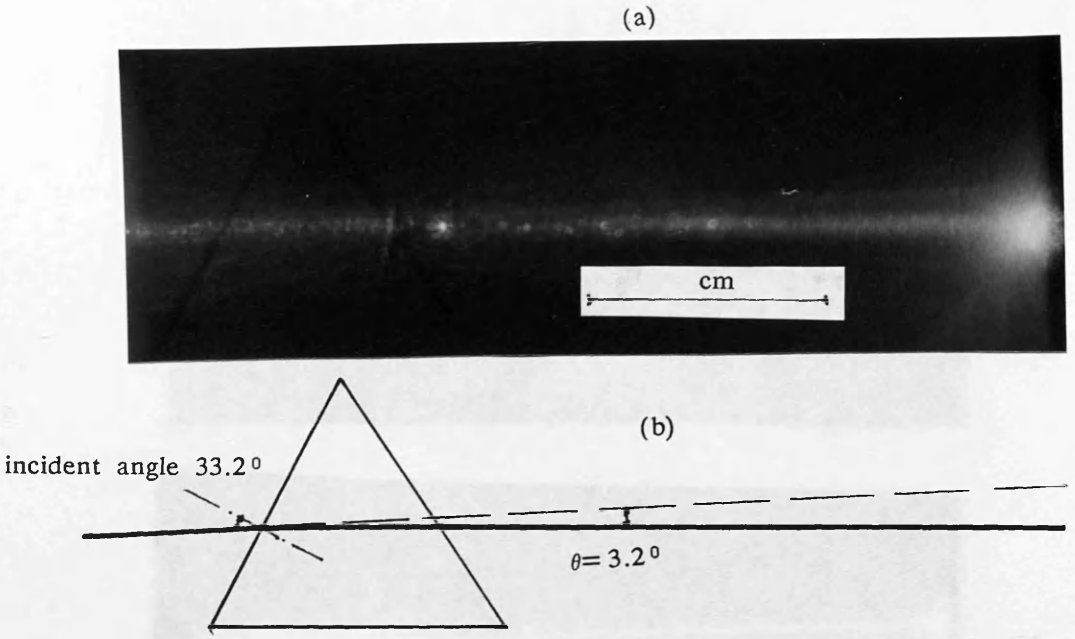

Figure 5－4. (a):Waveguide triangle prism on x－cut $LiNbO_3$ by Ti indiffusion and proton exchange. (b): Sketch of (a). The deflection angle θ is deduced as 3.2°.

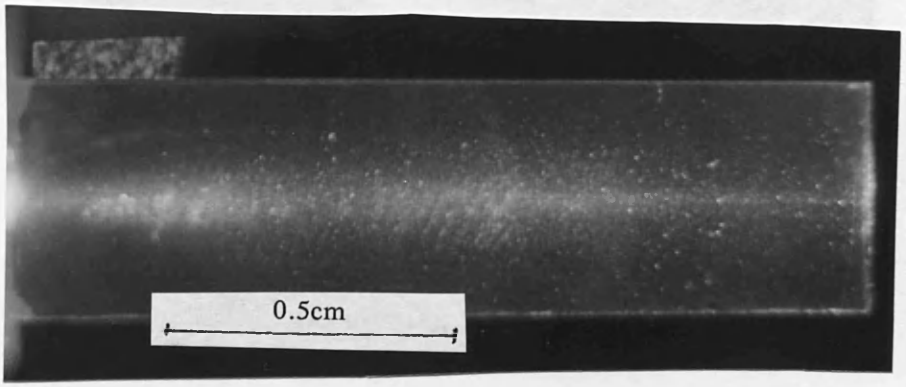

Figure 5－5. 4－element waveguide lens on z－cut $LiNbO_3$ by Ti indiffusion and proton exchange.

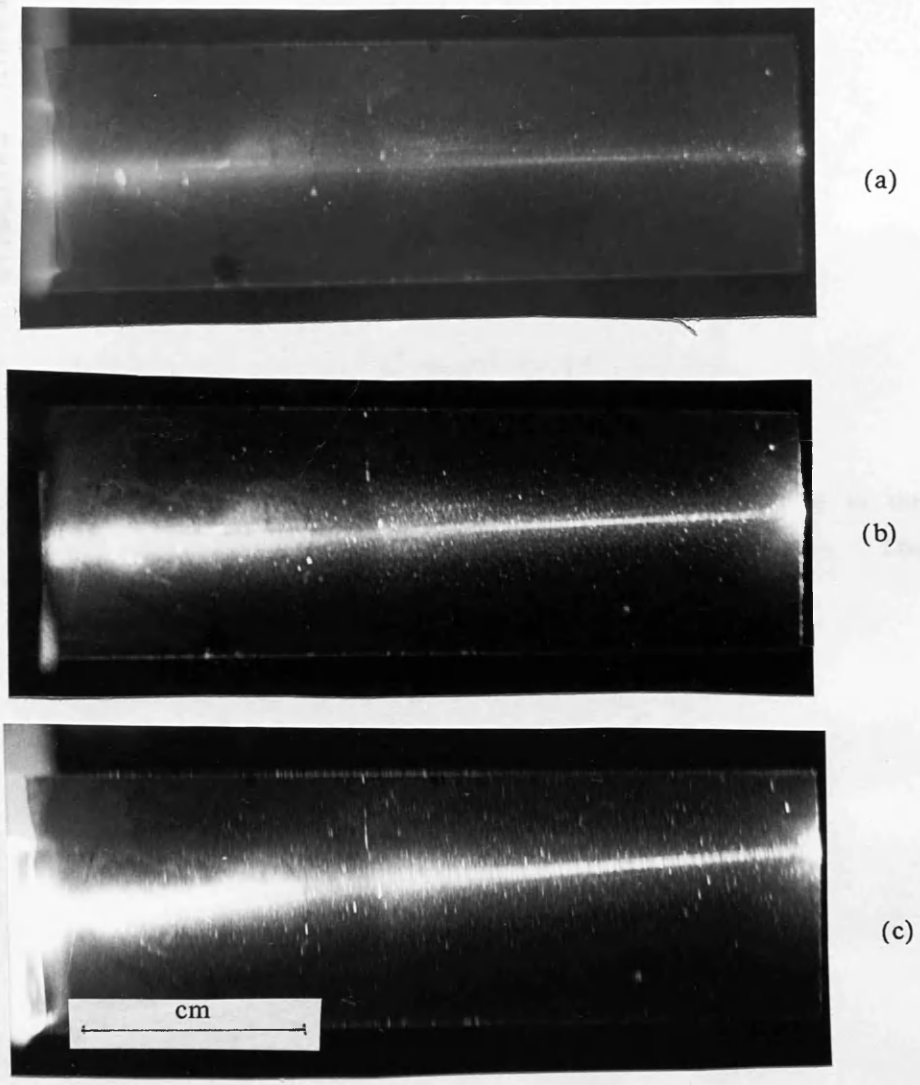

Figure 5−6. One−element waveguide lens on z−cut $LiNbO_3$ by Ti indiffusion and proton exchange. Incident angle of (a):0^0, (b):3^0 and (c)6^0.

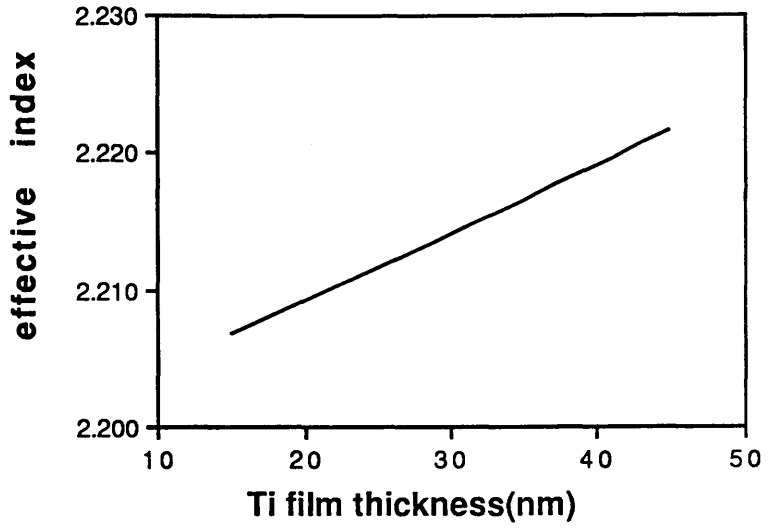

Figure 5−7. Effective index of fundamental TM mode in TI waveguide vs the thickness of Ti film, for a fixed annealing time of 4 hours. The slope is 0.000498/nm.

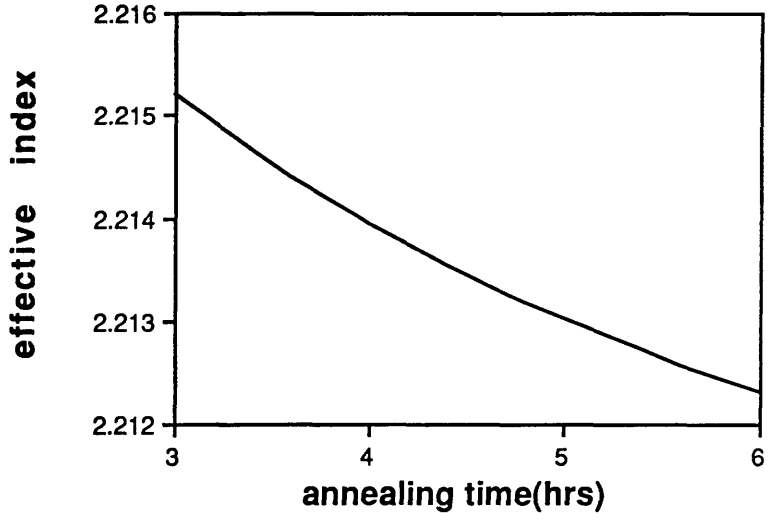

Figure 5−8. Effective index vs the annealing time for a fixed Ti film thickness of 30nm. The curve can be approximately fitted by a straight line with a slope of −0.000955/hour

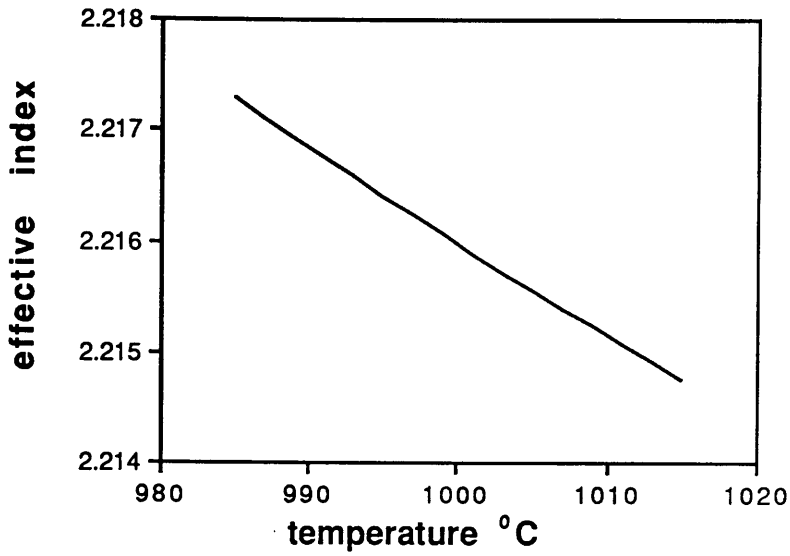

Figure 5–9. Effective index vs temperature with fixed Ti film thickness of 30nm and annealing time of 4 hours. The slope is −0.0000846/degree.

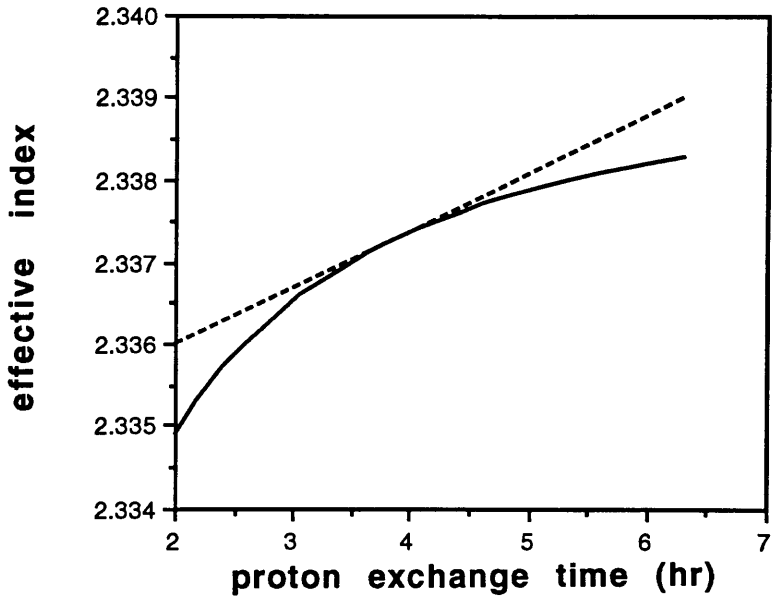

Figure 5–10. Effective index vs proton exchange time at 235°C and fixed waveguide index of 2.34 and substrate index of 2.20. The tangent at t= 4hr has a slope of 0.000661/hour

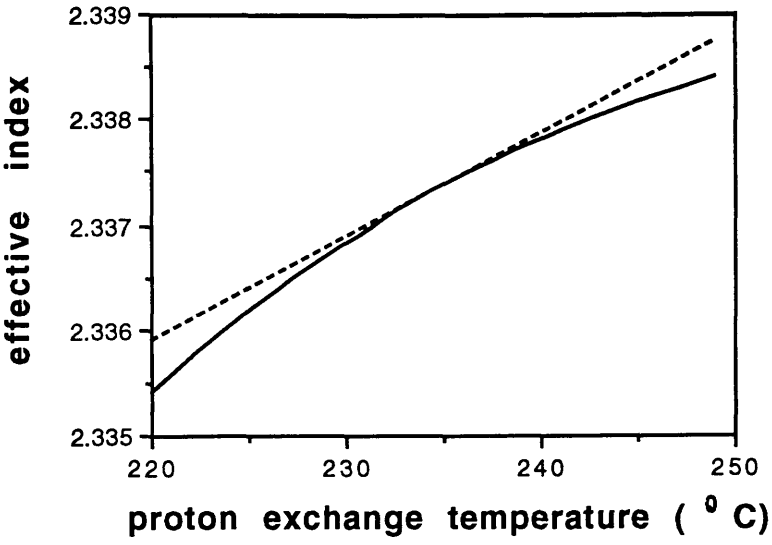

Figure 5−11. Effective index vs proton exchange temperature with fixed proton exchange time of 4 hours and fixed waveguide and substrate indices as in figure 5−9. The tangent at T=235 °C has a slope of 0.000096/degree

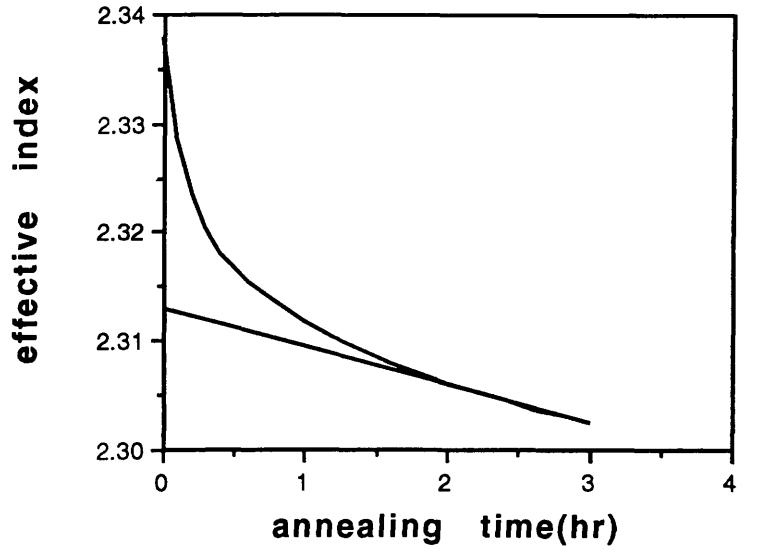

Figure 5−12. Effective index vs annealing time at 300 °C. The initial waveguide has index increase of 0.14 and depth of 3μm. The tangent at t= 3hr has a slope of −0.003$\frac{1}{2}$5/hr.

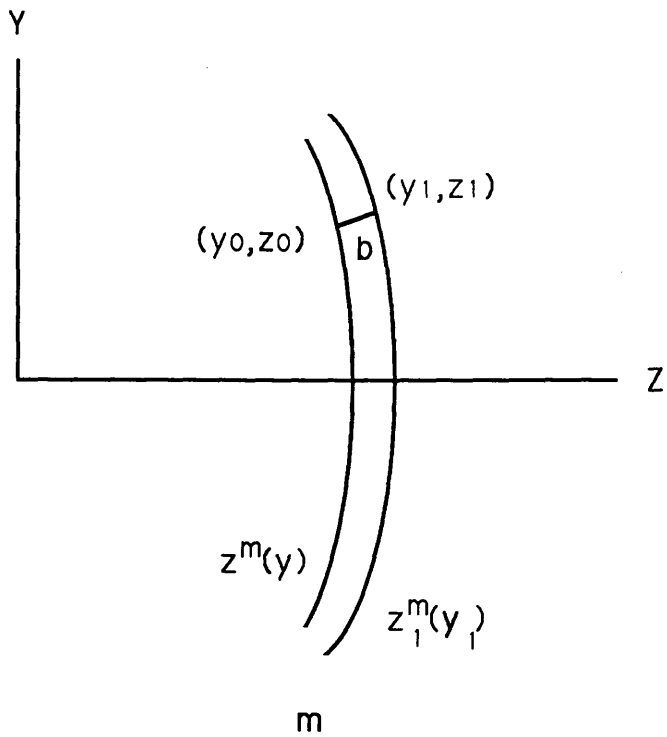

Figure 5-13 Lens contour expand

CHAPTER SIX: CONCLUSIONS

The following aspects of waveguide lenses have been studied: anisotropic aberration analysis, lens performance analysis, lens design, boundary losses, lens fabrication and fabrication tolerances. A new integrated optics device, the buried waveguide polariser, and a new method of Er doping, were developed. The work will be summarised in the next section and some suggestions for further study will be presented in the last section.

VI.1. Summary of the Work

The application of waveguide lenses in integrated optics devices requires that they have high resolution and are free of field curvature at the focus over several degrees, with reasonable relative aperture and signal–to–noise ratio. A small ratio of high and low refractive indices results in weak refraction power and complicates the lens design even though the 2–dimensional form has eased the fabrication of acircular boundaries and provided more freedom for lens design. Use of multi–element lens is an effective way to compensate the disadvantage of small index difference but the boundary losses limit its use.

When the lenses are working in x–cut or y–cut $LiNbO_3$, anisotropic aberration will affect the lens performances and must be taken into consideration. A method of lens analysis in anisotropic waveguide was developed and a comprehensive understanding of lens behaviour in such waveguides was obtained. The analysis and the computer programmes are also valid for lenses on isotropic waveguides.

When the lenses optimised for isotropic waveguide are working on anisotropic waveguide, the spot sizes are slightly larger, the background noise rises a little and the focal length extends.

The analysis showed that the existing one-element lenses had a big aberration of the focal plane. A new design of one-element lens was proposed, allowing for anisotropic aberration. There was no aberration of the focal plane. The optical performance was obviously worse than that of the four-element lens but the resolution was acceptable and the single element lens could be readily fabricated to give efficient light transmission.

Coupling efficiency on the boundary of two waveguides was studied in detail both theoretically and experimentally.

Various types of index profiles were chosen for the purpose of mode match analysis for both TE and TM modes. The overlap integral between two fundamental modes in two waveguides (with the low index waveguide just below the cut-off of the first order mode) with the same type of index profile could be about 99%, subject to the feasibility of fabrication of the waveguides with certain types of index profile. Experimentally, an overlap integral of optical intensity profile of about 99% was obtained in a TIPE $LiNbO_3$ system for both TE and TM modes.

Even though the mode mismatch and boundary reflection did not significantly affect the coupling efficiency on the boundary, the boundary scattering losses reduced the power transmission and was the major problem in waveguide lens fabrication. Therefore, multi-element lenses would not be suggested for use before this problem is solved.

Un-annealed DPE waveguide had high attenuation, while annealed DPE waveguide had a spread-out index profile and was difficult for the high index waveguide to

match. TI waveguide had low attenuation and was stable afterwards. The fundamental mode in TI waveguide could be well matched by that in TIPE waveguide. So TI waveguide was chosen as the low index waveguide in waveguide lens fabrication.

Suppression of Li_2O out-diffusion is important in waveguide lens fabrication, but unfortunately complete suppression can not be well controlled. It seemed that effective suppression might be achieved by chance (for the specific material used).

Plasma deposited SiO_2 gave better masking performance in blocking proton exchange than Si_3N_4 and Al, but post annealing was necessary to remove plasma damage on the $LiNbO_3$ surface.

Waveguide optical components of prism and single-element lenses were fabricated by TIPE technology with SiO_2 as the masking layer, while the boundary losses restricted the fabrication of multi-element components.

The tolerance of fabrication processing on lens performance was analysed. The inaccuracy of the ratio of effective index (adjustable by annealing) could be 0.0001, which resulted in a change of focal length of about 30μm (for the newly designed one-element lens) without significantly changing other optical parameters. The accuracy of the position of the focal plane should be controlled to within 3μm so that the design performance could be achieved.

A slight expansion of lens contour by photolithography would result in a shift of the focal plane. In an anisotropic waveguide, the focal length of the one-element lens became 3μm longer after 1μm expansion of the lens contour.

In addition to the main project on waveguide lenses, some other interesting work was carried out. A TI waveguide supporting ordinary-polarisation waveguide modes was

effectively buried by subsequent proton–exchange and the index profile was adjusted readily by annealing to near symmetric, which would benefit the coupling between integrated optical devices and an optical fiber. The cladding layer strongly attenuated the surface TM mode and led to a high extinction ratio TE mode polariser.

The indiffusion of Er was significantly enhanced by the presence of Ti and the annealing time needed to drive in the Er was dramatically reduced. In our experiment, the annealing temperature was lower, and the annealing time was much shorter than that used by other groups [Brinkmann 1991, Gill 1992] but an effective Er:Ti:$LiNbO_3$ waveguide was still obtained.

VI.2. Suggestions for Future Work

More time should be spent on the design of one–element lens, on either isotropic or anisotropic waveguides. It should be able to produce a one–element lens without curvature of field but with resolution of more than 1000 spots in a field of view of a few degrees and with a background noise level much lower than that of the present design (5.7dB).

Boundary loss is the biggest problem in lens fabrication and limits the application of multi–element lenses which would otherwise provide better optical performance. The mechanism of boundary losses is not quite clear. The inhomogenity of refractive index near the defined boundary and the imperfection of the boundary are possible sources.

Using hybrid photodetectors [Yi–Yan 1991] to form an array on $LiNbO_3$ can provide a curved detection surface. Then the curvature of focal field of the lenses will be no longer a problem and the lens parameters such as background noise and resolution can be improved without worrying about curvature of field in the lens

design.

Li_2O out-diffusion is still a problem in lens fabrication. Some groups found that the complete suppression of Li_2O depended on material, so it is suggested that various manufacturing sources be tried.

The design of Fresnel lens could be improved. The existing Fresnel lens has a basically elliptic or hyperbolic shape, with quantised phase shifting. As has been shown, these lenses may have bad off-axis performance. The lens contour could be improved by redesigning, as was done in the newly designed one-element lens, or by introducing high order polynomial terms (taking anisotropic aberration into consideration) before phase shifting. This could reduce aberrations, especially at off-axis angles, as in the case of homogenous refracting lenses.

It would be interesting to use an ordinary index TIPE waveguide system, as discussed in section IV.4., for Fresnel lens fabrication, because of the perfect mode match between the lens region and the surrounding waveguide region and its isotropic operation on x-cut and y-cut $LiNbO_3$.

REFERENCES

Anderson, D. B., Davis, R. L., Boyd, J. T. and August, R. R., 1977, "Comparison of optical-waveguide lens technologies", IEEE Journal of Quantum Electronics, Vol.QE-13, pp.275-282

Becker, R.A., 1983, "Comparison of guided-wave interferometer modulators fabricated on $LiNbO_3$ via Ti indiffusion and proton exchange', Applied Physics Letters, Vol.43, pp.131-133

Brinkmann, R., Sohhler, W. and Suche, H., 1991, "Continuous-wave erbium-diffused $LiNbO_3$ waveguide laser", Electronics Letters, Vol.27, pp.415-417

Burns, W.K., Bulmer, C. H. and West, E. J., 1978, "Application of Li_2O compensation techniques to Ti-diffused $LiNbO_3$ planar and channel waveguides', Applied Physics Letters, Vol.33, pp.70-72

Canali, C., Carnera, A., Mazzoldi, P. and De La Rue, R. M., 1984, "$LiNbO_3$ optical waveguide fabrication by Ti indiffusion and proton exchange: process, performances and stability", SPIE, Vol.517, Integrated Optical Circuit Engineering, pp.119-127

Chandler, P.J., Zhang,L. and Towsend, P.D., 1990, "Ion implanted waveguides in doped $LiNbO_3$", Electronics Letters, Vol.26, pp.332-334

Chartier, G. H., Laybourn, P. J. R. and Girod, A., 1986, "Masking process for double-ion-exchanged glass optical waveguide", Electronics Letters, Vol.22, pp.925-926

Ctyroky, J. and Henning, H. J., 1986, "Thin-film polariser for Ti:$LiNbO_3$ waveguides at $\lambda = 1.3\mu m$", Electronics Letters, Vol.22, pp.756-758

Davis, R. L., 1984, "Acousto-optic Bragg diffraction in proton exchanged waveguide", SPIE, Vol.517, Integrated Optical Circuit Engineering, pp.74-81

Dawar, A., De La Rue, R. M., Doughty, G. F., Finayson, N., Al-Shukri, S. M. and Singh, J., 1984, "Acousto-optic techniques in integrated optics", SPIE, Vol.517, Integrated Optical Circuit Engineering, pp.64-73

De Micheli, M., Botineau, J., Sibillot, P., Ostrowsky, D. B. and Papuchon, M., 1982, "Fabrication and characterization of titanium indiffused proton exchanged (TIPE) waveguides in lithium niobate", Optics Communications, Vol.42, pp.101-103.

De Micheli, M., 1983, "Nonlinear effects in TIPE-$LiNbO_3$ waveguides for optical communications", Journal of Optical Communications, Vol.4, pp.25-31

Dricsoll, W. G., (editor), 1978, Handbook of Optics, (New York.Toronto.London: McGraw-Hill Book Company).

Esdaile, R. J., 1978, "Closed-tube control of out-diffusion during fabrication of optical waveguides in $LiNbO_3$", Applied Physics Letters, Vol.33, pp.733-734

Fouchet, S., Carenco, A., Daguet, C., Guglielmi, R. and Riviere, L., 1987, "Wavelength dispersion of Ti induced refractive index change in $LiNbO_3$ as a function of diffusion parameters", Journal of Lightwave Technology, Vol.LT-5, pp.700-708

Goto, N. and Yip, Gar Lam, 1989, "Characterization of proton-exchange and annealed $LiNbO_3$ waveguides with pyrophosphoric acid", Applied Optics, Vol.28,

pp.60－65

Han, K.G., Kim, S., Kim, D.H., Jo, J.C. and Choi, S.S., 1991, "Ti:$LiNbO_3$ polarization splitters using an asymmetric branching waveguide", Optics Letters, Vol.14, pp.1086－1088.

Hinkov, V. and Ise, E., 1986, "Control of birefringence in Ti:$LiNbO_3$ optical waveguide by proton exchange of lithium ions", Journal of Lightwave Technology, Vol.LT－5, pp.444－448

Hunsperger, R. G., Yariv, A. and Lee, A., 1977, "Parallel end－butt coupling for optical integrated circuits", Applied Optics, Vol.16, pp.1026－1032

Jackel, J., 1980, "High－Δn optical waveguides in $LiNbO_3$: Thallium－lithium ion exchange", Applied Physics Letters, Vol.37, pp.739－741

Jackel, J., Rice, C. and Veselka, J., 1982a, "Proton exchange for high－index waveguides in $LiNbO_3$", Applied Physics Letters, Vol.41, pp.607－608

Jackel, J. L., 1982b, "Suppression of outdiffusion in titanium diffused $LiNbO_3$: a review", Journal of Optical Communications, Vol.3, pp.82－85

Jackel, J. L. and Rice, C. E., 1984, "Short and long term stabilities in proton－exchanged $LiNbO_3$ waveguides", SPIE, Vol.460, pp.43－

Jackel, J. L., 1991, "Buried proton－exchanged Lithium Niobate waveguides", Proceeding of Integrated Photonics Research 1991, USA, April 1991, pp.59－60

Kaminow, I. P. and Carruthers, J. R., 1973, "Optical waveguiding layers in $LiNbO_3$ and $LiTaO_3$", Applied Physics Letters, Vol.22, pp.326－328

Laybourn, P. J. R. and Righini, G. C., 1986, "New design of thin-film lens", Electronics Letters, Vol.22, pp.343-344

Laybourn, P. J. R., Molesini, G. and Righini, G. C., 1988, "Homogenous refracting lenses for integrated optical circuits", Journal of Modern Optics, Vol.35, pp.1029-1048

Longhurst, R. S., 1957, Geometrical and Physical Optics, (London.New York. Toronto: Longmans, Green and Co.).

Loni, A., De La Rue, R. M. and Winfield, J. M., 1988, "Very Low-Loss Proton-Exchange $LiNbO_3$ Waveguide with a Substantially Restored Electro-Optic Effect", Proc.Topical Meeting on Integrated & Guided-Wave Optics, paper no-3, Santa Fe, New Mexico

Loni, A., Hay, G., De La Rue, R. M. and Winfield, J. M., 1989, "Proton-exchanged $LiNbO_3$ waveguides: the effects of post-exchange annealing and buffered melts as determined by infrared spectroscopy, optical waveguide measurements, and hydrogen isotopic exchange reactions", IEEE Journal of Lightwave Technology, Vol.7, pp.911-920

McLachlan, A. D., 1981, "Theoretical and experimental investigations of titanium diffused lithium niobate waveguides", PhD thesis, Department of Electrical and Electronics Engineering, University of Glasgow

Neyer, A., 1987, "Fabrication of low-loss titanium-diffused $LiNbO_3$ waveguides using a closed platinum crucible", Electronics Letters, Vol.23, pp.1187-1188

Neyer, A., 1990, "Integrated-optic devices in lithium niobate: technology and

applications", SPIE, Vol.1274, Electro-Optic and Magneto-Optic Materials II, pp.2-17

Pitt, C. W., Reid, S., Reynolds, S. and Skinner, J., 1988, " Waveguiding Fresnel lenses: modelling and fabrication", Journal of Modern Optics, Vol.35, pp.1079-1111

Pun, E. Y. B., Loi, K. K. and Mak, C. F., 1991, "Optical waveguides in $MgO/LiNbO_3$ by H^+/Li^+ exchange using a new proton source: adipic acid", 17th ECOC 91 and 8th IOOC 91, Paris, Sept., 1991

Ramaswamy, R. V. and Srivastava, R., 1988, "Ion-exchanged glass waveguides: A review", Journal of Lightwave Technology, Vol.6, pp.984-1001

Reid, S. A., Varasi, M. and Reynolds, S., 1989, "Double dilute melt proton exchange Fresnel lenses for $LiNbO_3$ optical waveguides", Journal of Optics Communications, Vol.10, pp.67-73

Righini, G. C., Russo, V., Sottini, S. and Toraldo di Francia, G., 1973, "Geodesic lenses for guided optical waves", Applied Optics, Vol.12, pp.1477-1481

Righini, G. C. and Laybourn, P. J. R., 1986, "Novel thin-film lenses for integrated optics", SPIE, Vol.701, 1986 European Conference on Optics, Optical Systems and Applications, pp.195-199

Righini, G. C. and Molesini, G., 1987, "Refractive waveguide lenses: a new design", Electronics Letters, Vol.23, pp.302-303

Schmidt, R. V. and Kaminow, I. P., 1974, "Metal-diffused optical waveguides in $LiNbO_3$", Applied Physics Letter, Vol.25, pp.458-460

Shubert, R., and Harris, J. H., 1968, "Optical surface waves on thin films and their application to integrated data processors", IEEE Trans. Microwave Theory Tech., MTT-16, pp.1048-1054

Stock, G., 1988, "Realisation of integrated optical polarisers for Ti:$LiNbO_3$ with Au, Al and Ti metal cladding", Electronics Letters, Vol.24, pp.899-901

Suhara, T., Nishihara, H. and Koyama, J., 1982, "A folded-type integrated-optic spectrum analyzer using butt-coupled chirped grating lenses", IEEE Journal of Quantum Electronics, Vol.QE-18, pp.33-35

Suhara, T., Fujiwara, S. and Nishihara, H., 1986, "Proton exchanged Fresnel lenses in Ti:$LiNbO_3$ waveguides", Applied Optics, Vol.25, pp.3379-3383

Tatsumi, K., Nakaguchi, T. and Ito, S., 1988, "Wide field angle bi-aspherical waveguide lens in $LiNbO_3$ fabricated by proton-exchange", Electronics Letters, Vol.24, pp.546-548

Zang, D. Y., 1983, "Waveguide optical planar lenses in $LiNbO_3$ - theory and experiments", Optics Communications, Vol.47, pp.248-250

Taylor, H. F., 1987, "Application of guided-wave optics in signal processing and sensing", Proceedings of the IEEE, Vol.75, pp.1524-1535

Tsai, C. S., 1979, "Guided-wave acoustooptic Bragg modulators for wide-band integrated optic communications and signal producing", IEEE Transactions on Circuits and Systems, Vol.CAS-26, pp.1072-1098

Tsai, C. S., 1988, "Integrated-optical device modules in $LiNbO_3$ for computing and signal processing", Journal of Modern Optics, Vol.35, pp.965-977

Ulrich, R., and Martin, R. J., 1971, "Geometrical optics in thin film light guides", Applied Optics, Vol.10, pp.2077-2085

Valette, S., Morque, A. and Mottier, P., 1982, "High-performance integrated Fresnel lenses on oxidised silicon", Electronics Letters, Vol.18, pp.13-15

Varasi, M., Annuli, A., Vannucci, A. and Reid, S., 1987, "Dilute Melt Proton Exchange(DMPE) in Y-cut $LiNbO_3$ fo the Fabrication of Monomode Optical Waveguide(MOWG)", SPIE, Vol.866, Materials and Technologies for Optical Communication, pp.110-116

Verber, C. M., 1984, "Integrated-optical approaches to numerical optical processing", Proceedings of the IEEE, Vol.72, pp.942-953

Voges, E. and Neyer, A., 1987, "Integrated-optic devices on $LiNbO_3$ for optical communication", Journal of Lightwave Technology, Vol.LT-5, pp.1229-1238

Vu, T. Q., Norris, J. A. and Tsai, C. S., 1989a, "Planar waveguide lenses in GaAs by using ion milling", Applied Physics Letters, Vol.54, pp.1098-1100

Vu, T. Q. and Tsai, C. S., 1989b, "Ion-milled waveguide lenses and lens arrays in GaAs", Journal of Lightwave Technology, Vol.7, pp.1559-1566

Warren, C., Forouhar, S. and Chang, W. S. C., 1983, "Double ion exchanged chirp grating lens in lithium niobate waveguides", Applied Physics letters, Vol.43, pp.424-426

Yariv, A., 1973, "Coupled-mode theory for guided-wave optics", IEEE Journal of Quantum Electronics, Vol.QE-9, pp.919-933

Yi-Yan, A., 1989, "Grafted GaAs Detectors on Lithium Niobate and Glass Optical Waveguides", IEEE Photonics Technology Letters, Vol.1, pp.379-380

Zang, D. Y., 1983, "Waveguide optical planar lenses in $LiNbO_3$ - theory and experiments", Optics Communications, Vol.47, pp.248-250

Zang, D. Y. and Tsai, C. S., 1985, "Single-mode waveguide microlenses and microlens arrays fabrication in $LiNbO_3$ using titanium indiffused proton exchange technique", Applied Physics Letters, Vol.46, pp.703-705

Zang, D. Y. and Tsai, C. S., 1986, "Titanium-indiffused proton-exchenged waveguide lenses in $LiNbO_3$ for optical information processing", Applied Optics, Vol.25, pp.2264-2271

Zernike, F., 1974, "Luneburg lens for optical waveguide use", Optics Communications, Vol.12, pp.379-381

Zhou, Wujun, Ji, Guangda and Ristic, V. M., 1990, "A Design of Waveguide Collimating Lenses in the Presence of Anisotropic Aberrations", Journal of Lightwave Technology, Vol.8, pp.1187-1190

Zhou, Wujun and Ristic, V. M., 1989, "Anisotropic aberrations in planar waveguide lenses", IEEE Journal of Quantum Electronics, Vol.25, pp.749-754

APPENDIX

APPENDIX A Computing Programmes for Raytracing and Huygens–Fresnel Analysis on Anisotropic Waveguides

The main programme is used for raytracing. It will call the data file FILE.LENSDATA, which stores the parameters of the lens set, the subroutine programmes SRAYTRA.FORTRAN, SANINDE.FORTRAN and SWAISTS.FORTRAN, which are all listed thereafter. It will store the data of positions and phases of the analysed rays in a data file FILE.TEMPORAL for Huygens–Fresnel analysis.

Programme HUYFRE.FORTRAN is used for Huygens–Fresnel analysis. It will call the data file FILE.TEMPORAL and will store the data of optical intensity profile in the data file FILE.INTENS.

I. MAIN PROGRAMME

```
C   ************************************************************** 0010
C   *    RAYTRACING ON ANISOTROPIC WAVEGUIDES                    * 0020
C   *    This is the main programme.  The data file of the lens  * 0030
C   *    parameters should have been stored in the file named     * 0040
C   *    FILE.LENSDATA.  The subroutines to be called by this    * 0050
C   *    main programme are SRAYTRA.FORTRAN, SANINDE.FORTRAN and * 0060
C   *    SWAISTS.FORTRAN.  The number of boundaries of the lens  * 0070
C   *    M should be set in this main programme before runnuing  * 0080
C   ************************************************************** 0090
                                                                    0100
        IMPLICIT DOUBLE PRECISION (A-H,O-Z)                         0110
        DIMENSION C(8),RK(8),B1(8),B2(8),B3(8),B4(8),SPC(8),        0120
     &    OPL(201),XR(10,201),YR(10,201),AR(10,201),RNIN(10,201)   0130
        COMMON/P/PI                                                 0140
        WRITE(6,*)'RAYTRACY OF m/2-ELEMENT LENS ON ANISOTROPIC      0150
     &  MATERIAL'                                                   0160
                                                                    0170
```

```
C   ==== set the number of the boundaries of the lens set ====      0180
        M=3                                                        0190
                                                                   0200
C   ============================================================== 0210
C   =  read lens parameters from FILE.LENSDATA which should have  = 0220
C   =  been available.  C is the paraxial curvature, K is the     = 0230
C   =  conic coefficient and the Bi coefficients are the ith-     = 0240
C   =  order deformation terms                                    = 0250
C   ============================================================== 0260
        OPEN (UNIT=1,FILE='LENSDATA',STATUS='OLD')                 0270
        DO 1 L=1,M                                                 0280
           READ (1,*)C(L),RK(L),B1(L),B2(L),B3(L),B4(L),SPC(L)     0290
  1     CONTINUE                                                   0300
        CLOSE(UNIT=1,STATUS='KEEP')                                0310
                                                                   0320
C   = effective ordinary and extraordinary indices used to form  = 0330
C   = effective index profiles in low and high index waveguides  = 0340
        RNLO=2.2922D0                                              0350
        RNLE=2.2080D0                                              0360
        RNHO=2.2451D0                                              0370
        RNHE=2.3293D0                                              0380
                                                                   0390
        PI=3.141592653589000D0                                     0400
                                                                   0410
C  ====  input the diameter(mm) of the beam analysed  ====         0420
        BW=4.0D0                                                   0430
                                                                   0440
C  ====  N is the number of rays constituting the beam   ====     0450
        N=100                                                      0460
                                                                   0470
        DO 5 K=1,N+1                                               0480
           OPL(K)=0.0D0                                            0490
  5     CONTINUE                                                   0500
                                                                   0510
C   ==== input incident beam angle AFI(degree) from Key Board  ==== 0520
        WRITE(6,*) 'ANGLE OF INCIDENT LIGHT?'                      0530
        READ(5,*) AFI                                              0540
                                                                   0550
C   ==== calculate effective index RNLE of incident beam  ====     0560
        BETA=(90.0D0-AFI)*PI/180.0D0                               0570
           IF(AFI.LT.1.0D-8) THEN                                  0580
              THETAL=90.0D0                                        0590
              GOTO 7                                               0600
           ENDIF                                                   0610
        THETAL=(180.0D0/PI)*DATAN(DTAN(BETA)/RNONEL)               0620
  7     CALL SANINDE (THETAL,RNEL,RNLO,RNLE)                       0630
                                                                   0640
C   ==== initial positions of the rays in the beam  ====           0650
        A0=AFI*PI/180.0D0                                          0660
        DO 10 I=1,N+1                                              0670
           B=(2.0D0*(I-1.0D0)/N-1.0D0)*BW/2.0D0                    0680
           RNIN(1,I)=RNEL                                          0690
           AR(1,I)=A0                                              0700
      XR(1,I)=-DCOS(AR(1,I))*(DCOS(AR(1,I))+B*DSIN(AR(1,I)))+SPC(1) 0710
           YR(1,I)=DCOS(AR(1,I))*(B*DCOS(AR(1,I))-DSIN(AR(1,I)))   0720
  10    CONTINUE                                                   0730
                                                                   0740
C   ==== poistions of the rays at the (j-1)th surface  =====       0750
        SPCT=0.0D0                                                 0760
```

```
          DO 30 J=2,M+1                                                  0770
          RNONEL=(RNLO/RNLE)**2                                          0780
            SPCT=SPCT+SPC(J-1)                                           0790
            DO 20 I=1,N+1                                                0800
               X=XR(J-1,I)                                               0810
               Y=YR(J-1,I)                                               0820
               A=AR(J-1,I)                                               0830
               RNL=RNIN(J-1,I)                                           0840
         CALL SRAYTRA(X,Y,A,XN,YN,AN,C(J-1),RK(J-1),B1(J-1),B2(J-1),     0850
     &         B3(J-1),B4(J-1),SPCT,RNL,RNR,RNHO,RNHE,RNONEL)            0860
               XR(J,I)=XN                                                0870
               YR(J,I)=YN                                                0880
               AR(J,I)=AN                                                0890
               RNIN(J,I)=RNR                                             0900
             RNEFEL=DSQRT((RNLO*DSIN(A))**2+(RNLE*DCOS(A))**2)           0910
             OPL(I)=RNEFEL*DSQRT((XN-X)**2+(YN-Y)**2)+OPL(I)             0920
  20         CONTINUE                                                   0930
                                                                         0940
C   ====    exchange indices on both sides of the boundary  ====        0950
            RNOT=RNLO                                                    0960
            RNLO=RNHO                                                    0970
            RNHO=RNOT                                                    0980
            RNET=RNLE                                                    0990
            RNLE=RNHE                                                    1000
            RNHE=RNET                                                    1010
  30      CONTINUE                                                       1020
                                                                         1030
C   ================================================================     1040
C   = calculate waist and it's position.  if you set BAFO=0 you  =       1050
C   = will get the minmum waist size and its position(back focal =       1060
C   = length) BAFON. if you set BAFO>1, you will get the beam    =       1070
C   = size on that position                                      =       1080
C   ================================================================     1090
          BAFO=0.0D0                                                     1100
          CALL SWAISTS(SPCT,XR,YR,AR,BW,N,M,WAIST,BAFO,BAFON)            1110
          WRITE(6,*) 'WAIST=(um)',WAIST,'AT FOCUS=(mm)',BAFON            1120
                                                                         1130
C  =output the data file FILE.TEMPORAL for Huygens-Fresnel analysis=     1140
          OPEN (UNIT=2,FILE='TEMPORAL',STATUS='NEW')                     1150
          WRITE(2,*) SPCT,N                                              1160
          DO 80 I=1,N+1                                                  1170
             WRITE(2,*)XR(M+1,I),YR(M+1,I),AR(M+1,I),OPL(I)              1180
  80      CONTINUE                                                       1190
                                                                         1200
        WRITE(2,*)'TEMPORAL DATA FOR HUYGENS-FRESNEL ANALYSIS,',         1210
     &'BEAM DIAMETER',BW,'INCIDENT ANGLE',AFI,'BACK FOCAL LENGTH',       1220
     & BAFON                                                             1230
                                                                         1240
          STOP                                                           1250
          END                                                            1260
```

II. FILE.LENSDATA

```
 0.194955210000000004        -1.57877500000000004
-0.126524000000000000E-03    -0.611483999999999989E-04
-0.306717000000000006E-05     0.354368000000000001E-08
 5.00000000000000000
 0.270918599999999997E-01     1.65104399999999996
 0.308406000000000001E-03    -0.110415000000000001E-04
-0.107605000000000006E-05    -0.359954999999999999E-08
 1.09880000000000000
 0.206210409999999997        -0.481859999999999997E-01
-0.798695000000000016E-04     0.123801000000000001E-04
 0.776387000000000002E-06    -0.987955000000000061E-07
 0.114000000000000004
-0.126940140000000007        -1.90943100000000010
 0.147574000000000000E-03    -0.477244999999999994E-05
-0.217914000000000007E-05     0.545041999999999996E-07
 2.29750000000000010
 0.892185100000000009E-01    -1.75026400000000004
-0.274140999999999990E-03     0.199732000000000005E-04
 0.548245999999999998E-06    -0.379726000000000002E-07
 0.640100000000000002
-0.188198589999999999        -0.947816000000000006
 0.128491000000000000E-03    -0.197848999999999992E-05
-0.106986000000000008E-05    -0.150240000000000001E-06
 2.65159999999999996
 0.755856999999999970E-02   142.455762000000000
-0.394213999999999990E-03    -0.128449000000000000E-04
-0.625077000000000006E-06    -0.166810999999999997E-06
 0.419600000000000001
-0.237642580000000006        -0.888111999999999999
 0.652228999999999992E-03     0.263365000000000010E-04
 0.149899999999999996E-05    -0.940160000000000029E-08
 2.03689999999999993
```

```
C  ***************************************************************************
C  * This is a data programme FILE.LENSDATA which is to be used in the *
C  * main progromme.  The data are stored in the order of:             *
C  * C(1), K(1), B1(1), B2(1), B3(1), B4(1), SPACE(1)                  *
C  * ........                                                         *
C  * C(M), K(M), B1(M), B2(M), B3(M), B4(M), SPACE(M)                  *
C  * The present file includes the data of 4-element lens             *
C  * where M is the number of boundaries of the lens set              *
C  ***************************************************************************
```

```
C   ********************************************************************** 0010
C   * This is the subroutine programme SRAYTRA.FORTRAN to be used * 0020
C   * in the main programme to calculate the refractive angle on  * 0030
C   * the boundary of two waveguide in a anisotropic material.    * 0040
C   * From the ray position (X,Y) on the last boundary and its    * 0050
C   * direction A,  the ray position (XN,YN) on the new boundary  * 0060
C   * and its direction AN after refraction are obtained.        * 0070
C   ********************************************************************** 0080
                                                                          0090
      SUBROUTINE SRAYTRA (X,Y,A,XN,YN,AN,C,RK,B1,B2,B3,B4,SPC,            0100
     &                    RNEL,RNEH,RNHO,RNHE,RNONEL)                     0110
      IMPLICIT DOUBLE PRECISION (A-H,O-Z)                                 0120
      COMMON/P/PI                                                         0130
                                                                          0140
C  ====  calculate ray position on the new boundary, (XN,YN)  ====        0150
      DX=0.5D0                                                            0160
      XX=X                                                                0170
      YY=Y                                                                0180
   80 Y1=DABS(YY)                                                         0190
      IF (Y1.LT.1E-6)THEN                                                 0200
         Y10=0.0D0                                                        0210
            ELSE                                                          0220
         Y10=YY**10                                                       0230
      END IF                                                              0240
      IF (Y1.LT.1E-8)THEN                                                 0250
         Y8=0.0D0                                                         0260
            ELSE                                                          0270
         Y8=YY**8                                                         0280
      END IF                                                              0290
      IF (Y1.LT.1E-11)THEN                                                0300
         Y6=0.0D0                                                         0310
            ELSE                                                          0320
         Y6=YY**6                                                         0330
      END IF                                                              0340
      IF (Y1.LT.1E-17)THEN                                                0350
         Y4=0.0D0                                                         0360
            ELSE                                                          0370
         Y4=YY**4                                                         0380
      END IF                                                              0390
      XXX=C*YY**2/(1.0D0+SQRT(1.0D0-(1.0D0+RK)*(C*YY)**2))                0400
      XXX=XXX+B1*Y4+B2*Y6+B3*Y8+B4*Y10                                    0410
      BBB=XXX-XX+SPC                                                      0420
      XAB=DABS(BBB)                                                       0430
      IF(XAB.LT.1D-7) THEN                                                0440
        GOTO 90                                                           0450
      END IF                                                              0460
      IF(BBB.LT.1D-7) THEN                                                0470
        DX=-0.6D0*DABS(DX)                                                0480
      ELSE                                                                0490
        DX=ABS(DX)                                                        0500
      END IF                                                              0510
      XX=XX+DX                                                            0520
      YY=(XX-X)*DTAN(A)+Y                                                 0530
      GOTO 80                                                             0540
   90 XN=XX                                                               0550
```

```
          YN=YY                                                          0560
                                                                         0570
C  == direction of the boundary normal, XY, at the incident point =     0580
          Y2=DABS(YY)                                                    0590
          IF (Y2.LT.1E-7)THEN                                            0600
             Y9=0.0D0                                                    0610
                ELSE                                                     0620
             Y9=YY**9                                                    0630
          END IF                                                         0640
          IF (Y2.LT.1E-9)THEN                                            0650
             Y7=0.0D0                                                    0660
                ELSE                                                     0670
             Y7=YY**7                                                    0680
          END IF                                                         0690
          IF (Y2.LT.1E-13)THEN                                           0700
             Y5=0.0D0                                                    0710
                ELSE                                                     0720
             Y5=YY**5                                                    0730
          END IF                                                         0740
          IF (Y2.LT.1E-23)THEN                                           0750
             Y3=0.0D0                                                    0760
                ELSE                                                     0770
             Y3=YY**3                                                    0780
          END IF                                                         0790
         ZZ=DSQRT(1.0D0-(1.0D0+RK)*(C*YN)**2)                            0800
     XY=C*YN*(2.0D0+(C*YN)**2*(RK+1.0D0)/(ZZ*(1.0D0+ZZ)))/(1.0D0+ZZ)     0810
                                                                         0820
          XY=XY+4.0D0*B1*Y3+6.0D0*B2*Y5+8.0D0*B3*Y7+10.0D0*B4*Y9          0830
                                                                         0840
C  ====  calculate the incident angle, E0, on the boundary  ====         0850
           IF(DABS(A).LT.1D-8) THEN                                      0860
               GAMAL=0.0D0                                               0870
               GOTO 155                                                  0880
             ENDIF                                                       0890
         BETAL=PI/2.0D0-A                                                0900
         THETAL=DATAN(DTAN(BETAL)/RNONEL)                                0910
         GAMAL=PI/2.0D0-THETAL                                           0920
            IF(GAMAL.GT.PI/2.0D0) THEN                                   0930
               GAMAL=GAMAL-PI                                            0940
            ENDIF                                                        0950
  155     GAMAL=GAMAL                                                    0960
                                                                         0970
          E0=GAMAL+DATAN(XY)                                             0980
          AB=SIN(E0)*RNEL                                                0990
         E0SI=DSIGN(1.0D0,E0)                                            1000
                                                                         1010
C   ==== find refractive angle, E1, on the rafractive plane and ===     1020
C   ==== direction, AN, of the refracted ray                  ===     1030
          RNSI=-DSIGN(1.0D0,2.25D0-RNHE)                                 1040
          DTH=0.0050D0*E0SI*RNSI                                         1050
          THETAH=90.0D0-GAMAL*180.0D0/PI                                 1060
          IF(E0.EQ.0.0D0) THEN                                           1070
             DTH=0.0D0                                                   1080
          END IF                                                         1090
  160     THETAH=THETAH+DTH                                              1100
          CALL SANINDE (THETAH,RNEH,RNHO,RNHE)                          1110
          GAMAR=(90.0D0-THETAH)*PI/180.0D0                               1120
          E1=GAMAR+DATAN(XY)                                             1130
          BA=SIN(E1)*RNEH                                                1140
```

```
          AA=(AB-BA)*EOSI*RNSI                                          1150
          BB=DABS(AA)                                                   1160
          IF (BB.LT.1.0D-15) THEN                                       1170
            GOTO 180                                                    1180
          ENDIF                                                         1190
          IF (AA.GT.1.0D-15) THEN                                       1200
           DTH=-DABS(DTH)*0.63D0*EOSI*RNSI                              1210
              ELSE                                                      1220
           DTH=DABS(DTH)*EOSI*RNSI                                      1230
          ENDIF                                                         1240
          GOTO 160                                                      1250
 180     THETAR=THETAH*PI/180.0D0                                       1260
           IF(DABS(THETAH-90.0D0).LT.1D-8) THEN                         1270
              AN=0.0D0                                                  1280
              GOTO 182                                                  1290
            ENDIF                                                       1300
         RNONER=(RNHO/RNHE)**2                                          1310
         BETAR=DATAN(DTAN(THETAR)*RNONER)                               1320
         AN=PI/2.0D0-BETAR                                              1330
            IF(AN.GT.PI/2.0D0) THEN                                     1340
              AN=AN-PI                                                  1350
            ENDIF                                                       1360
  182    AN=AN                                                          1370
                                                                        1380
          RETURN                                                        1390
          END                                                           1400
```

IV. SANINDE.FORTRAN

```
C    ************************************************************    0010
C    *   This is the subroutine progromme SANINDE.FORTRAN to be  *    0020
C    *   used in the main programme to calculate the refractive  *    0030
C    *   index RINDEX of wave normal K in anisotropic waveguide. *    0040
C    ************************************************************    0050
                                                                       0060
          SUBROUTINE SANINDE (THETA,RINDEX,RNO,RNE)                    0070
          IMPLICIT DOUBLE PRECISION (A-H,O-Z)                          0080
          COMMON/P/PI                                                  0090
          THR=THETA*PI/180.0D0                                         0100
        RINDEX=RNO*RNE/SQRT((RNO*SIN(THR))**2+(RNE*COS(THR))**2)       0110
          RETURN                                                       0120
          END                                                          0130
```

V. SWAISTS.FORTRAN

```
C    ************************************************************    0010
C    *  This is the subroutine SWAISTS.FORTRAN to be used in the *    0020
C    *  main programme to calculate the waist size WAIST and its *    0030
C    *  position (back focal length) BAFON                       *    0040
C    ************************************************************    0050
                                                                       0060
```

```
      SUBROUTINE SWAISTS (SPCT,XR,YR,AR,BW,N,M,WAIST,BAFO,BAFON) 0070
      IMPLICIT DOUBLE PRECISION (A-H,O-Z)                        0080
      DIMENSION XR(10,201),YR(10,201),AR(10,201)                 0090
                                                                 0100
      IF (BAFO.GT.1.0D0) THEN                                    0110
          X=BAFO+SPCT                                            0120
          KKK=999                                                0130
          GOTO 40                                                0140
      END IF                                                     0150
         KKK=0                                                   0160
         X=XR(M+1,N/2.0)-YR(M+1,N/2.0)/DTAN(AR(M+1,N/2.0))       0170
         X=X-5.0D0                                               0180
      W2=BW                                                      0190
      DX=0.5D0                                                   0200
 40   WH=-10.0D0                                                 0210
      WL=10.0D0                                                  0220
      DO 50 I=1,N+1                                              0230
         Y=(X-XR(M+1,I))*DTAN(AR(M+1,I))+YR(M+1,I)               0240
         IF (Y.GT.WH) THEN                                       0250
           WH=Y                                                  0260
         END IF                                                  0270
         IF (Y.LT.WL) THEN                                       0280
           WL=Y                                                  0290
         END IF                                                  0300
 50   CONTINUE                                                   0310
      WAIST=WH-WL                                                0320
      IF (KKK.GT.10) THEN                                        0330
         GOTO 65                                                 0340
      END IF                                                     0350
      IF(DABS(DX).LT.1E-7) THEN                                  0360
         GOTO 60                                                 0370
      END IF                                                     0380
      IF (WAIST.GT.W2) THEN                                      0390
         DX=-DX*0.6D0                                            0400
      END IF                                                     0410
      W2=WAIST                                                   0420
      X=X+DX                                                     0430
      GOTO 40                                                    0440
 60   BAFON=X-SPCT                                               0450
 65   WAIST=WAIST*1000.0D0                                       0460
      RETURN                                                     0470
      END                                                        0480
```

VI. HUYFRE.FORTRAN

```
C   ************************************************************** 0010
C   *  This is the programme for Huygens-Fresnel Analysis on     * 0020
C   *  anisotropic waveguide.  Use the data file FILE.TEMPORAL   * 0030
C   *  calculated in the main programme.  Output the data of     * 0040
C   *  intensity profile in percentage and dB in the data file   * 0050
C   *  FILE.INTENS                                               * 0060
C   ************************************************************** 0070
                                                                   0080
      IMPLICIT DOUBLE PRECISION (A-H,O-Z)                          0090
      DIMENSION X0(301),Y0(301),AN(301),OPL(301),AM(301),          0100
```

```
     &              X1(3001),Y1(3001),E(3001),E1(3001)                  0110
                                                                        0120
       WRITE(6,*)'H-F INTENSITY PROFILE ON ANISOTROPIC WAVEGUIDE.       0130
     & E(Y)=SUM((EXP(-iK*L)).  USING DATA FROM FILE.TEMPORAL'           0140
                                                                        0150
C    === N1 is the number of analysed points on the focal plane ===     0160
          N1=100                                                        0170
                                                                        0180
C    ==== set wavelength(um)   ====                                     0190
          WL=0.8300d0                                                   0200
          WL=WL/1000.0d0                                                0210
                                                                        0220
C    ==== you must give the position (back focal length) BAFO   ====   0230
C    ==== of the focal plane.  after several choices you can    ====   0240
C    ==== find an optimum one.                                  ====   0250
          WRITE(6,*)'BAFO'                                              0260
          READ(5,*)BAFO                                                 0270
                                                                        0280
C    ==== AGD is the ratio of Gaussian width to beam diameter  ====     0290
          AGD=1.0D0                                                     0300
                                                                        0310
C    ==== ordinary and extraordinary refractive indices of the ====     0320
C    ==== waveguide where the focus is                         ====     0330
          RNLO=2.2451D0                                                 0340
          RNLE=2.2800D0                                                 0350
                                                                        0360
          PI=3.141592653589000D0                                        0370
                                                                        0380
C    ==== read FILE.TEMPORAL, assuming the original incident ====       0390
C    ==== beam has a Gaussian intensity profile              ====       0400
          OPEN(UNIT=1,FILE='TEMPORAL',STATUS='OLD')                     0410
          READ(1,*) SPC2,N0                                             0420
          ATO=0.0D0                                                     0430
          DO 10 I=0,N0                                                  0440
          READ(1,*)X0(I),Y0(I),AN(I),OPL(I)                             0450
          AM(I)=DEXP(-((2.0D0*I/N0-1.0D0)/AGD)**2)                      0460
          ATO=ATO+AM(I)                                                 0470
   10     CONTINUE                                                      0480
          ATO=ATO*ATO                                                   0490
          CLOSE(UNIT=1,STATUS='KEEP')                                   0500
                                                                        0510
C    ==== calculate the intensity profile  ====                         0520
          EAM=0.0D0                                                     0530
          NC=N0/2                                                       0540
          X=BAFO+SPC2                                                   0550
          YC=Y0(NC)+(X-X0(NC))*DTAN(AN(NC))                             0560
C    ==== YRANG(mm) is the range in which you want to carry out ====    0570
C    ==== the Huygens-Fresnel Analysis                         ====     0580
          YRANG=0.020D0                                                 0590
          YD=YRANG/N1                                                   0600
                                                                        0610
C    ================================================================  0620
C    =    YL is the point of low side of the analysis range       =    0630
C    =    and YL+YRANG is the high side of the analysis range     =    0640
C    =    sometime you have to use a big YRANG at first to        =    0650
C    =    find where the intensity peak is and decide where       =    0660
C    =    the YL is                                               =    0670
C    ================================================================  0680
          YLD=-0.0210D0                                                 0690
```

```
      YL=YC+YLD                                                          0700
                                                                         0710
C     ==== calculate intensity profile in the range of YRANG ====        0720
      YLS=YL-YD                                                          0730
      DO 20 J=1,N1+1                                                     0740
        X1(J)=X                                                          0750
        YLS=YLS+YD                                                       0760
        Y1(J)=YLS                                                        0770
        ES=0.0D0                                                         0780
        EC=0.0D0                                                         0790
        DO 30 I=0,N0                                                     0800
          RL=DSQRT((X0(I)-X1(J))**2+(Y0(I)-Y1(J))**2)                    0810
          IF (DABS(Y1(J)-Y0(I)).LT.1.0D-20) THEN                         0820
              A=0.000D0                                                  0830
          GOTO 15                                                        0840
          END IF                                                         0850
        A=DATAN((Y1(J)-Y0(I))/(X1(J)-X0(I)))                             0860
                                                                         0870
   15   RNEF=DSQRT((RNLO*DSIN(A))**2+(RNLE*DCOS(A))**2)                  0880
                                                                         0890
          RLP=(RNEF*RL+OPL(I))/WL                                        0900
          PP=(RLP-INT(RLP))*2.0D0*PI                                     0910
          ES=ES+AM(I)*DSIN(PP)                                           0920
          EC=EC+AM(I)*DCOS(PP)                                           0930
   30     CONTINUE                                                       0940
          E0=ES*ES+EC*EC                                                 0950
          E(J)=(E0/ATO)*100.0D0                                          0960
          IF(E(J).GT.EAM) THEN                                           0970
             EAM=E(J)                                                    0980
             YEAM=(Y1(J)-YC)                                             0990
          END IF                                                         1000
   20     CONTINUE                                                       1010
          WRITE(6,*)'Yc(mm)',Yc,'Ymax(mm)',yeam                          1020
                                                                         1030
C     ==== intensity normalization and output to FILE.INTENS ====       1040
          OPEN(UNIT=2, FILE='INTENS', STATUS='NEW')                      1050
          DO 40 J=1,N1+1                                                 1060
          E(J)=E(J)/EAM*100.0D0                                          1070
          Y1(J)=(Y1(J)-(YC+YEAM))*1000.0D0                               1080
          WRITE(2,*)Y1(J),E(J)                                           1090
    40    CONTINUE                                                       1100
                                                                         1110
C     ==== intensity in dB and output to FILE.INTENS ====               1120
          DO 50 J=1,N1+1                                                 1130
          E1(J)=10.0D0*(DLOG10(E(J))-2.0D0)                              1140
          WRITE(2,*)Y1(J),E(J)                                           1150
    50    CONTINUE                                                       1160
                                                                         1170
          WRITE(2,*)'Huygens-Fresnel intensity, Back Focal               1180
         & Length (mm)',BAFO                                             1190
C     ==== Yc+Yeam is the distance between the spot and the lens ====    1200
C     ==== axis                                                  ====    1210
          WRITE(2,*)'Yc(mm)',Yc,'Ymax(mm)',yeam                          1220
                                                                         1230
          CLOSE(UNIT=2, STATUS='KEEP')                                   1240
                                                                         1250
          STOP                                                           1260
          END                                                            1270
```

APPENDIX B Publication List and Reprints

P. Jiang, W. Zhang and P. J. R. Laybourn, "Waveguide Coupling Efficiency in Thin-Film Homogeneous Lenses", IEE Proceedings, Vol.137, Pt.J, pp.255-260, 1990.

Pisu Jiang, P. J. R. Laybourn and G. C. Righini, "Homogeneous Thin-Film Lens on $LiNbO_3$", Proc.SPIE, Vol.1362, pp.899-906, Physical Concepts of Materials for Novel Optoelectronic Device Applications, Aachen, FRG, Oct.28-Nov.2, 1990

Pisu Jiang, P. J. R. Laybourn and G. C. Righini, "Homogenous Planar Lens on Anisotropic Waveguide", Journal of Modern Optics, Vol.39, pp.121-132, 1992

Pisu Jiang and P. J. R. Laybourn, "Waveguide Lens on $LiNbO_3$: A New Design", The 2nd IEEE International Workshop on Photonic Networks, Components and Applications, Montebello, Canada, 9-11 March 1992

Pisu Jiang and P. J. R. Laybourn, "Coupling Efficiency of TM modes on the Boundary of Two Waveguides", to be published

Pisu Jiang, Feng Zhou, P. J. R. Laybourn and R. M. De La Rue, "Buried Optical Waveguide Polariser by Titanium Indiffusion and Proton-Exchange in $LiNbO_3$", to be published in IEEE Photonics Technology Letters, Vol.4, August 1992

F. Zhou, P. S. Jiang, R. M. De La Rue, C. N. Ironside, T. Han, B. Henderson and A. I. Ferguson, "Spectroscopic Studies of Erbium-Titanium Codoping of Lithium Niobate Waveguides for Active Device Applications", postdeadline paper PD5, Integrated Photonics Research, New Orleans, USA, April 13-16, 1992

G. C. Righini, S. Pelli, P. J. R. Laybourn, P. Jiang and R. Shen, "Waveguide Collimator Design for Integrated Optical Signal Processing Devices", to be published in GRIN'92 Topical Meeting, Galicia, Spain, October 1992

Waveguide coupling efficiency in thin-film homogeneous lenses

P. Jiang
W. Zhang
P.J.R. Laybourn

Indexing terms: Waveguides and waveguide components, Optical processing

Abstract: Homogeneous thin-film lenses for integrated optical signal processing devices consist of alternating regions of high and low index waveguide. Boundary losses depend on coupling efficiency between fundamental modes in the two regions. Coupling efficiency has been calculated for various assumed index profiles, and also for measured optical field profiles in glass and lithium niobate waveguides. The glass system showed poor performance, but a system consisting of Ti-indiffused and annealed proton-exchanged waveguides had well matched modes between which the coupling efficiency calculated from measured field profiles was 99%.

1 Introduction

There is a continuing interest in thin-film planar lenses for integrated optical signal processing applications, as exemplified by the integrated acousto-optical spectrum analyser [1]. Because of the expense and difficulty in fabricating geodesic lenses [2], other, planar methods of making thin-film lenses on lithium niobate have been investigated [3]. Fresnel diffraction lenses have been designed and produced experimentally [4, 5], and homogeneous refracting multielement lenses have been designed and predicted to have superior performance, particularly in off-axis focusing and efficiency [6]. In homogeneous thin-film lenses [7], guided light is refracted at the boundary between two regions of disparate waveguide (Fig. 1). On a lithium niobate substrate, the two waveguide regions may be titanium-diffused, with low effective index, and proton-exchanged, with high effective index. Alternatively for the low effective index region *dilute* proton change may be employed. Having optimised the design of a homogeneous multielement lens, involving the positioning of the boundaries between low and high index waveguide regions, the lenses will in practice be limited by the efficiency of light transfer across that boundary, which is the coupling efficiency between the fundamental waveguide modes in the two waveguides. Light may be lost by scattering out into the substrate, or by coupling to modes other than the fundamental $m = 0$ mode in the second guide. The coupling efficiency η may be expressed as the overlap integral between the transverse electric field profiles E_l and E_h in the low and high index guiding regions, respectively. Early multielement lens designs [8] using circular lens boundaries required of the order of 30 elements (and 60 boundaries) so that η would have to be very close to 100% at each boundary. Later designs using acircular lens elements need only 4 or 5 elements, with 8 or 10 boundaries, so that while coupling loss will be important a satisfactory overall performance will be more readily achievable [6].

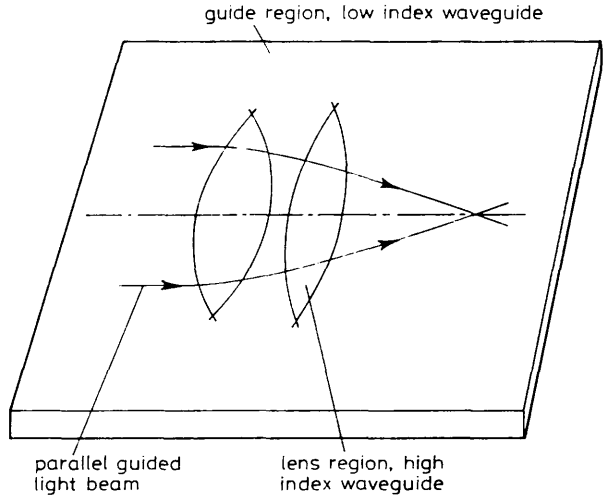

Fig. 1 *Homogeneous thin film lens*

It is clear that in order to reduce light in unwanted modes (which would be refracted differently from the fundamental mode and hence would constitute a background noise signal around the focused spot) the low index waveguide at least should only support one mode. It will be shown later that the high index guide will inevitably be multimode for optimum coupling efficiency η, but any higher mode excited in the high index lens element by coupling from the fundamental mode of the low index waveguide region, at low efficiency, will be recoupled at exit from the lens element at equally low efficiency to the fundamental guide mode, and although mis-focused, should not present significant background noise if η is high. If, however, higher modes were supported in the guide region there could be significant coupling of light to them from higher modes in the lens region.

Various refractive index profiles have been considered for the two guiding layers. Using step profiles the solution of the waveguide characteristic equation is straightforward and electric field profiles are easily calculated.

Paper 7364J (E13), received 23 November 1989

The authors are at the Department of Electronics and Electrical Engineering, University of Glasgow, Glasgow G12 8QQ, United Kingdom

W. Zhang is on leave from the Department of Electronics, Shandong University, People's Republic of China

Such a profile could be used to model a proton-exchanged waveguide. For diffused waveguides various profiles approximate to the true profile, and waveguides with Gaussian, exponential and error function complement refractive index profiles have been solved numerically to determine their electric field profiles. First experiments to measure mode profiles and the coupling efficiency obtained were made on glass substrates with potassium and silver ion-exchanged waveguides, while recent results deal with x-cut $LiNbO_3$ on which are formed Ti-diffused and TIPE waveguides.

2 Field overlap calculation

The coupling efficiency, η, between two TE modes at a boundary between two dissimilar planar waveguides can be expressed as the overlap integral of the transverse electric field profiles [9]:

$$\eta = \frac{[\int E_l(x) \times E_h(x)\, dx]^2}{[\int E_l^2(x)\, dx] \times [\int E_h^2(x)\, dx]} \quad (1)$$

where $E_l(x)$ and $E_h(x)$ are the electric field profiles of the guiding modes in the low index waveguide and high index waveguide, respectively. The electric profile $E(x)$ in a planar waveguide is a solution of:

$$\frac{d^2E(x)}{d^2x} + k^2 \times [n^2(x) - n_e^2] \times E(x) = 0 \quad (2)$$

where $n(x)$ is the refractive index profile; n_e is the guide effective index, β/k; $k = 2\pi/\lambda_0$; and λ_0 is the free-space wavelength. Calculations and measurements have been made with $\lambda_0 = 633$ nm.

The characteristic equation of the step-index planar waveguide is simply solved, yielding the effective index n_e as a function of waveguide depth, when the transverse field may be written as

$$E(x) = \begin{cases} \exp(x \times R) & x < 0 \text{ (superstrate: air)} \\ \cos(x \times Q) + \dfrac{R}{Q}\sin(x \times Q) & 0 \leqslant x < d \\ \left[\cos(d \times Q) + \dfrac{R}{Q}\sin(d \times Q)\right] & \\ \quad \times \exp[P \times (d - x)] & d \leqslant x \end{cases} \quad (3)$$

d is the waveguide thickness and

$$R = k \times (n_e^2 - 1)^{1/2}$$
$$Q = k \times (n_1^2 - n_e^2)^{1/2}$$
$$P = k \times (n_e^2 - n_2^2)^{1/2}$$

n_1 and n_2 are the waveguide and substrate refractive indices, respectively.

For gradient index profile, planar waveguides with a known index profile $n(x)$, $E(x)$ may be written as:

$$E(x) = \begin{cases} E_1(x) = \exp(x \times R) & x < 0 \text{ (air)} \\ E_2(x) & x > 0 \end{cases}$$

where

$$R = k \times (n_e^2 - 1)^{1/2}$$
$$E_2(0) = E_1(0) = 1$$
$$E_2' = E_1'(0) = R$$

Assuming a value for n_e the resulting electric field profile $E_2(x)$ can be calculated numerically from the superstrate/guide interface down into the graded index guiding region by using eqn. 2 over successive increments of x. It is found that only when the true solution for n_e is taken does $E_2(x)$ approach zero for very large x. Then the corresponding electric field profile is also known. The method has shown to be in good agreement with known solutions of planar waveguides.

Having calculated the electric field profiles E_l and E_h in two adjacent waveguide sections, with low and high refractive indices, the coupling efficiency across the interface is numerically calculated by using eqn. 1.

3 Computed solutions

(i) *Step–step index profile*

Both waveguide regions, with low and high indices, are assumed to possess step refractive index profiles: the refractive index is constant across the waveguide region. Fig. 2 shows the coupling efficiency η as a function of the depth of the high index guide for a particular low-index guide depth d_l of 2.2144 μm, in a waveguide system where the substrate index $n_2 = 2.202$, and the guide indices are $n_l = 2.212$, $n_h = 2.322$.

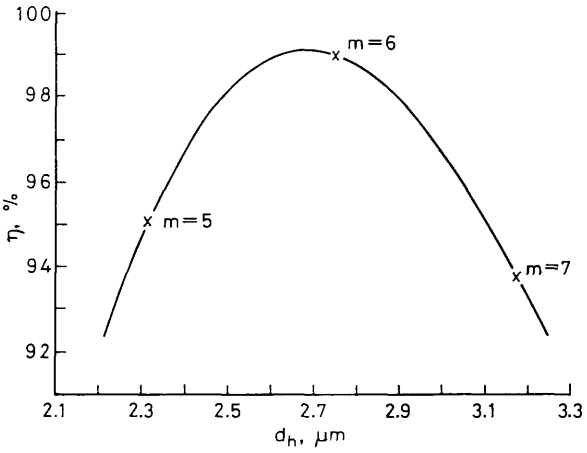

Fig. 2 *Coupling efficiency vs high index waveguide depth*
$n_l = 2.212$, $n_h = 2.322$, $n_2 = 2.202$, $d_l = 2.2144$ μm

The high-index guide is multimoded around the depth d_h for optimum coupling efficiency, and the cut-off depths for modes $m = 5$, 6, 7 are shown on the graph. The optimum coupling efficiency is seen to occur for d_h around 2.68 μm, slightly deeper than the low-index guide. Fig. 3 is a plot of such optimum efficiencies as a function of the low-index guide depth, where we see that increasing d_l continues to increase the coupling efficiency. However, the guide region in an optical signal processor should be single-mode, so that the optimum low-index guide depth will be just below the cut-off depth for $m = 1$ (shown in Fig. 3). In the following cases the low-index guide depths are also selected to be just below the cut-off depth for $m = 1$ mode.

Fig. 4 shows the electric field profiles of the modes in the two coupled waveguides, with η maximised at 99.1% for the particular refractive indices chosen.

The optimum value of d_h, the high index waveguide depth, is plotted against the low index guide depth d_l in Fig. 5, from which it is clear that $d_h > d_l$ for optimum coupling efficiency. The point $m = 1$ is the single-mode limit of d_l.

(ii) *Gaussian–step index profiles*

The Gaussian refractive index profile is expressed as

$$n(x) = n_2 + \Delta n \times \exp\{-(x/d)^2\}$$

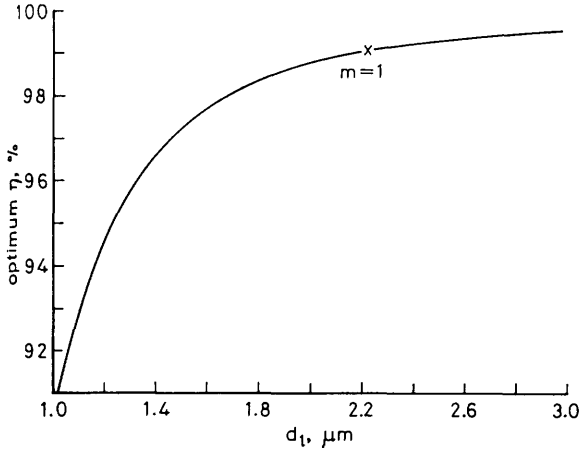

Fig. 3 *Optimum efficiency vs low index waveguide depth*
$n_1 = 2.212$, $n_h = 2.322$, $n_2 = 2.202$

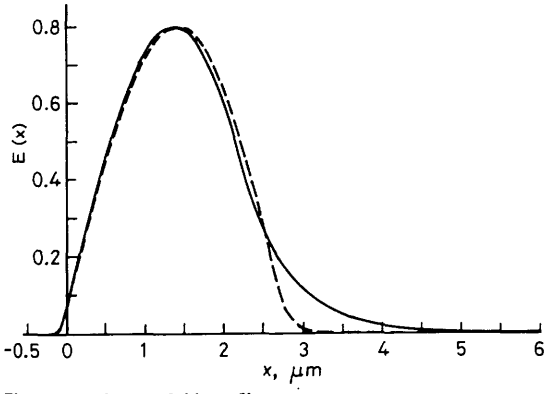

Fig. 4 *Electric field profiles*
$n_1 = 2.212$, $n_h = 2.322$, $n_2 = 2.202$, $d_1 = 2.2144$ μm, $d_h = 2.677$ μm, $\eta = 99.1\%$
——— low index
- - - - high index

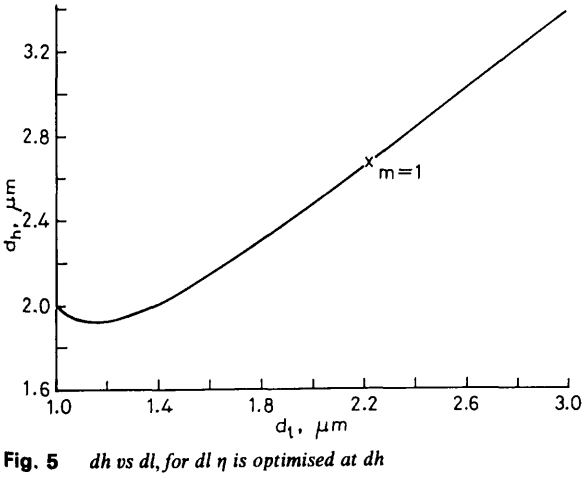

Fig. 5 *dh vs dl, for dl η is optimised at dh*
$n_1 = 2.212$, $n_h = 2.322$, $n_2 = 2.202$

where d is $1/e^2$ depth and Δn is the increase in surface refractive index over that of the substrate. The low index waveguide is approximated by the Gaussian profile, the high index waveguide by the step index profile, modelling Ti-indiffused and proton exchanged regions. For given refractive indices, waveguide depths have again been optimised, and an example is shown in Fig. 6, modelling the Ti/PE system. Because the electric field distributions are a relatively poor match, the overlap integral can only predict a maximum η of 95.6%.

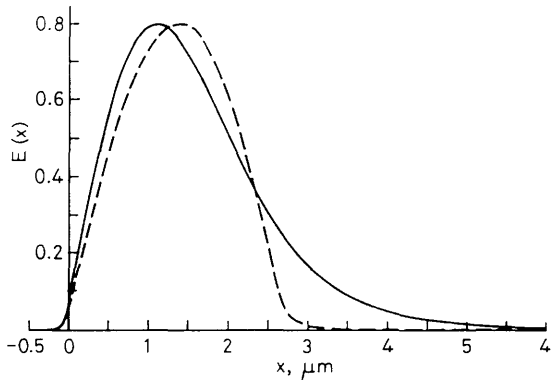

Fig. 6 *Electrical field profiles*
$n_1 = 2.202 + 0.01^*\exp(-(x/2.0)^2)$, $n_2 = 2.202$, $n_h = 2.322$, $d_h = 2.609$ μm, $\eta = 95.6\%$
——— low index
- - - - high index

(iii) *Gaussian–Gaussian index profiles*

In this and the following two examples various graded index approximations were used to simulate silver and potassium ion-exchanged glass waveguides.

If both high and low index guiding regions are Gaussian in refractive index distribution, the fundamental modes can be well matched, as shown in Fig. 7. An optimised coupling efficiency of 99.6% was predicted.

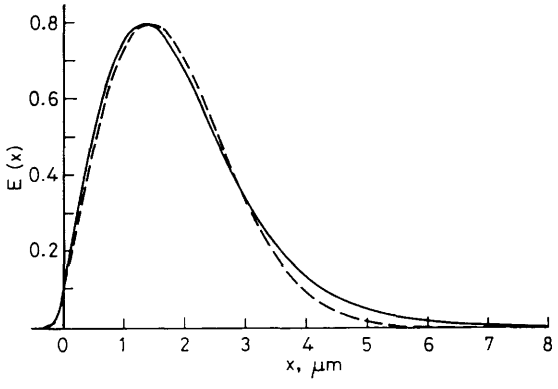

Fig. 7 *Electric field profiles*
$n_1 = 1.512 + 0.009^*\exp(-(x/2.0)^2)$, $n_h = 1.512 + 0.100^*\exp(-(x/12.37)^2)$, $\eta = 99.6\%$
——— low index
- - - - high index

However, the high index waveguide depth is then about 12 μm, and the waveguide supports 27 modes. Even though it might be possible to achieve such a depth, transverse diffusion would be going on simultaneously, degrading the lens boundary definition between the two waveguides.

(iv) *Exponential–exponential and erfc–erfc index profiles*

The exponential index profile may be expressed as:

$$n(x) = n_2 + \Delta n \times \exp(-x/d)$$

while the complementary error function (erfc) profile is:

$$n(x) = n_2 + \Delta n \times \operatorname{erfc}(x/d)$$

$$= n_2 + \Delta n \times \left(1 - \frac{2}{\sqrt{\pi}} \int_0^{x/d} e^{-x^2}\, dx\right)$$

Figs. 8 and 9 show optimised electric field profiles. Again, high maximum coupling efficiencies are predicted, but the optimum high index waveguide depths are now 70 μm and 60 μm, respectively, outside the limits of good wave-

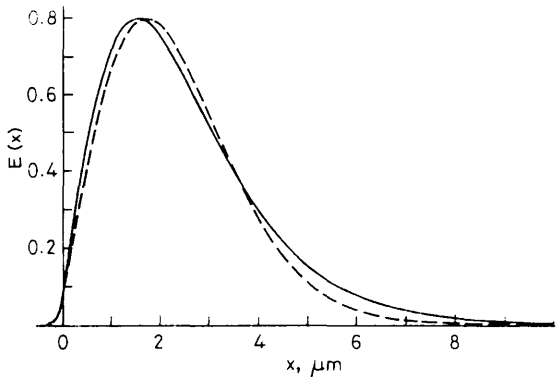

Fig. 8 *Electric field profiles*
$n_l = 1.512 + 0.009^* \exp(-x/1.8)$, $n_h = 1.512 + 0.100^* \exp(-x/71.63)$, $\eta = 99.4\%$
——— low index
- - - - high index

guide fabrication. With these three highly overmoded graded index profiles, it is clear that the fundamental mode is confined to the region of highest refractive index, very near to the waveguide surface, and the large diffusion depth is needed to extend the electric field profile sufficiently to match the wider-spread low index field profile.

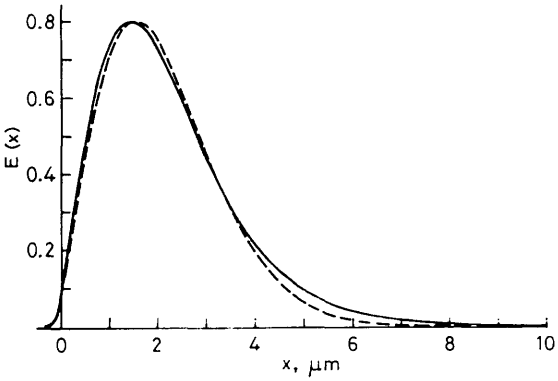

Fig. 9 *Electric field profiles*
$n_l = 1.512 + 0.009^* \text{erfc}(x/3.5)$, $n_h = 1.512 + 0.100^* \text{erfc}(x/62.75)$, $\eta = 99.7\%$
——— low index
- - - - high index

4 Experiment

Two substrate materials have been considered as the basis for experimental lens preparation, soda-lime glass and single-crystal lithium niobate. It was hoped that the lens preparation on glass substrates would prove to be relatively straightforward, using silver and potassium ion exchange with the sodium in the glass to provide the high and low index waveguide regions [10], rather than the more involved but more useful lens production on lithium niobate by proton exchange and titanium indiffusion. It happens that the refractive index ratio between high and low index guides is similar in the two systems, allowing the same lens designs to be used, since the refractive index ratio is the only material parameter appearing in the designs [6, 8].

Measurements of electric field intensity profiles were carried out on waveguides fabricated on glass and lithium niobate substrates. One end of each sample was polished to optical quality. Light was coupled into the waveguide by prism coupler, to excite only the lowest order mode. A microscope objective ($\times 40$) was used to image the polished waveguide end face onto a vidicon, recording the near field intensity profile of the guided wave. The magnification of the system was fixed so that the recorded mode profiles of all samples were comparable. The transverse intensity profile $I(x)$ of the lowest order mode in each guide was sampled and stored by an associated computer, and from pairs of intensity profiles measured in low and high index guides on the same substrate material the predicted coupling efficiency was calculated using a numerical approximation of the overlap integral, eqn 1. The range of samples was limited, and the position of the air-guide interface had to be estimated from the measured profiles. Examples of measured profiles are shown in Figs. 10 to 14. In all cases there is a

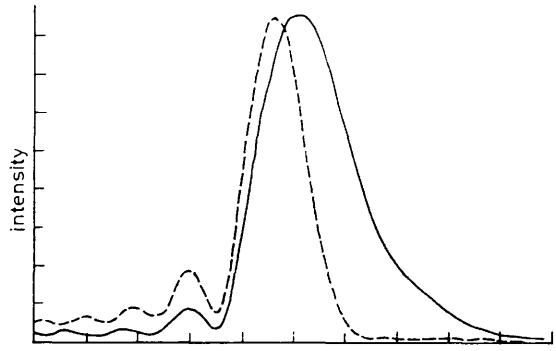

Fig. 10 *Measured optical intensity profiles*
$\eta = 90.9\%$
Low index waveguide: k^+ exchange, 20 min. at 375°C; high index waveguide: Ag^+ exchange, 180 min. at 225°C
——— low index
- - - - high index

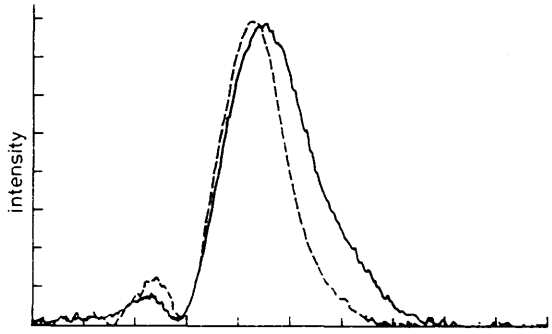

Fig. 11 *Measured optical intensity profiles*
$\eta = 93.4\%$
Low index waveguide: 25 mm Ti, 1000°C, 4 hrs; high index waveguide: Benzoic acid, 236°C, 3 hrs
——— low index
- - - - high index

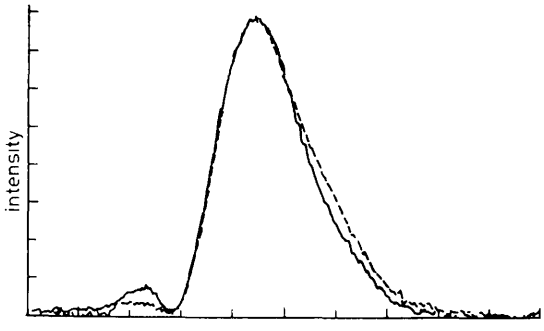

Fig. 12 *Measured optical intensity profiles*
$\eta = 99.1\%$
Low index waveguide: 25 nm Ti, 1000°C, 4 hrs; high index waveguide: Benzoic acid, 236°C, 3 hrs, annealing, 300°C, 3 hrs
——— low index
- - - - high index

ecaying oscillatory field outside the surface of the guide ut for the purpose of calculating the overlap, this part of ie measured profile was discounted, and the first inimum was taken as the position of the surface.

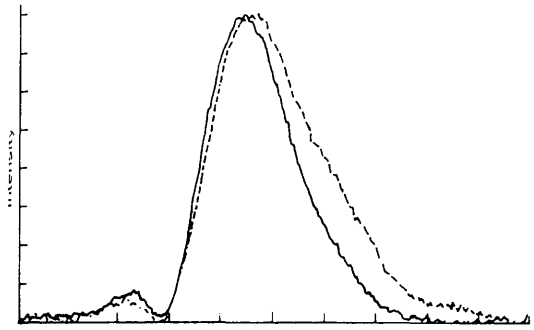

Fig. 13 *Measured optical intensity profiles*

= 95.5%
low index waveguide: 25 nm Ti, 1000°C, 4 hrs; high index waveguide: Benzoic id, 236°C, 3 hrs, annealing, 300°C, 6 hrs
—— low index - - - - high index

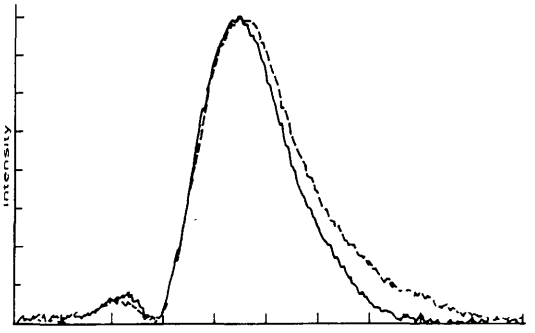

Fig. 14 *Measured optical intensity profiles*

= 96.5%
low index waveguide: 25 nm Ti, 1000°C, 4 hrs; high index waveguide: Benzoic id, 236°C, 3 hrs, annealing, 300°C, 9 hrs
—— low index - - - - high index

(i) *K^+ and Ag^+ ion exchanged glass waveguides*

The ion exchange temperatures used were 375°C for K^+ exchange and 225°C for Ag^+ exchange. A diffusion time of 20 minutes was used for the potassium exchange, forming a single-mode waveguide. Different diffusion times were used to form various overmoded silver-exchanged guides, as shown in Table 1, in an attempt to produce a guide that would be deep enough to support a fundamental mode well matched to the potassium-exchanged guide. Examples of measured optical field profiles in potassium and silver ion exchanged guides are shown in Fig. 10, where it can be seen that even with 3 h of diffusion time, the depth of the fundamental mode in the high index guide is insufficient to match the mode profile in the low index guide. The computed coupling efficiency resulting frm the measured mode profiles is shown in Table 1. It is apparent that the efficiency is rising very slowly with diffusion time.

Table 1: Coupling efficiency between K^+ exchanged waveguide (20 min at 375°C) and Ag^+ exchanges waveguide (at 225°C)

Ag^+ exchange time, h	3	6	10	12
Number of modes	5	8	10	11
η, %	90.9	86.3	91.2	91.3

(ii) *Titanium–indiffused and proton-exchanged waveguides on $LiNbO_3$*

Low-effective index waveguides were made by titanium indiffusion into lithium niobate. A 25 nm film of Ti was deposited on x-cut lithium niobate substrates. The samples were heated to 1000°C for four hours in flowing wet oxygen, resulting in a single mode waveguide. TE propagation was used in the y direction. The effective mode index was measured to be 2.2065, while the substrate extraordinary index was 2.2015. The optical mode intensity profile was recorded as before.

One Ti-diffused sample was then subjected to proton exchange in benzoic acid at 236°C for three hours. The sample was left to stabilise for 16 days [11], after which time the intensity profile of the fundamental mode was measured (Fig. 11). The sample was then annealed for three hour periods at 300°C in wet oxygen, and the optical mode profile remeasured after each period of annealing (Figs. 12 to 14). After the first annealing period the profile is seen to match very well to the Ti-diffused low index profile. However, subsequent annealing degrades the good mode match. The calculated coupling efficiency, shown in Table 2, confirms the matching properties of the waveguides.

Table 2: Coupling efficiency between TI waveguide (25 nm Ti, 4 h at 1000°C) and annealed TIPE waveguide (Benzoic Acid, 3 h at 236°C, annealing at 300°C)

Annealing time, h	0	3	6	9
Number of modes	7	10	10	10
η, %	93.4	99.1	95.5	96.5

5 Discussion

The experimental results of mode profile measurements on glass ion exchanged waveguides may be compared with a Gaussian model for the profile [12]. The electric field profiles of the low and high Gaussian refractive index profiles give a high theoretical optimum efficiency, calculated to be 99.6% for the particular waveguides considered. However, to achieve this optimum efficiency the high index waveguide profile has to be about 12 μm deep and support 27 modes. In the experimental Ag^+ exchanged guides the longest diffusion time of 12 hours only produced a guide supporting 11 modes, and consequently the best coupling efficiency calculated from measured field profiles was only 91.3%. Step index guides could be expected to result in better-matched mode profiles, and can be produced by electric-field-assisted ion exchange [12]. In such a high index guide the step index profile would result in a deeper fundamental mode profile, and hence a shallower optimum guide depth. However, the added difficulties of electric field assistance make its use less desirable, while the guides produced by simple ion exchange do not seem to offer a good medium for experimental lens fabrication.

The index profiles of the multimode proton-exchanged waveguides were calculated from the mode effective indices measured after each annealing step (and plotted in Fig. 16), and are shown in Fig. 15. After annealing the proton-exchanged region assumed an index profile very close to rectangular, with the three hour-annealed guide showing a good mode profile match to the Ti-diffused guide. Further annealing, although not changing the refractive index profile greatly, evidently had sufficient effect on the mode intensity profile of the proton-exchanged guide to reduce significantly the match between the high and low index guides and the resulting computed coupling efficiency. Indeed, the optimum coupling efficiency is much better than would have been expected from the theoretical modelling of the Ti-indiffused waveguide by a Gaussian profile and the

proton-exchanged waveguide by a step profile, as discussed in Section 3(ii).

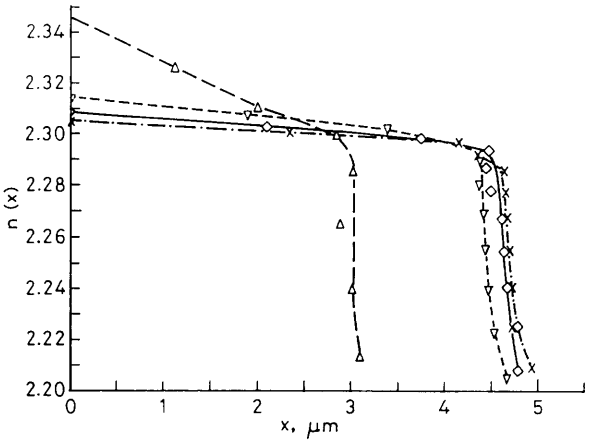

Fig. 15 *Variation of index profile vs annealing time*
Benzoic acid, 236°C, 3 hrs, annealing temperature 300°C
Δ —— 0 hr
▽ ------- 3 hrs
◇ —— 6 hrs
× -·-·-· 9 hrs

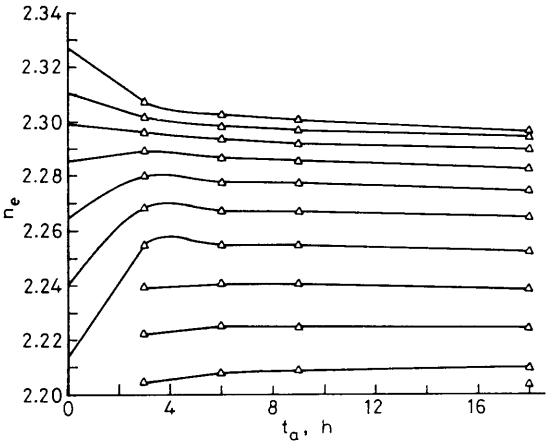

Fig. 16 *Effective index vs annealing time*
x-cut $LiNbO_3$, Benzoic acid, 236°C, 3 hrs, annealing temperature 300°C

6 Conclusions

The experiments that have been performed on glass and lithium niobate optical waveguides suggest that while the Ti/PE double waveguide system might be used successfully to produce homogeneous refracting thin-film lenses for signal-processing applications, simple ion exchange on a soda-lime glass substrate will not model the lithium niobate lens system well, notwithstanding a similar effective index ratio. It seems that the problem with high effective index graded-index waveguides is a concentration of the electric field at the peak of the index profile, restricting the width of the fundamental mode profile and producing a poor match to a mode in a low-effective-index guide. With 99% coupling efficiency at a single boundary in the $LiNbO_3$ Ti/PE waveguide system, a 5 element acircular lens might be expected to contribute a loss of only 10% or 0.05 dB overall which is an acceptable figure.

7 Acknowledgment

Pisu Jiang wishes to thank Mrs. M. Howes and Mr. F.S. Howes of Montreal, Canada and ORS Committee of UK for the financial supports.

8 References

1 ANDERSON, D.B., BOYD, J.T., HAMILTON, M.C., and AUGUST, R.R.: 'An integrated-optical approach to the Fourier transform', *IEEE J. Quant. Elec.*, 1977, **13**, pp. 268–275
2 DOUGHTY, G.F., DE LA RUE, R.M., SINGH, J., SMITH, J.F., and WRIGHT, S.: 'Fabrication techniques for Geodesic lenses in lithium niobate', *IEEE Trans.*, 1982, **CHMT-5**, pp. 205–209
3 ANDERSON, D.B., DAVIS, R.L., BOYD, J.T., and AUGUST, R.R.: 'Comparison of optical-waveguide lens technologies', *IEEE J. Quant. Elec.*, 1977, **13**, pp. 275–282
4 PITT, C.W., SKINNER, J.D., and TROTTER, G.R.: 'Computer simulation of thin film lenses', *Opt. Com.*, 1985, **53**, pp. 87–90
5 REID, S.A., VARASI, M., and REYNOLDS, S.: 'Double dilute melt proton exchange Fresnel lenses for $LiNbO_3$ optical waveguides', *J. Opt. Com.*, 1989, **10**, pp. 67–73
6 LAYBOURN, P.J.R., MOLESINI, G., and RIGHINI, G.C.: 'Homogeneous refracting lenses for integrated optical circuits', *J. Modern Opt.*, 1988, **35**, pp. 1029–1048
7 ZANG, D.Y., and TSAI, C.S.: 'Single-mode waveguide microlenses and microlens arrays fabrication in $LiNbO_3$ using titanium indiffused proton exchange technique', *Appl. Phys. Lett.*, 1985, **46**, pp. 703–705
8 LAYBOURN, P.J.R., and RIGHINI, G.C.: 'New design of thin-film lens', *Elec. Lett.*, 1986, **22**, pp. 343–344
9 HUNSPERGER, R.G., YARIV, A., and LEE, A.: 'Parallel end-butt coupling for optical integrated circuits', *Appl. Opt.*, 1977, **16**, pp. 1026–1032
10 CHARTIER, G.H., LAYBOURN, P.J.R., and GIROD, A.: 'Masking process for double-ion-exchanged glass optical waveguide', *Elect. Lett.*, 1986, **22**, pp. 925–926
11 JACKEL, J.L., and RICE, C.E.: 'Short and long term stabilities in proton-exchanged $LiNbO_3$ waveguides', *SPIE*, 1984, **460**, p. 43
12 RAMASWAMY, R.V., and SRIVASTAVA, R.: 'Ion-exchanged glass waveguides: A review', *J. Lightwave Tech.*, 1988, **6**, pp. 984–1001

Homogeneous thin film lens on $LiNbO_3$

Pisu Jiang, P.J.R.Laybourn and G.C.Righini *

Department of Electronics and Electrical Engineering
University of Glasgow, Glasgow G12 8QQ, UK
*IROE/CNR, 50127 Florence, Italy

ABSTRACT

Problems in the fabrication of homogeneous integrated lenses on lithium niobate were investigated. TIPE and double proton exchange waveguide fabrication methods were compared, and various masking systems tested. Mode matching between a low index single-mode DMPE waveguide and a high index multi-mode PE waveguide was optimized.

1.INTRODUCTION

There is a continuing interest in thin-film planar lenses for optical signal processing applications. Recent reports have described Fresnel lenses made on $LiNbO_3$ [1,2] and on GaAs [3] and single-element homogeneous TIPE lens on $LiNbO_3$ [4]. However, when working at off-axis input beam angles the quality of the focused spot deteriorates severely. Multi-element acircular homogeneous lens designs, as in Fig.1, offer the possibility of excellent off-axis performance [5,6]. For such multi-element lenses, some problems in fabrication, giving rise to coupling loss at the boundaries and loss through out-diffusion modes and scattering must be addressed. Some recent work will be reported on designing the waveguides in which the multi-element homogeneous lenses will be fabricated for minimum throughout coupling loss, and in fabricating those designs on lithium niobate waveguides.

2.FABRICATION OF WAVEGUIDES AND LENS

2.1. Waveguide System

In order to obtain a sufficiently high effective index, proton exchange must be used on $LiNbO_3$ for the high-index lens region. But for the low index planar guide region, either titanium indiffusion(TI) or dilute melt proton exchange(DMPE) may be utilized, both of which processes can provide a good quality waveguide. TI requires high temperature processing and is stable during subsequent processes, but DMPE is not, and it is more complicated to match DMPE and PE waveguides for good coupling efficiency as will be described later. However, with TI, Li_2O out-diffusion may occur, introducing a spurious waveguide and resulting in an index profile which is a combination of the out-diffused waveguide and the TI or TIPE waveguide, and there might be some guided modes additional to the pure TI or TIPE modes. When the light beam crosses the boundary of two waveguides some energy will inevitably be coupled into the out-diffused guide, and this has been observed in the m-lines of a prism coupler as shown in Fig.2, even though the loss was small in some cases. In a 4-element planar lens light was coupled into out-diffusion modes at every boundary as shown in Fig.3, decreasing signal level and constituting noise.

Several techniques have been suggested for the suppression of lithium oxide out-diffusion. Carrying out the Ti indiffusion in a flowing atmosphere containing water vapour seems to reduce the mobility of Li and Ti by occupying some of the vacancies with H^+ ions [7]. Out-diffusion cannot be suppressed completely by this mechanism, but if it can be reduced sufficiently the out-diffused layer may be too shallow to support a guided mode, the out-diffusion can be considered to be suppressed. On the other hand, if the out-diffusion is to such an extent that the mode confined

in the TI layer and the modes in the TI plus out–diffusion layer are mismatched with each other, the excited TI mode is hardly coupled into out–diffusion modes at the boundary of two different waveguides. This phenomenon was observed by another group where on some TI strip waveguide samples, in which no major defects had been produced during processing which would scatter guided light into out–diffusion modes, pure TI strip mode was seen by suitable adjusting the incident light even though there was an out–diffusion waveguide all over the sample[8]. Some authors did not find an out–diffusion mode on the sample just by using a dry oxygen and argon atmosphere[9]. By saturating the atmosphere in which the diffusion is carried out with Li_2O vapour out–diffusion may be fully suppressed: indeed, lithium *in*–diffusion has been reported by this means[10]. But care should be taken to guarantee surface quality. If the atmosphere is closed and of small enough volume the substrate itself may be able to supply the saturated vapour pressure without the generation of an out–diffused layer capable of supporting a mode[11,12,13]. But the reproducibility of some system[11] was found questionable.

In a first series of experiments, out–diffusion modes were always found by prism coupling in slab waveguide samples processed at 1000 °C for 4h or longer in flowing wet oxygen. The oxygen was bubbled at 1.0 to 1.5ℓ/minute through a 15cm high water column at >90 °C. In a second series of experiments the sample was placed polished face up on a bed of $LiNbO_3$ powder, to provide a local atmosphere rich in Li_2O vapour. The quartz boat containing the sample and powder was covered with platinum foil, and either dry or wet oxygen flowed through the furnace tube. In some cases no out–diffusion mode was seen but then the crystal surface was damaged and the TI waveguide mode suffered from scattering.

A platinum box[13] containing a sample was buried in $LiNbO_3$ powder and annealed at 1000 °C for 4 hours. An out–diffusion mode was still found. For a fourth series of experiments, in an attempt to provide a local atmosphere saturated with Li_2O vapour, two samples were placed face–to–face and buried in $LiNbO_3$ powder while being annealed in air at 1000 °C for 4 hours. Out–diffusion modes could not be observed in a pair of virgin samples but were seen in a pair of TI samples.

It seems that complete suppression of out–diffusion is very difficult. In some applications, e.g. strip waveguide[8], out–diffusion may not incur trouble. But in the case of a multi–element lens, there are 2m boundaries for an m–element lens and the energy will be coupled from the fundamental mode into out–diffusion modes at every boundary, as in Figs.2 and 3. So the coupling into out–diffusion mode must be minimised. To circumvent the problem of out–diffusion, DMPE can be used as an alternative for the low index waveguide. Annealing the DMPE sample at a higher temperature than that of later processes can stabilize the index profile, but it will be shown in the next section that annealing makes it difficult for the low index DMPE waveguide to match high index PE waveguide. It was reported that annealing improved waveguide quality on y–cut[14] and x–cut[15] but worsen it on z–cut $LiNbO_3$[15].

There are some advantages of using DPE waveguide as low index waveguide in thin film lens fabrication. The threshold of photorefractive damage is higher than that of TI waveguide[16]. This is important in thin film lenses where the light energy density is very high in the beam focus region. If a 1mm wide incident beam is focused into a 1 μm wide spot with 3dB(50%) loss through the lens, the light energy density at the focus is 500 times that of incident beam. A DMPE waveguide can be made shallower than a TI waveguide, which is important for high frequency SAW applications[17]. Calculation[18] shows that if both low and high index waveguides have step–like index profiles, by means of DMPE and PE, respectively, the coupling efficiency is much better than that if the low index waveguide has a gradient index profile while the high index waveguide has a step–like index profile, by means of TI(or annealed DMPE) and TIPE, respectively. A disadvantage of DMPE waveguide is its higher scattering loss, especially for un–annealed samples. An advantage of using TI waveguide is its higher electro–optic effect accompanying with acousto–optic effect resulting large Bragg diffraction[19].

2.2. Masking Layers for Proton Exchange

Computer-generated multi-element lens masks[6] were defined on the low index waveguide to block PE outside the lens region. Masking layers of Al, Si_3N_4 and SiO_2 were tried.

A 200nm Al film prevented the effective index of the existing guide from increasing while immersing the sample in benzoic acid at 236 °C for 3hrs, but the waveguide deteriorated after processing. For PE less than 30min, strong in-plane scattering was observed in the output m-line. If PE was for greater than 30min, light coupling into or out of the waveguide was very poor. Post-annealing in O_2 at 300 °C for 3hrs partly restored the waveguide in some cases, even after PE for 3hrs, but scattering was strong.

60nm films of Si_3N_4 and SiO_2 prevented an increase in effective index after PE at 236 °C for 3hrs, but strong scattering was observed. With thicker films of 200nm, the guides improved. Using Si_3N_4, and post-annealing as before, light could be easily coupled in, while with SiO_2 no post-annealing was necessary. Clearly, a sufficient masking thickness is needed to block both H^+ and Li^+ diffusion through the masking film. Observation of the OH^- absorptions at 3505cm^{-1} showed that for a 200nm Al-masked sample the absorption increased, while for a 200nm Si_3N_4 sample it stayed constant after immersion in benzoic acid at 236 °C for 3hrs.

An advantage of the SiO_2 masking layer, besides its better masking performance, is its ease of etching and removal in dilute HF, without risk of damage to the $LiNbO_3$ surface.

3.MODE-MATCHING ACROSS THE LENS BOUNDARIES

In a thin-film homogeneous lens, the guided light in the fundamental mode is refracted at the boundary between two different waveguides, one low index single-mode and the other high index multi-mode. At the same time, some mismatch may occur between the modes in the two guides, resulting in coupling at the boundary into higher order modes or substrate modes. The light in higher order modes is refracted at different angles because of different effective refractive indices, giving rise to spatially distributed background noise in the focal plane. Fig.4 shows a fundamental mode in a low index single-mode waveguide refracting into all modes in a high index multi-mode waveguide in different directions. For a 4-element lens, a coupling efficiency of 92% is required on each boundary to achieve an overall transmission efficiency of 50% or −3dB. The modelling and computation of the electric field overlap integral between two waveguides for several pairs of index profiles were carried out, and optical field intensity profile measurements were made on ion exchanged glass waveguides and TIPE $LiNbO_3$ waveguides[18]. It was shown that the coupling efficiency between two waveguides with the same type of index profile can be >99%, and an optical field overlap of 99% was obtained between TI and TIPE waveguides.

Matching between fundamental modes of a DMPE waveguide and a PE waveguide is more complicated because the index profile of DMPE waveguide changes during subsequent processing at elevated temperatures including PE of the lens region. Coupling efficiency was assessed by monitoring the light intensity distribution in m-line with various fabrication parameters of DMPE and PE waveguides. The measurement arrangement is like that in Fig.2(a) but with DMPE and PE waveguide regions (instead of TI and TIPE). Fig.5 shows m-lines of a z-cut $LiNbO_3$ sample which was proton exchanged in 1% diluted benzoic acid at 210 °C for 50 minutes and annealed at 320 °C for 10 minutes to form the low index waveguide and then in pure benzoic acid at 235 °C for 3hrs with half of the waveguide surface covered by a layer of SiO_2 to form the high index half of the waveguide region. For the DPE waveguide annealed at 320 °C for 10 minutes, it was difficult for the PE waveguide to match because the waveguide was too deep and had a gradient index profile; low coupling efficiency for such a waveguide and a step-like PE waveguide was expected[18]. Most of the energy is in the highest order mode. Prolonging PE time can deepen the high index

waveguide and reduce the coupling into the highest mode, but the waveguide will become highly multimoded in which case much energy will be coupled and scattered into those high order modes at the boundary, and in the waveguide by scattering among the modes. Post annealing did not improve the matching. Fig.6 shows the m-lines of a sample of which the processing is the same as the sample of Fig.5 except that no annealing was done. Most energy is concentrated in the fundamental mode.

4.CONCLUSIONS

Computer modelling of the two-waveguide lens boundaries has shown that by optimum mode-matching, transmission efficiency across one boundary can be as high as 99%, sufficient to allow multi-element acircular lens designs to operate effectively[18]. Reasonable coupling efficiency of two fundamental modes was got for TIPE system and un-annealed double proton exchange system. But scattering at imperfect boundaries, inter-mode scattering and waveguide attenuation decreases the overall transmission efficiency of the lens. Suppression of out-diffusion in the TIPE process is especially important for multi-element thin film lens fabrication, and from our experiments it seems that there still is no reliable method to suppress out-diffusion, particularly in the visible region. Un-annealed DMPE waveguide has some advantages over TI waveguide but suffers from large scattering. A SiO_2 masking film appears to block proton exchange satisfactorily, and with the advantage of ease in subsequent processing.

5.ACKNOWLEDGMENTS

The authors thank Mr. Dejie Li, Dr. A. Loni, Prof. R. M. De La Rue and Dr. M. R. Shenoy for useful discussions. Pisu Jiang thanks the University of Glasgow for J. D. Gray Postgraduate Scholarship and ORS committee of UK for ORS Award.

6.REFERENCES

1. T.Suhara, S.Fujiwara and H.Nishihara, 'Proton-exchanged Fresnel Lenses in Ti:$LiNbO_3$ Waveguides', *Appl.Opt.*, Vol.25, pp.3379-3383, 1986.
2. S.A.Reid, M.Varasi and S.Reynolds, 'Double Dilute Melt Proton Exchange Fresnel Lenses for $LiNbO_3$ Optical Waveguides', *J.Opt.Com.*, Vol.10, pp.67-73, 1989.
3. T.Q.Vu, J.A.Norris and C.S.Tsai, 'Planar Waveguide Lenses in GaAs by Using Ion Milling', *Appl.Phys.Lett.*, Vol.54, pp.1098-1100, 1989.
4. D.Y.Zang and C.S.Tsai, 'Titanium-indiffused Proton-exchanged Waveguide Lenses in $LiNbO_3$ for Optical Information Processing', Appl.Opt., Vol.25, pp.2264-2271, 1986.
5. G.C.Righini and G.Molesini, 'Refractive Waveguide Lenses: A New Design', *Elec.Lett.*, Vol.23, pp.302-303, 1987.
6. P.J.R.Laybourn, G.Molesini and G.C.Righini, 'Homogeneous Refracting Lenses for Integrated Optical Circuits', *J.Mod.Opt.*, Vol.35, pp.1029-1048, 1988.
7. J.L.Jackel, 'Suppression of Outdiffusion in Titanium Diffused $LiNbO_3$: A Review', *J.Opt.Com.*, Vol.3, pp.82-85, 1982.
8. Dejie Li, private communication, Dept. of Information Elec., Univ. of Tsinghua, P.R.China.
9. S.Fouchet, A.Carenco, C.Daguet, R.Guglielmi and L.Riviere, 'Wavelength Dispersion of Ti Induced Refractive Index Change in $LiNbO_3$ as a Function of Diffusion Parameters', *J.Lightwave Tech.*, Vol.5, pp.700-708, 1987.
10. W.K.Burns, C.H.Bulmer and E.J.West, 'Application of Li_2O Compensation Techniques to Ti-diffused $LiNbO_3$ Planar and Channel Waveguides', *Appl.Phys.Lett.*, Vol.33, pp.70-72, 1978.
11. R.J.Esdaile, 'Closed-tube Control of Out-diffusion during Fabrication of Optical Waveguides in $LiNbO_3$', *Appl.Phys.Lett.*, Vol.33, pp.733-734, 1978.
12. E.Voges and A.Neyer, 'Integrated-optic Devices on $LiNbO_3$ for Optical Communication', *J.Lightwave Tech.*, Vol.5, pp.1229-1238, 1987.

13. A.Neyer and T.Pohlmann, 'Fabrication of Low-loss Titanium-Diffused $LiNbO_3$ Waveguides Using a Closed Platinum Crucible', *Elec.Lett.*, Vol.23, pp.1187-1188, 1987.
14. M.Varasi, A.Annuli, A.Vannucci and S.Reid, 'Dilute Melt Proton Exchange(DMPE) in Y-cut $LiNbO_3$ for the Fabrication of Monomode Optical Waveguides(MOWG)', *SPIE*, Vol.866, *Materials and Technologies for Optical Communication*, pp.110-116, 1987.
15. A.Loni, R.M.De La Rue and J.M.Winfield, 'Very Low-Loss Proton-Exchange $LiNbO_3$ Waveguides with a Substantially Restored Electro-Optic Effect'. *Proc.Topical Meeting on Integrated & Guided-Wave Optics*, paper no-3, Santa Fe, New Mexico, 1988.
16. R.A.Becker, 'Comparison of Guided-Wave Interferometer Modulators Fabricated on $LiNbO_3$ via Ti Indiffusion and Proton Exchange', *Appl.Phys.Lett.*, Vol.43, pp.131-133, 1983.
17. C.S.Tsai, 'Guide-Wave Acoustooptic Bragg Modulators for Wide-Band Integrated Optic Communication and Signal Processing', *IEEE Tran. Circuits and Systems*, Vol.26, pp.1072-1098, 1979.
18. P.Jiang, W.Zhang and P.J.R.Laybourn, 'Waveguide Coupling Efficiency in Thin-film Homogeneous Lenses', *IEE Proc.*, Vol.137, Pt.J, pp.255-260, 1990.
19. R.L.Davis, 'Acousto-optic Bragg Diffraction in Proton Exchanged Waveguide', *SPIE*, Vol.517, Integrated Optical Circuit Engineering, pp.74-81, 1984

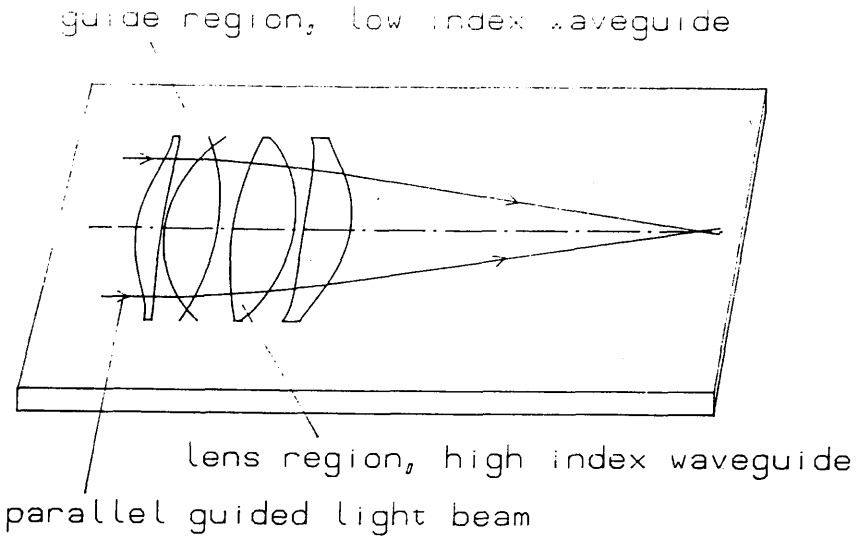

Fig.1 4-Element Homogeneous Thin Film Lens[6]

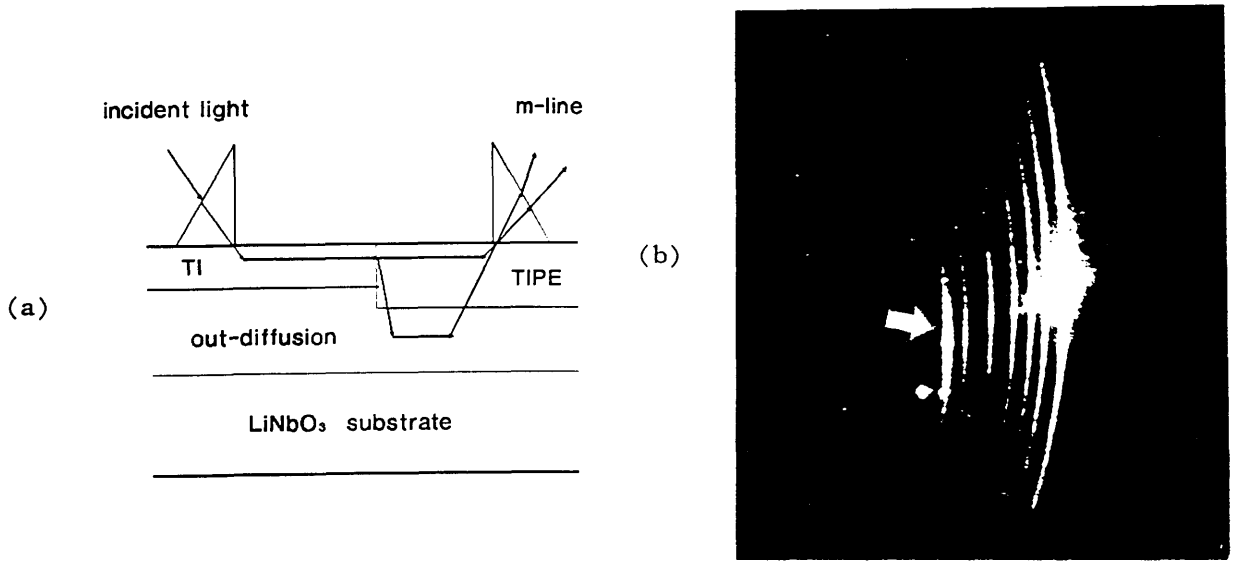

Fig.2 Coupling from TI mode into out-diffusion mode (shown by arrow in (b)) at a single boundary of TI waveguide and TIPE waveguide

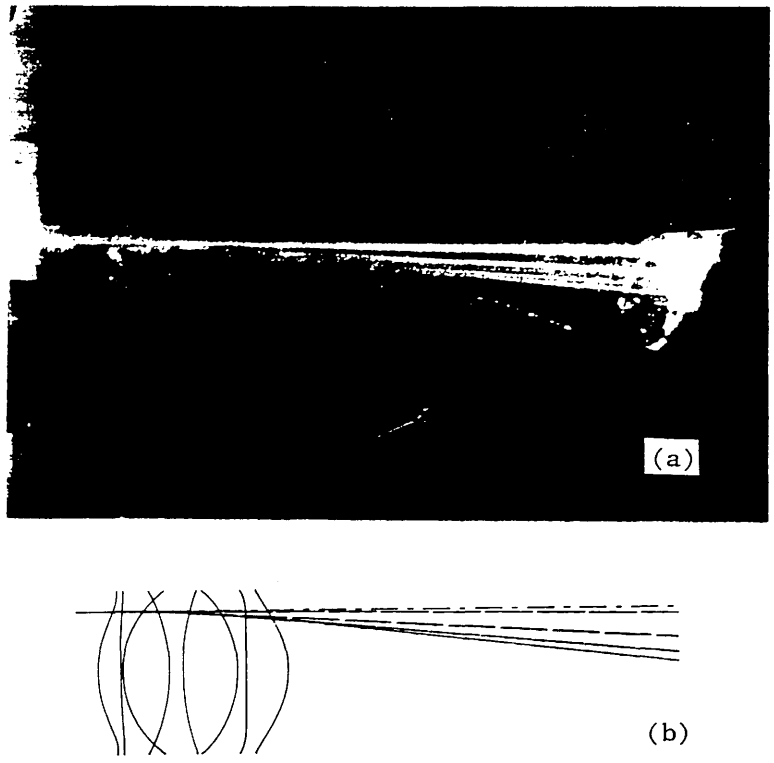

Fig.3 Coupling from a fundamental mode into out-diffusion modes at the boundaries of 4-element lens. (a):experimental result; (b): computing model

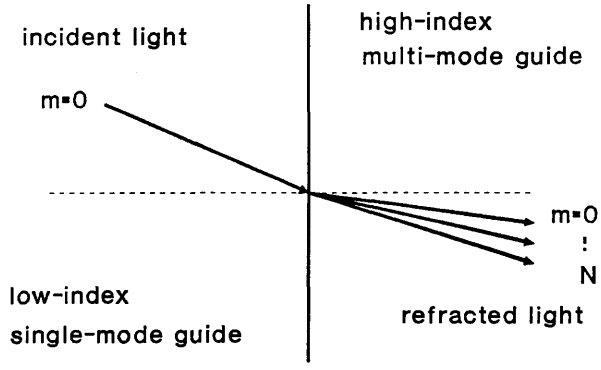

Fig.4 Refraction from a fundamental mode in a low index single mode waveguide into all modes in a high index multi-mode waveguide

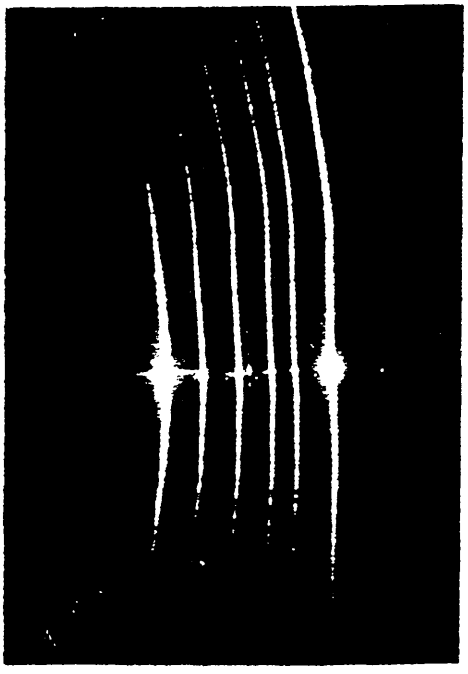

Fig.5 Coupling from a fundamental mode in DMPE waveguide into the modes in PE waveguide.
DPE: 1% dilute benzoic acid, 210°C 50min
annealing: 320°C 10min
PE: 235°C 3 hours

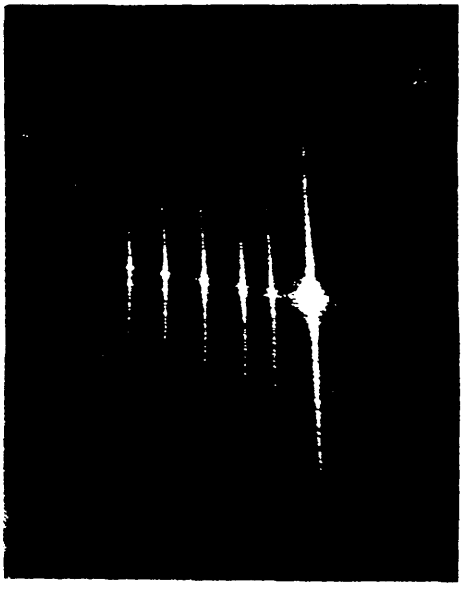

Fig.6 Coupling from a fundamental mode in DMPE waveguide into the modes in PE waveguide.
DPE: 1% dilute benzoic acid, 210°C 50min
PE: 235°C 3 hours

JOURNAL OF MODERN OPTICS, 1992, VOL. 39, NO. 1, 121–132

Homogeneous planar lens on an anisotropic waveguide

PISU JIANG, P. J. R. LAYBOURN
Department of Electronics and Electrical Engineering,
University of Glasgow, Glasgow G12 8QQ, Scotland

and G. C. RIGHINI
Istituto di Ricerca sulle Onde Elettromagnetiche (IROE/CNR),
I-50127 Firenze, Italy

(*Received 14 March 1991; revision received 18 September 1991*)

Abstract. Anisotropic aberration of a four-element acircular homogeneous planar lens is calculated on anisotropic y cut or x cut $LiNbO_3$ waveguide. Ray-tracing shows that the beam waist size increases greatly with off-axis angle. Huygens–Fresnel analysis shows a focused spot size of 2·8 μm at −8·1 dB in the incident angle range of $\pm 8°$ indicating the number of resolvable spots to be 2100.

1. Introduction

The waveguide lens is a key element in the integrated optics spectrum analyser, giving a Fourier transform of the surface-acoustic-wave-diffracted light beam angle to the focal spot position. Earlier reports have described planar Fresnel lenses made on $LiNbO_3$ [1, 2] and on GaAs [3] and the single element homogeneous Ti indiffusion and proton exchange (TIPE) lens on $LiNbO_3$ [4]. The single element homogeneous lens has intrinsically large aberration when working at an off-axis incident angle [6]. Besides focusing degradation at off-axis incident angles, there are other disadvantages for Fresnel lens: low transmission efficiency and the difficulty of reproducing by photolithography a perfect lens pattern which consists of many micro features with dimension down to about 1 μm. Recently some multi-element acircular homogeneous lens designs were reported, which offer the possibility of excellent off-axis performance [5, 6]. All the lens designs mentioned above were based on isotropic material: glass, GaAs or z cut $LiNbO_3$ waveguide on which the propagation is completely ordinary like in an isotropic material. However the most interesting materials for acousto-optical applications are planar waveguides grown on y cut or x cut $LiNbO_3$, which are anisotropic. The planar lens designs must have modified parameters when used on an anisotropic waveguide. Zhou and Ristic have contributed to the study of anisotropic aberration of a single element homogeneous lens using geometrical optical analysis [7]. This paper reports some results of ray-tracing and Huygens–Fresnel analysis on the anisotropic aberration of the four-element homogeneous lens [6] and estimates the number of resolvable spots.

2. Ray-tracing on anisotropic material waveguide

The four-element homogeneous planar lens is depicted in figure 1. The substrate material is x cut $LiNbO_3$, while the analysis is identical for y cut $LiNbO_3$ because the two are optically similar. The optic axis of $LiNbO_3$ is along the Z direction, so the

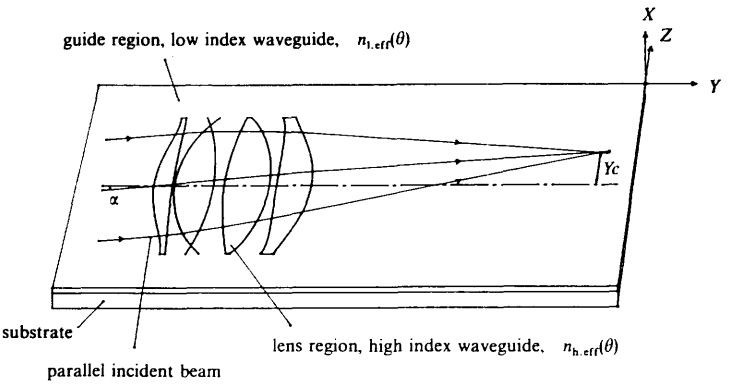

Figure 1. Four-element homogeneous planar lens on x cut $LiNbO_3$. The high-index waveguide with the lens contour is inserted in a low-index waveguide. The guided wave has effective refractive index $n_{l.eff}(\beta)$ and $n_{h.eff}(\beta)$ in guide region and lens region respectively, where β is the ray direction with respect to the Z axis. α is the incident off-axis angle. Yc is the distance between the focal spot and lens axis in the focal plan.

TE mode will see the extraordinary refractive index when propagating along the Y direction and see the ordinary refractive index when propagating along the Z direction. For refraction to take place, the lens region should be a high refractive index waveguide with effective refractive index $n_{h.eff}(\beta)$ and the surrounding guide region a low refractive index waveguide with effective refractive index $n_{l.eff}(\beta)$. These effective refractive indices vary with the angle β of the ray with respect to the Z axis in the YZ plane because the refractive indices of the waveguide material, i.e. $n_s(\beta)$ for the substrate, $n_h(\beta)$ for the high index waveguide and $n_l(\beta)$ for the low index waveguide, vary with β.

Because of the anisotropic performance of x cut and y cut $LiNbO_3$, ray-tracing in the planar waveguide is not straightforward. The light ray E (direction of propagation) and the wave normal K are not in the same direction, and on the boundary of two different waveguides the refraction of the wave normal K, not the ray E, obeys Snell's law, using effective index instead of material index. Ray E is the direction of energy flow and is to be used for ray-tracing. So it must be kept in mind that the direction and effective index of the ray E are used for ray-tracing and calculating the optical path, while the direction and effective index of the wave normal K are used for calculating angles of refraction.

2.1. *Material refractive indices*

A point light source polarized as a TE wave spreads out in the YZ plane with a elliptical energy velocity profile as shown in figure 2 (*b*). The velocity of ray E in the direction β is expressed as

$$v_E(\beta) = \frac{v_o v_e}{(v_o^2 \sin^2\beta + v_e^2 \cos^2\beta)^{1/2}}, \tag{1}$$

where v_o and v_e are velocities of ray E along the Z and Y directions respectively.

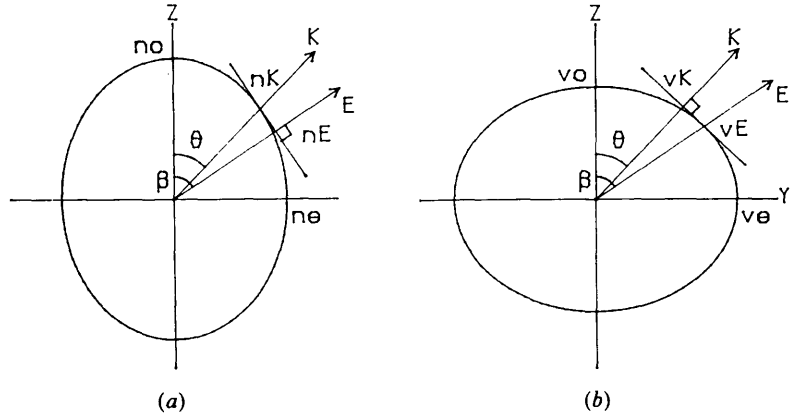

Figure 2. Elliptic sections of refractive index of wave normal K (*a*) and velocity of ray E (*b*) and relationship between K and E.

The wave normal K is in the direction θ. The velocity of K can be obtained as v_K, the cross point of the tangent through v_E and the wave normal K which is perpendicular to the tangent. The angles θ and β are related by:

$$\tan\beta = \frac{v_e^2}{v_o^2}\tan\theta = \frac{n_o^2}{n_e^2}\tan\theta, \tag{2}$$

where n_o is the ordinary refractive index and n_e is the extraordinary refractive index of the wave normal K. v_K can be obtained from v_E:

$$\begin{aligned} v_K(\theta) &= v_E(\beta)\cos\beta\frac{1+\tan^2\beta\, n_e^2/n_o^2}{(1+\tan^2\beta\, n_e^4/n_o^4)^{1/2}}, \\ &= v_E(\beta)\cos\theta\frac{1+\tan^2\theta\, n_o^2/n_e^2}{(1+\tan^2\theta\, n_o^4/n_e^4)}. \end{aligned} \tag{3}$$

The index of the wave normal K forms another elliptic section as shown in figure 2 (*a*) and is expressed as

$$n_K(\theta) = \frac{n_o n_e}{(n_o^2\sin^2\theta + n_e^2\cos^2\theta)^{1/2}}. \tag{4}$$

When n_o and n_e take the values in table 1, which are quoted as the parameters of Ti indiffused (TI) waveguide and TI plus proton exchange (TIPE) waveguide, $n_K(\theta)$,

Table 1. Ordinary and extraordinary refractive index for substrate, low-index waveguide, high-index waveguide and effective ordinary and extraordinary refractive index for low and high-index waveguide.

	Substrate n_s	Low-index waveguide n_l	High-index waveguide n_h	Low-index waveguide effective $n_{l.eff}$	High-index waveguide effective $n_{h.eff}$
n_o	2·287	2·287 + 0·008	2·287 − 0·040	2·292	2·245
n_e	2·201	2·201 + 0·010	2·201 + 0·131	2·208	2·329

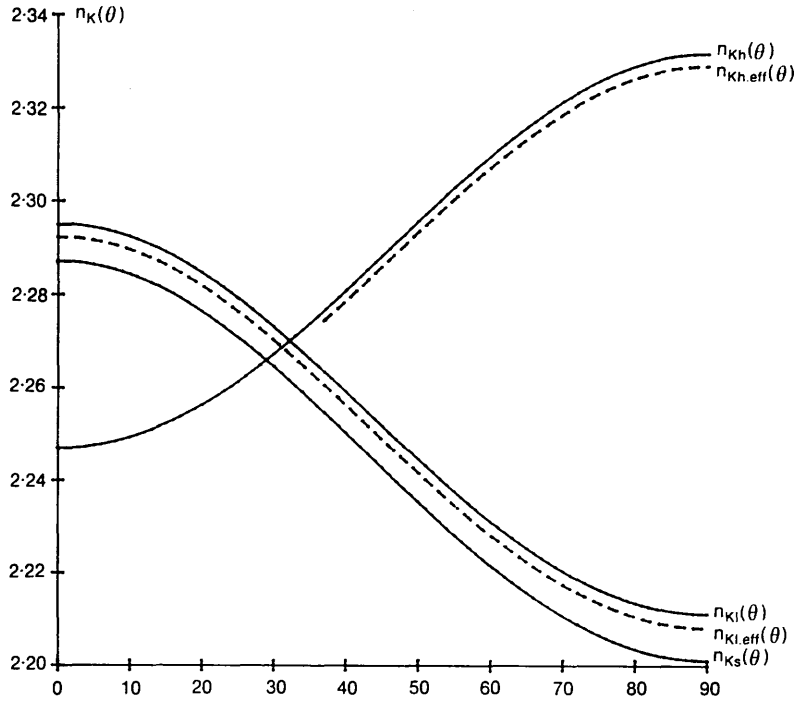

Figure 3. Refractive indices of $LiNbO_3$ substrate, TI waveguide and TIPE waveguide and effective refractive indices of low index and high index waveguide on x cut $LiNbO_3$.

expressed in (4), becomes the corresponding material indices of the substrate ($n_{Ks}(\theta)$), low index waveguide ($n_{Kl}(\theta)$), and high index waveguide ($n_{Kh}(\theta)$) for the wave normal K, which are plotted as function of θ in figure 3.

The index of the ray E is at the cross point of the tangent at n_K and the ray E which is perpendicular to the tangent. n_E is related to n_K:

$$n_E(\beta) = n_K(\theta)\cos\beta\frac{1+\tan^2\beta\, n_e^2/n_o^2}{(1+\tan^2\beta\, n_e^4/n_o^4)^{1/2}},$$

$$= n_K(\theta)\cos\theta\frac{1+\tan^2\theta\, n_o^2/n_e^2}{(1+\tan^2\theta\, n_o^4/n_e^4)^{1/2}}. \tag{5}$$

Substitute (2) and (4) into (5), giving

$$n_E(\beta) = (n_o^2\cos^2\beta + n_e^2\sin^2\beta)^{1/2}. \tag{6}$$

The following relationship always holds

$$v_o n_o = v_e n_e = v_K(\theta)n_K(\theta) = v_E(\beta)n_E(\beta) = c, \tag{7}$$

where c is the speed of light in vacuum.

2.2. *Waveguide effective index calculation*

The guided wave will see the effective refractive index of the waveguide. As with the material refractive index, we can find an effective refractive index profile for the wave normal K as a function of θ, $n_{K.eff}(\theta)$, and then the relationship between $n_{K.eff}(\theta)$

and effective refractive index of ray E, $n_{E.\mathrm{eff}}(\beta)$. Firstly we define the waveguide structure. Perpendicular to the plane YZ of propagation, in the X direction, the variation of material refractive index is steplike:

$$n(x,\theta)=\begin{cases}1, & x>0, & \text{air},\\ n_{\mathrm{w}}(\theta), & 0\geqslant x>-d, & \text{waveguide},\\ n_{\mathrm{s}}(\theta), & -d\geqslant x, & \text{substrate}.\end{cases}$$

The waveguide depth is d, and we have used the values calculated for maximum coupling efficiency on isotropic z cut $LiNbO_3$ waveguide [8]: d is 2·20 μm and 2·66 μm in the low-index and high-index guide sections, respectively. $n_{\mathrm{s}}(\theta)$ and $n_{\mathrm{w}}(\theta)$ are calculated from (4), using the values of ordinary and extraordinary index in each material layer given in table 1.

The effective refractive indices, $n_{Kl.\mathrm{eff}}(\theta)$ and $n_{Kh.\mathrm{eff}}(\theta)$ for the wave normal K in low- and high-index waveguide may be obtained by solving the wave equation [11]. However, an analytical solution is required in order to establish a relation between θ and β, the corresponding ray direction. We have used an approximation by analogy with the bulk material refractive indices. The equations (4), (6) and (2), used to determine $n_K(\theta)$, $n_E(\beta)$ and the relation between θ and β in anisotropic bulk medium, have been applied to the anisotropic waveguides to determine the equivalent effective indices and angles. In order to apply these equations we need the effective indices $n_{\mathrm{o.eff}}$ and $n_{\mathrm{e.eff}}$ in each waveguide. For the low-index waveguide they may be calculated, and for example, applied to equation (4) to give $n_{Kl.\mathrm{eff}}(\theta)$. The values of $n_{Kl.\mathrm{eff}}(\theta)$ calculated from (4), using $n_{\mathrm{ol.eff}}$ and $n_{\mathrm{el.eff}}$ in table 1, agree with values calculated from the wave equation [11] to $\Delta n_{Kl.\mathrm{eff}}(\theta)<2\times10^{-5}$, justifying the extension of the bulk index equation to the waveguide case. The function is shown in figure 3. In the high-index waveguide case, because of the anomalous variation of the bulk $n_K(\theta)$ with θ in TIPE waveguide, the guide is cut off for $\theta<31°$, and there is no physical meaning for $n_{Kh.\mathrm{eff}}(0)=n_{\mathrm{oh.eff}}$. However, a value for $n_{\mathrm{oh.eff}}$ can be obtained by calculating $n_{Kh.\mathrm{eff}}(\theta)$ from the wave equation [11] at an arbitrary value of θ, near to cut off, and substituting into equation (4). The approximated $n_{Kh.\mathrm{eff}}(\theta)$ is shown in figure 3 and is found to be good for θ large, well away from waveguide cutoff. The values of $n_{Kh.\mathrm{eff}}(\theta)$ calculated from (4), using $n_{\mathrm{oh.eff}}$ and $n_{\mathrm{eh.eff}}$ in table 1, agree with the values calculated from wave equation to $\Delta n_{Kh.\mathrm{eff}}(\theta)<2\times10^{-5}$ in the angle range of $\theta>75°$, where in our calculation the light ray lies in.

With any direction of ray E or wave normal K, the effective index can be obtained from (4) or (6), and the direction of the corresponding E or K calculated from (2). In the calculation that was made, the ratio of effective extraordinary indices of high- and low-index waveguide sections, shown in table 1, was 2·329/2·208 = 1·055. This ratio was used in optimising the performance of the four-element lens design on isotropic z cut $LiNbO_3$ waveguide [6].

2.3. *Ray-tracing procedure*

The ray-tracing is carried out as follows, and illustrated in figure 4 where WG1 and WG2 represent two different waveguide divided by refractive planes. A known incident ray $E_1(\beta_1)$ in WG1 is considered, propagating in direction β_1, with respect to the Z axis. The direction θ_1 of the corresponding wave normal $K_1(\theta_1)$ is obtained through (2) with n_{o} and n_{e} taking effective values of the related waveguide in table 1. The effective indices $n_{K_1.\mathrm{eff}}(\theta_1)$ and $n_{E_1.\mathrm{eff}}(\beta_1)$ are worked out from (4) and (6). Then

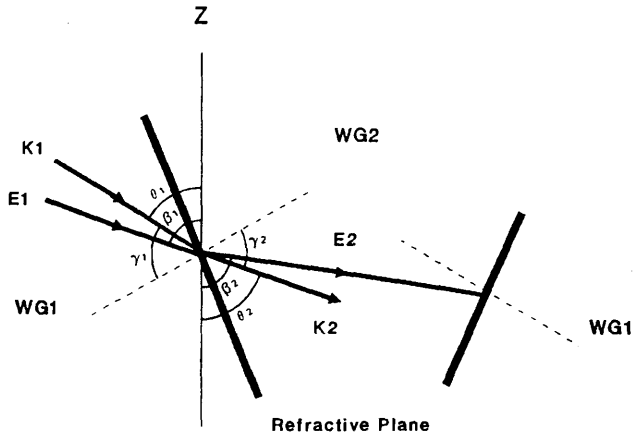

Figure 4. Illustration of ray-tracing on anisotropic material.

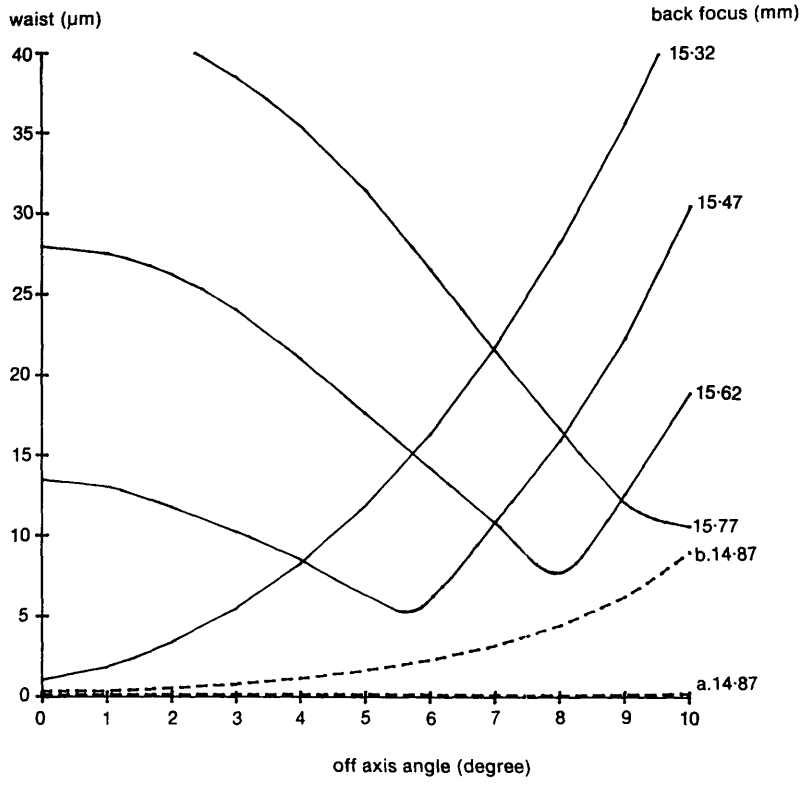

Figure 5. Anisotropic aberration of four-element lens. Waist size against incident angle on different positions of focal plane. Beam wide 2 mm. Dashed line: aberration on isotropic material for incident beam of 2 mm (*a*) and 6 mm (*b*) wide.

the ray $E_1(\beta_1)$ is traced to the first boundary and the optical path calculated. At the boundary the refraction of the wave normal is calculated by a successive approximation routine, necessary since the effective refractive index, $n_{K_2,\text{eff}}(\theta_2)$ to be used in Snell's law is itself dependent on θ_2, the direction of the wave normal $K_2(\theta_2)$ in the next waveguide section. β_2 is then calculated from θ_2 using equation (2). The process is repeated for each ray at every boundary, giving the position, direction and relative phase of each ray at any plane (including the focal plane).

3. Ray-tracing of homogeneous lens

A programme was written for light beam ray-tracing on anisotropic waveguides. Repeating the computation for 101 rays, forming a parallel incident beam, on all eight boundaries, the beam waist size can be obtained by ray analysis at the detection plane.

Figure 5 shows the performance of a four-element lens on anisotropic material. The waist varies with off-axis angle with back focal length as a parameter. The incident beam is 2 mm wide. The back focal length is taken as the distance from the back surface of the lens to the detection plane. As a comparison, the dashed lines in the figure show the waist size of the lens on isotropic material. For an Elliptical–Hyperbolic lens design [6], off-axis performance is much worse for both anisotropic and isotropic materials as expected.

4. Huygens–Fresnel analysis

Ray analysis breaks down as the focused spot size is within or near to the diffraction limit. The Huygens–Fresnel method allows the calculation of the amplitude and phase of the wave in the focal plane. The data on the positions and phases of all 101 rays on the last surface of the lens, as the result of ray-tracing, were then fed into another programme. Each position was considered as a new wavelet source with a calculated initial phase. All 101 wavelets interfere and, by summing in phase and out of phase components of all wavelets on the detection plane, the optical intensity profile can be obtained.

Figure 6 shows optical intensity profiles for a Gaussian intensity profile incident beam with Gaussian width $A=6$ mm, beam width $D=6$ mm and wavelength $\lambda=0{\cdot}633$ μm at the incident angle of 0°, 2°, 5° and 8°. The spot size σ is listed in table 2. From the figures and the table we can see that at the focal plane 15·91 mm away from the last lens surface the focal spot size can be held to 2·8 μm at −8·1 dB of peak intensity in the incident angle range of ±8°. The optimum focal surface is still considered to be a plane, or straight line in this 2-D planar lens case. The number of resolvable spots N then is estimated as in table 2, assuming an average diffraction

Table 2. Spot sizes and resolvable spot number for four-element lens on anisotropic material.

θ°	Yc(mm)	σ(μm) at −8·1 dB	σ(μm) at −10·0 dB	σ(μm) at −10·9 dB	N
0		2·8	3·0	3·1	
±2	±0·793	2·8	3·0		566
±5	±1·847	2·8			1319
±8	±3·023	2·8			2159

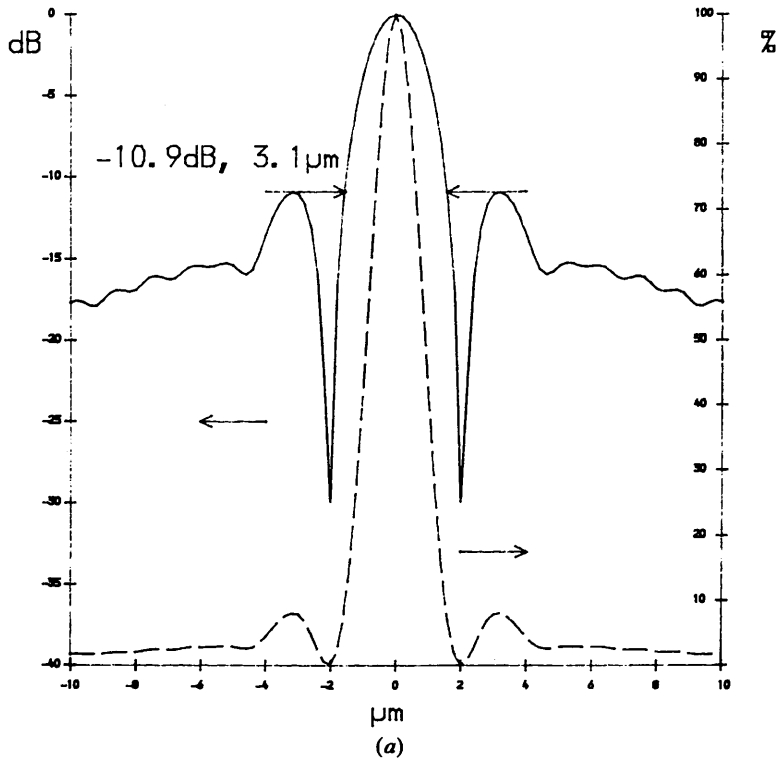

(*a*)

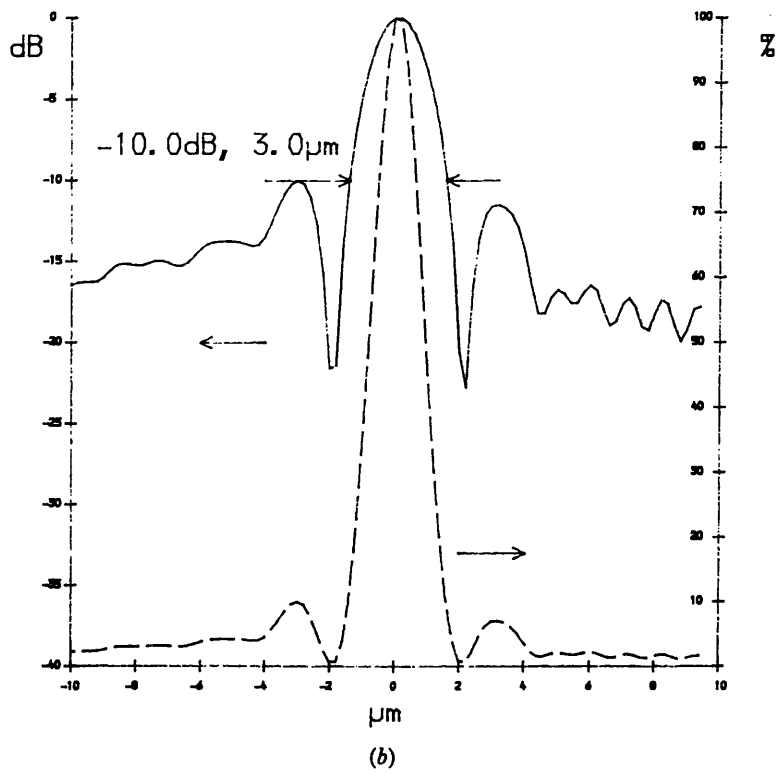

(*b*)

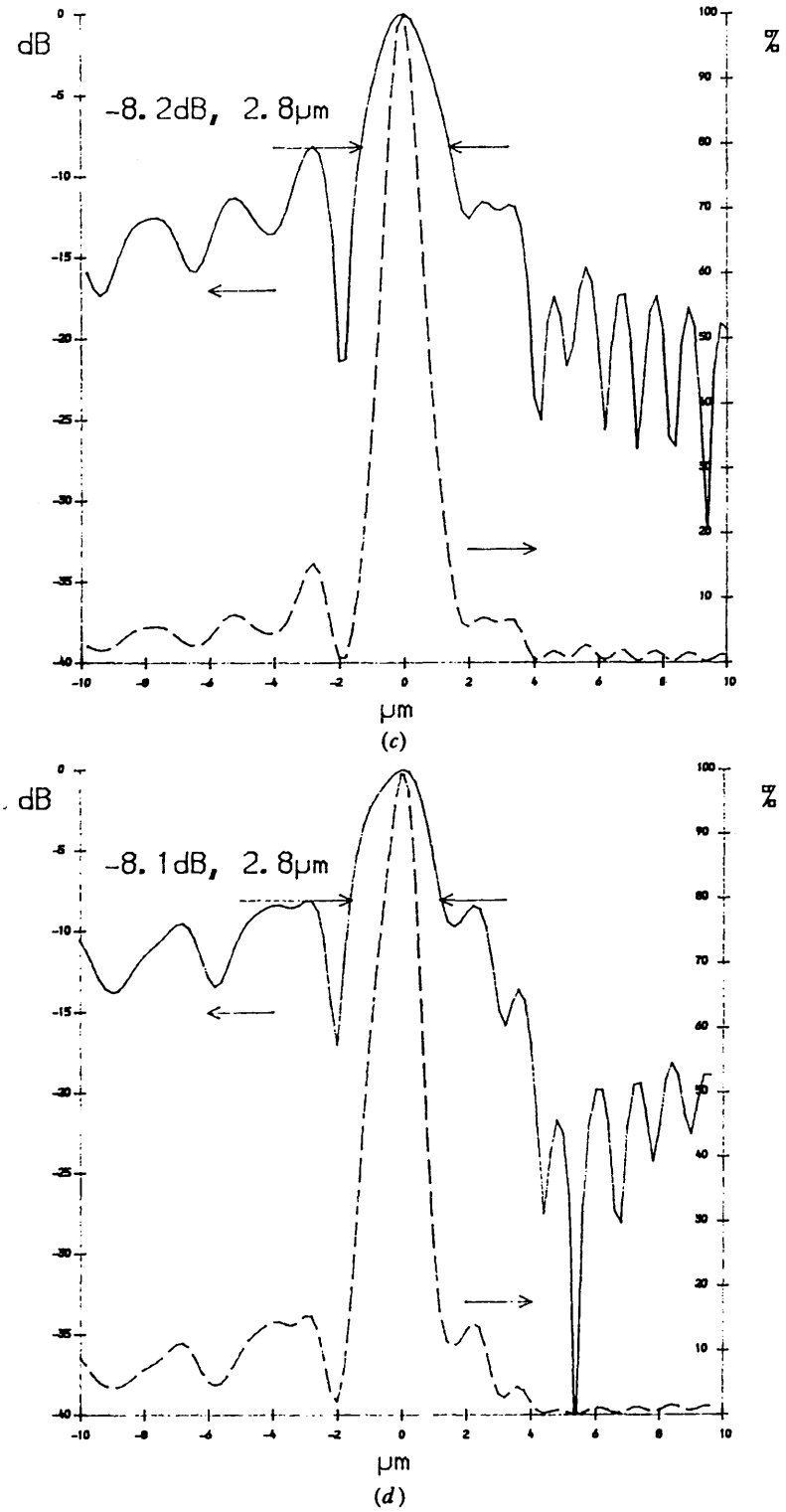

Figure 6. Diffraction intensity profile for four-element lens on anisotropic material. $\lambda = 0{\cdot}633\,\mu m$. Incident beam $D = 6\,mm$ wide with Gaussian width $A = 6\,mm$. Back focal length $f = 15{\cdot}91\,mm$. Incident angle $\alpha = 0°$ (*a*), 2° (*b*), 5° (*c*) and 8° (*d*).

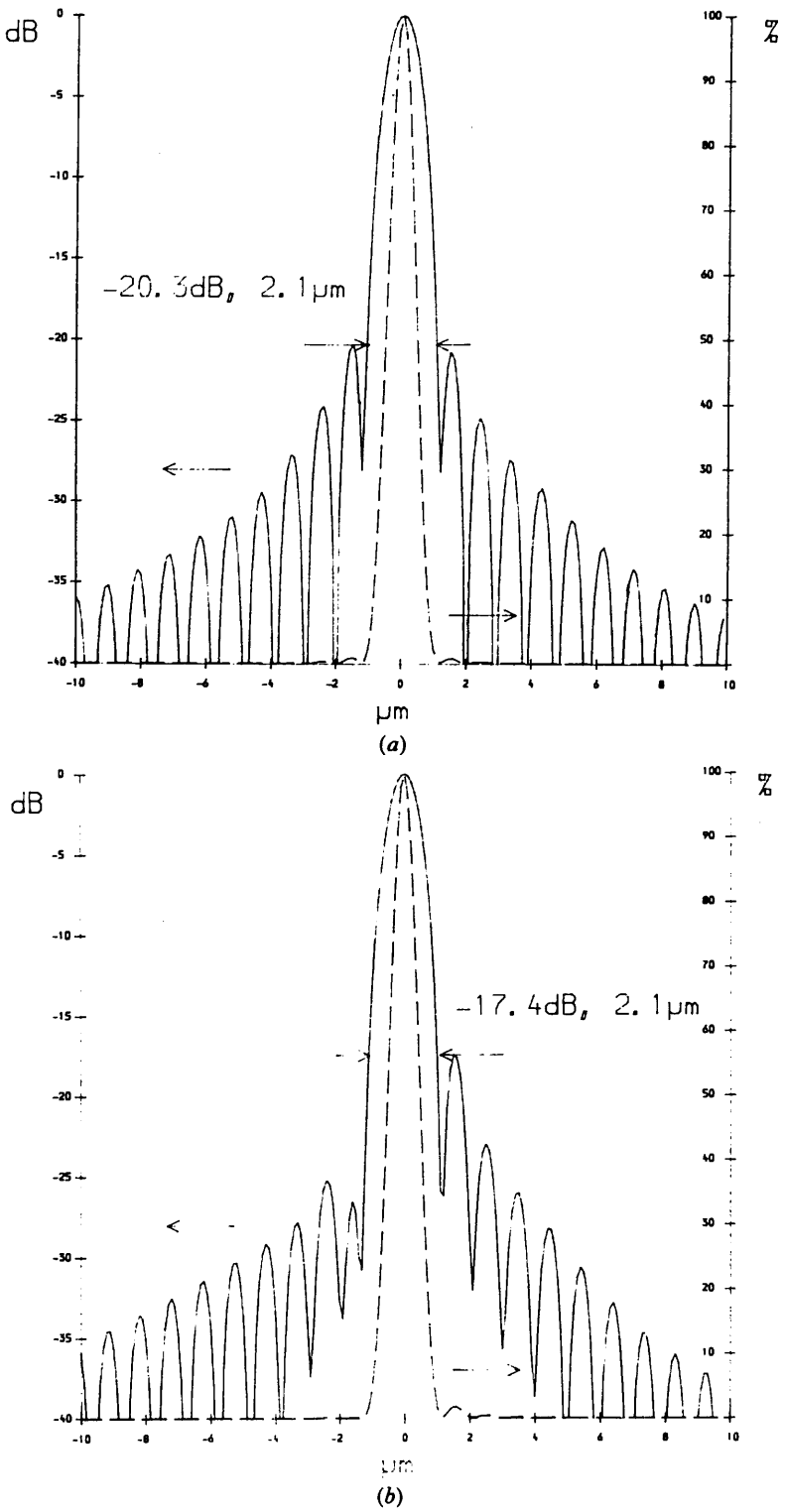

Figure 7. Diffraction intensity profile for four-element lens on isotropic material. $\lambda = 0{\cdot}633\,\mu m$. Incident beam $D = 6\,mm$ wide with Gaussian width $A = 6\,mm$. Back focal length $f = 14{\cdot}87\,mm$. Incident angle $\alpha = 5°$ (*a*) and 8° (*b*).

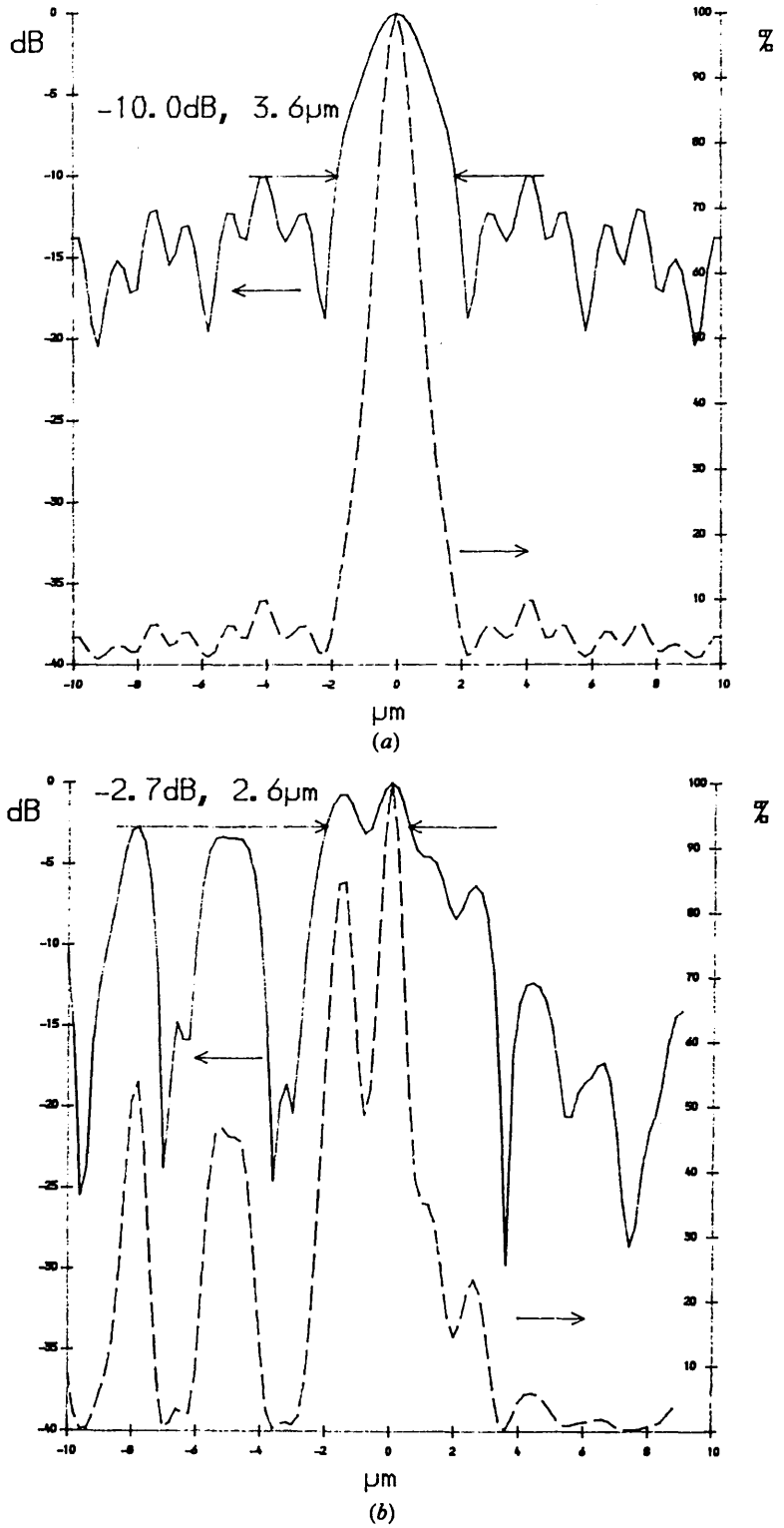

Figure 8. Diffraction intensity profile for Elliptical–Hyperbolic lens on anisotropic material. $\lambda = 0{\cdot}633$ μm. Incident beam $D = 6$ mm wide with Gaussian width $A = 6$ mm. Back focal length $f = 11{\cdot}07$ mm. Incident angle $\alpha = 0°$ (*a*) and 2° (*b*).

Table 3. Spot sizes and resolvable spot number for four-element lens on isotropic material.

$\theta°$	Yc(mm)	σ(μm) at −10 dB	σ(μm) at −17·4 dB	σ(μm) at −20·3 dB	σ(μm) at −20·6 dB	N
0		1·6	2·0	2·1	2·1	
±2	±0·691	1·6	2·0	2·1	2·1	691
±5	±1·732	1·7	2·0	2·1		1732
±8	±2·784	1·7	2·1			2784

spot size of $\sigma = 2{\cdot}8$ μm in the range of Yc on the focal plane, while Yc is the distance between the spot and lens axis in the focal plane (shown in the figure 1), and $N = 2\,Yc/\sigma$.

Using a 2 mm wide incident beam the focused spot widened, because the stronger diffraction, and the sidelobes were reduced somewhat. *Vice versa*, with a wider beam, the spot size decreases, but at the same time the background noise increases, as the sidelobes rise up.

As a comparison with the isotropic case (z cut $LiNbO_3$ waveguide), figure 7 shows optical intensity profiles for an incident beam of $D = A = 6$ mm wide and $\lambda = 0{\cdot}633$ μm at the incident angles of 5° and 8°. At the focal plane 14·87 mm away from the last lens surface the focal spot size can be maintained at about 2 μm at −17 dB in the incident angle range of ±8°. The spot sizes and estimated resolvable spot numbers are listed in table 3.

Figure 8 shows intensity profiles for an Elliptical–Hyperbolic lens [6] used on anisotropic material. The on-axis performance is acceptable but the off-axis performance is greatly degraded.

5. Summary

When the four-element lens which is optimized on isotropic material is used on anisotropic material, the optimum focal surface is still plane, the spot size becomes a little wider and the sidelobe rises. The spot size is still acceptable, with the number of resolvable spots estimated to be about 2100 in the incident angle range of ±8°, or 1300 in a range of ±5°. The major drawback will be the higher background noise which will reduce the main lobe intensity and hence the signal-to-noise ratio. It should be pointed out that better optical performance should be obtained if the lens is redesigned and optimized on anisotropic materials.

Acknowledgments

The authors would like to thank Professor R. M. De La Rue for helpful discussions. Pisu Jiang thanks the University of Glasgow for the D. L. Gray Postgraduate Scholarship and the ORS committee of the UK for an ORS Award.

References

[1] Suhara, T., Fujiwara, S., and Nishihara, H., 1986, *Appl. Optics*, **25,** 3379.
[2] Reid, S. A., Varasi, M., and Reynolds, S., 1989, *J. opt. Com.*, **10,** 67.
[3] Vu, T. Q., Norris, J. A., and Tsai, C. S., 1989, *Appl. Phys. Lett.*, **54,** 1098.
[4] Zang, D. Y., and Tsai, C. S., 1986, *Appl. Optics*, **25,** 2264.
[5] Righini, G. C., and Molesini, G., 1987, *Electron Lett.*, **23,** 302.
[6] Laybourn, P. J. R., Molesini, G., and Righini, G. C., 1988, *J. mod. Optics*, **35,** 1029.
[7] Zhou, Wujun and Ristic, V. M., 1989, *IEEE J. quant. Electron*, **25,** 749.
[8] Jiang, P., Zhang, W., and Laybourn, P. J. R., 1990, *IEE Proc.*, **137,** Pt.J, 255.
[9] Longhurst, R. S., 1957, *Geometrical and Physical Optics* (London, Longmans).
[10] Driscoll, W. G. (editor), 1978, *Handbook of Optics* (New York: McGraw-Hill).
[11] Yariv, A., 1973, *IEEE J. quant. Electron*, **9,** 919.